The Removal of Phosphate ions from aqueous solution by Fly

ash, Slag, Ordinary Portland Cement and related blends

by

Nana Mensah Agyei

Submitted in partial fulfilment of the requirements for the degree

Philosophiae Doctor

CHEMISTRY

in the Faculty of Natural & Agricultural Science

University of Pretoria

Pretoria

April 2004

The Removal of Phosphate ions from aqueous solution by Fly ash,

Slag, Ordinary Portland Cement and related blends

by

Nana Mensah Agyei

Supervisor: Prof. C.A. Strydom

Department of Chemistry

University of Pretoria

Co-supervisor: Prof. J.H. Potgieter

Department of Chemical & Metallurgical Engineering

Technikon Pretoria

Degree: Philosophiae Doctor

SUMMARY

Phosphate ions have been removed from aqueous solution by fly ash (FA), slag, OPC and related cement blends. Characterisation of the adsorbents was done using XRD, XRF and laser Fraunhofer diffractometry. The rate and efficiency of phosphate removal was found to increase in the order: FA, slag, OPC, apparently mimicking the order of increasing percentage CaO in the adsorbents. Blending OPC with FA or slag evidently results in diminished phosphate removal efficiency.

Better removal was obtained with smaller particles, at higher solute concentration, acidic pH and higher temperature. The speed of mixing was not found to have a significant effect. A 400 mg/l PO_4^{3-}-P solution was fed at a steady velocity of 2.0 cm/min through a 2-cm fixed-bed column (at pH 9.0 and 25°C) to construct breakthrough curves. Adsorption capacity values of 32, 60, 75, 78 and 83 mg PO_4^{3-}-P/g adsorbent were obtained for FA, slag, OPC/FA, OPC/slag and OPC, respectively.

Adsorption is evidently the major phosphate removal mechanism, with a contribution from precipitation by calcium ions released into solution via dissolution and hydration. The Frumkin isotherm was found to be the appropriate equation for modelling the experimental adsorption data, and values have been

obtained for the isotherm constants. A first order kinetic model was used to obtain values for overall sorption rate constants and intra-particle diffusion constants.

The use of a fixed bed consisting of a mixture of sand and OPC, OPC/slag or OPC/FA evidently offers a potential alternative to the established methods of large-scale phosphate removal using chemical and/or microbiological agents. An envisaged added value of this proposed method is that bed, after exhaustion with respect to phosphate removal, may be used for the production of masonry bricks. This will obviate the challenge of disposing of the spent bed.

Die verwydering van fosfaatione uit waterige oplossing deur vlieg-as, slak, gewone Portland sement en verwante mengsels

deur

Nana Mensah Agyei

Studieleier: Prof. C.A. Strydom

Department Chemie

Universiteit van Pretoria

Mede-studieleier: Prof. J.H. Potgieter

Department Chemiese & Metallurgiese Ingenieurswese

Technikon Pretoria

Graad: Philosophiae Doctor

ACKNOWLEDGEMENTS

Table of Contents

LIST OF ABBREVIATIONS AND SYMBOLS

PO_4^{3-}-P	Phosphate phosphorus (i.e., the P in PO_4^{3-})
FDPA	Fraunhofer diffraction pattern analysis
XRF	X-ray fluorescence
XRD	X-ray diffraction
UV/VIS	Ultraviolet/visible
OPC	Ordinary Portland cement
FA	Fly ash
ACBFS	Air-cooled blast furnace slag
GGBFS	Ground granulated blast furnace slag
CAC	Commercial activated carbon
GAC	Granular activated carbon
ACC	Clothe activated carbon
PAC	Powder activated carbon
ACF	Fibre activated carbon
CEC	Cation exchange capacity
A	Al_2O_3
C	CaO
H	H_2O
CH	$Ca(OH)_2$
S	SiO_2

$\underline{S}$	SO_3
C_2S	Dicalcium silicate
C_3S	Tricalcium silicate
C_3A	Tricalcium aluminate
C_4AF	Calcium aluminoferrite
$U(t)$	Fractional attainment of equilibrium
k'	First-order rate constant, per hour
D	Intra-particle diffusion constant, cm^2/s
α, β	Frumkin isotherm constants
h_Z	Height of the mass transfer zone, cm
h_T	Bed height, cm
t_E	Breakthrough time, min
X_0	Influent concentration, mg/l PO_4^{3-}-P
X	Effluent concentration, mg/l PO_4^{3-}-P
V_E	Effluent volume at breakthrough, cm^3
V_T	Effluent volume at bed exhaustion, cm^3
V_Z	V_T minus V_Z, cm^3
C_T	Specific dynamic adsorption capacity, mg/g

CHAPTER 1

ADSORPTION FROM SOLUTION

Adsorption from solution is a phenomenon that is applicable to many important processes. These include chromatography, heterogeneous catalysis, the dyeing of textiles, and the removal of impurities from wastewater and effluents. Adsorbents investigated in this regard, i.e. for wastewater and effluent treatment, include naturally occurring materials such as zeolites, chitosan, clays and various oxides; industrial by-products such as fly ash, iron (III) hydroxide, waste slurry, lignin, blast-furnace slag and sawdust; as well as a variety of miscellaneous adsorbents. Research efforts have focussed almost entirely on the removal of heavy metals, due to their well-known toxicity.

1.1.   Literature review

Commercial activated carbon (CAC) is the most widely used adsorbent in wastewater applications. The large number of pores produced within the particles during activation and the extremely large specific surface area (on the order of 1000 m^2/g) makes CAC a very efficient adsorbent. However, CAC is expensive, and this fact has led to on-going research into the feasibility of using lower-cost adsorbents as alternatives to CAC.

1

Several workers have investigated the removal of heavy metals from aqueous solution by granular activated carbon (GAC). Netzer and Hughes (1984) reported that GAC removed 99 % Co and 93 % Cu, respectively, from 10 ppm solutions at pH 4.0. An adsorption capacity of 30 mg Pb^{2+}/g GAC was reported by Reed and Arunachalam (1994), who also showed that the portion of Pb^{2+} not removed represented the amount that was complexed with by the EDTA added to improve the removal performance of the adsorbent. The adsorption capacity value of 145 mg Cr^{6+}/g GAC type Filtrasorb 400 at pH 3.0 reported by Sharma and Forster (1996) is several orders of magnitude higher than the value of only 0.18 Cr^{6+}/g GAC reported by Han et al. (2000) in a comparative study.

Leyva-Ramos et al (1997) reported an adsorption capacity value of 8 mg Cd^{2+}/g GAC at pH 8.0. They also made the observation that the adsorption capacity decreased with increasing temperature, indicating that the adsorption process was exothermic. It has also been reported (Aggarwal et al, 1999) that chemical modification of the surface of GAC with nitric acid led to a three-fold increase in the adsorption capacity for Cr^{3+} to 30 mg Cr^{3+}/g GAC. This can be ascribed to the larger negative charge on the surface of the oxidised GAC compared to the GAC as received.

Other types of CAC have also been investigated. Using clothe activated carbon (ACC), adsorption capacities of 65, 2.0 and 3.8 mg/g ACC were reported (Babi et

al, 2002) for Hg^{2+}, Zn^{2+} and Cd^{2+} respectively. The removal of Hg^{2+} using powder activated carbon (PAC) was studied by Huang and Blankkenship (1984). They reported 99-100 % removal of 0.2 mM Hg^{2+} in the pH range 4.0-5.0. Oxidative treatment of fibrous activated carbon (ACF) with nitric acid was reported (Rangel-Mendez and Streat, 2002) to result in a marked increase Cd^{2+} in removal. An adsorption capacity of 146 mg Cd^{2+}/g ACF was obtained in the pH range 5.0-6.0.

In addition to removing heavy metals, CAC has also been used widely for deodorising wastewater by removing colour- and odour- producing refractory organic materials (Smethurst, 1979).

Zeolites occur as crystalline aluminosilicates consisting of a framework of tetrahedral molecules interlinked by shared oxygen atoms. The unique capability of zeolites to preferentially exchange constituent cations such as Al^{3+}, K^+ and Na^+ for heavy metal ions makes them good candidates for research and application in wastewater treatment. The family of zeolites consist of a wide variety of species, with clinoptilolite and chabazite being the two commonest types.

Malliou et al (1992) reported adsorption capacities of 1.4 mg Pb^{2+} and 1.2 mg Cd^{2+}/g clinoptilolite. It was further observed (Malliou et al, 1994) that higher temperatures favoured metal uptake. This can be attributed to activation of the metal ions, which enhances adsorption at the coordination site of zeolites.

Chabazite was found to be superior to clinoptilolite with respect to the removal of Pb^{2+}, Cd^{2+}, Cu^{2+}, Zn^{2+}, Ni^{2+} and Co^{2+} from effluents (Ouki and Kavanagh, 1997). This was attributed to the fact that the former zeolite has a higher Al substitution of Si than the latter, providing a negative framework more favourable for cation exchange. Several workers (Ouki et al, 1993; Semmens and Martin, 1988; Curkovic et al, 1997) have reported that pre-treatment of zeolites influences the cation exchange capacity (CEC). For example, treating chabazite (and clinoptilolite) with NaOH solution was reported by Ouki et al (1993) to result in CECs in excess of 100 mg/g for Pb^{2+} and Cd^{2+}; 137 mg Cd^{2+} and 175 mg Pb^{2+}/g chabazite (and 70 mg Cd^{2+} and 62 mg Pb^{2+}/g clinoptilolite).

For column operation, effluent flow rate has been found to be an important parameter influencing the CEC of zeolites. In a study using an Italian zeolite containing chabazite and phillipsite a CEC of 7.10 mg Cr^{3+}/g was obtained at a flow rate of 1.83 ml/min (Pansini et al, 1991). A similar study using a flow rate of 15 ml/min yielded a CEC of only 0.25 mg Cr^{3+}/g (Ibrahim et al, 2002). This observation can be attributed to the fact that at a lower flow rate there is a greater chance for physicochemical interactions to occur between the zeolite and the target heavy metal species.

Chitosan is produced by alkaline N-deacetylation of chitin, a natural biopolymer similar to cellulose in molecular structure and widely found in the exoskeleton of

4

crustaceans and shellfish. The large number of surface hydroxyl and primary amino groups, coupled with the flexible structure of the polymer chain, make chitosan a good candidate for the adsorption of metal ions.

The removal of heavy metals by chitosan has been investigated by several workers. McKay et al (1989) reported adsorption capacities of 75, 164, 222 and 815 mg/g for Zn^{2+}, Ni^{2+}, Cu^{2+} and Hg^{2+}, respectively. Another study (Huang et al, 1996) found adsorption capacities of 16.8, 8.5, 2.4, 16.4 and 51.6 mg/g for Cu^{2+}, Cd^{2+}, Ni^{2+}, Pb^{2+} and Hg^{2+}, respectively.

The effect of chitosan particle size on removal efficiency can be seen by comparing the results obtained by Annachhatre et al (1996) and Wan-Nga and Isa (1998). The former reported an adsorption capacity of 13 mg Cu^{2+}/g using 50 mesh chitosan, compared to the 4.7 mg Cu^{2+}/g obtained in the latter study, which used 200 mesh chitosan under similar conditions.

Chemical modification of chitosan has been reported to enhance its removal efficiency for metal ions. For example, Guibal et al (1994) obtained a high adsorption capacity of 450 mg V^{5+}/g using the oxo-2-glutaric acid derivative of chitosan. They also reported an optimum pH of 3.0 for vanadium (V) removal and fitted the experimental adsorption data to the Freunlich isotherm. Nga et al (2002) reported adsorption capacities of 45.9, 62.5 and 59.7 mg Cu^{2+}/g for chitosan cross

linked with ethylene glycol diglycidyl ether (EGDA), epichlorohydrin (EC), and glutaraldehyde (GD), respectively, at a pH of 6.0. Although it improves the stability of chitosan, cross linking was reported (Schmuhl et al, 2001) to reduce the capacity of the adsorbent for metal ion removal.

The essential constituents of clay are kaolinite and other hydrous aluminous minerals like smectites (e.g. montmorillonite, wollastonite and bentonite), micas and fine particles (less than 2 μm diameter). An obvious attraction of clays for adsorption studies is its relatively low cost and easy local availability.

Srivastava et al (1989) compared the removal of cadmium and lead by kaolinite and montmorillonite. They obtained adsorption capacities of 0.72 mg Cd^{2+}/g and 0.68 mg Pb^{2+}/g on montmorillonite and 0.32 mg Cd^{2+}/g and 0.12 mg Pb^{2+}/g on kaolinite. They also observed that the uptake of metal ions is improved in the presence of anionic surfactants and attenuated in the presence of cationic surfactants. Montmorilonite was reported (Undaybeytia et al, 1996) to adsorb Zn^{2+} more efficiently than Cd^{2+}. This was ascribed to the fact that Zn^{2+} has a higher ionic potential than Cd^{2+}. Panday et al (1986) studied the removal of Cu^{2+} using homogeneous mixtures of adsorbents such as wollastonite/China clay, wollastonite/fly ash and China clay/fly ash. The wollastonite/fly ash mixture yielded the maximum adsorption capacity, 1.18 mg Cu^{2+}/g.

Chantawong et al (2001) reported adsorption capacities of 4.3 and 1.4 mg Pb^{2+}/g, respectively, for kaolinite and illite from Thailand. They observed that an increase in pH improved the efficiency of lead uptake, and that co-ions such as Cd^{2+}, Cu^{2+} and Zn^{2+} reduce Pb^{2+} adsorption because they bind strongly with organic matter present in clay. Both the Langmuir and Freundlich isotherms were used to model the experimental adsorption data. China clay and wollastonite were used to evaluate the effect of temperature on lead removal (Yadava et al, 1991). The adsorption capacity was found to decrease with increasing temperature (e.g. 1.68 and 1.10 mg Pb^{2+}/g wollastonite at 20 and 40°C, respectively); negative ΔH values were obtained, indicating an exothermic adsorption process. This happens to be opposite to the observation made by Khan et al (1995), who found that the sorption of Cr^{6+} on the clay mineral bentonite is favoured at higher temperatures (0.33 and 0.57 mg Cr^{6+}/g at 20 and 40°C, respectively). Bentonite has also been used to remove radioactive waste (Pusche, 1992).

Several natural oxides have been investigated for their ability to remove heavy metals from aqueous waste. Srivastava et al (1996) reported adsorption capacities of 31 mg Cd^{2+}/g and 33 mg Pb^{2+}/g for aluminium oxide, and 72 mg Cd^{2+}/g and 230 mg Pb^{2+}/g for goethite (a ferric oxide). Iron oxide coated with sand was used to develop a unit that can be used domestically to remove over 80 % of the As^{3+} and As^{5+} from ground water (1.0 ppm arsenic), regardless of the chemical origin of the arsenic (Joshi and Chaudhuri, 1996). Manganese oxide has also been used to

remove arsenic compounds from ground water (Chakaravarty et al, 2002). Bailey et al (1992) successfully removed 99 % of 0.038 mM Cr^{6+} from aqueous solution using iron oxide coated with sand.

Several solid waste materials generated as by-products in a variety of industrial processes have been investigated for potential use as adsorbents; finding new applications for a particular by-product adds economic value to the process involved in its generation.

Iron (III) hydroxide and waste slurry are both by-products generated in the fertilizer industry. Namasivayam and Ranganathan (1992) reported an adsorption capacity of 0.47 mg Cr^{6+}/g iron (III) hydroxide at pH 5.6. Very high adsorption capacities of 1030 mg Pb^{2+}/g, 560 mg Hg^{2+} and 640 mg Cr^{6+}/g were reported for waste slurry (Srivastava et al, 1989). Lignin, a by-product of paper manufacturing, reportedly (Srivastava et al, 1994) has outstanding adsorption capacities for Pb^{2+} (1865mg/g) and Zn^{2+} (95 mg/g). They found that the high adsorption capacity can be ascribed to the presence of polyhydric phenol groups on the surface of lignin, and that the efficiency of metal ion removal improved with increasing temperature. An adsorption capacity of 13.8 mg Cu^{2+}/g was reported (Ajmal et al, 1998) for sawdust, a by-product of the saw milling of timber.

Fly ash, a by-product of the combustion of coal to produce electrical power, has been investigated by many workers in this regard. It has been used to adsorb heavy metals such as Cr^{6+} (Dasmahapatra et al, 1996), Cu^{2+}, Pb^{2+} and Cd^{2+} (Apaka et al, 1998) and Hg^{2+} (Sen and De, 1987). Panday et al (1984) found that using fly ash in a 1:1 homogeneous mixture with wollastonite improved its removal efficiency for hexavalent chromium. They achieved an adsorption capacity of 2.92 mg Cr^{6+}/g mixed adsorbent at pH 2.0, and modelled the experimental adsorption data on the Langmuir isotherm. Sen and Arnab (1987) reported an adsorption capacity of 2.82 mg Hg^{2+}/g fly ash in the pH range 3.5-4.5. They found the Freundlich isotherm to be the appropriate isotherm for modelling the experimental adsorption data. Slag, which is a by-product of the manufacture of iron and steel in a blast furnace, has been investigated for its adsorptive capability. Srivastava et al (1997) reported adsorption capacities of 40 mg Pb^{2+}/g and 7.5 mg Cr^{6+}/g for slag.

Table 1.1 is a summary of the highest adsorption capacities (for heavy metals) reported in the publications that have been cited in this review. The values reflect the effectiveness of the different types of adsorbents for removing various heavy metals from aqueous solution.

As can be seen from the entries in the Table, a number of alternative adsorbents match and even surpass CAC with regard to their ability to remove toxic heavy metals from aqueous solution. Zeolites, chitosan, waste slurry and lignin exhibit

9

outstanding adsorption capacities. Zeolites can remove Pb^{2+} over 5 times better than CAC. Chitosan is superior to the other adsorbents for the removal of Hg^{2+}, Ni^{2+} and Cu^{2+}. Waste slurry has very high adsorption capacities for Pb^{2+}, Cr^{6+} and Hg^{2+}, and lignin has the highest reported adsorption capacities for Pb^{2+} and Zn^{2+}.

Table 1.1. Summary of cost and adsorption capacities for various adsorbents.

Material	Typical cost[a] (US \$/kg)	Adsorption capacity (mg/g)						
		Pb^{2+}	Cr^{6+}	Cd^{2+}	Hg^{2+}	Zn^{2+}	Ni^{2+}	Cu^{2+}
CAC	20	30	145	146	65	2		
Zeolites	0.12	175	3.6	137		5.5	4.5	5.1
Chitosan	16	16.4	50	8.5	815	75	164	222
Clays	0.04-0.12	4.3	0.6	11.4		4.5		1.2
Natural oxides	0.05	230		72				
Fly ash	N.O.		2.9		2.8			
Slag	38/t	40	7.5					
Iron (III) oxide	N.O.		0.5					
Waste slurry	N.O.	1030	640		560			
Lignin	0.06	1865				95		
Sawdust	N.O.							13.8

[a]Source: Virta, R., USGS Mineral Information, US Geological Survey Mineral Commodity Summary, 2002.

N.O.: Not obtained

The actual cost of a "low-cost" material is an important consideration in choosing it as a candidate adsorbent for research and/or application. It is hardly surprising that zeolites have received a lot of attention, considering that their adsorption capacities compare favourably to those of CACs but cost 20 times cheaper.

Although chitosan has high adsorption capacities for most heavy metals, it is not really a low-cost material considering that it costs nearly as much as CACs. Lignin appears to offer the best value for money for Pb^{2+} and Zn^{2+}. Although the adsorption capacities of clays appear to be modest, their low cost increases their attraction. It must be emphasised that in certain circumstances local availability is a consideration that might supersede cost.

Both fly ash and slag have also been used to remove chemical species other than heavy metals from aqueous solution. Akgerman and Zardkoohi (1996) obtained adsorption capacities of 67, 20 and 22 mg/g fly ash for phenol, chlorophenol and 2,4-dichlorophenol, respectively. Fly ash has been used for removing radionuclides (Aptak et al, 1996), colour (Gupta et al, 1998), and F^- (Piekos and Paslawska, 1999) and from aqueous solution.

The use of slag for the removal of nutrients such as phosphates from aqueous solution has also been studied. Johansson and Gustafsson (2000) concluded that Ca-P precipitation (probably as the hydroxyapatite) was the major phosphate removal mechanism. This conclusion was reached on the basis that with adsorption it is difficult to explain the observation they made, that there was a concomitant decrease in the concentration of dissolved Ca when increasing concentrations of PO_4^{3-} solution were added to the slag. This is not consistent with the findings of either Yamada et al (1986) or Sakadevan and Bavor (1998). Both

11

studies concluded that adsorption was the dominant mechanism for phosphate sorption by slag. The latter study fitted the experimental data to the Langmuir adsorption isotherm and used it to calculate an adsorption capacity of 44.2 mg P/g slag.

It must be pointed out that Johansson and Gustafsson (2000) did not report any adsorption data, whilst the other 2 studies (Yamada et al,1986; Sakadevan and Bavor, 1998) did not explicitly consider the possible contribution of Ca-P precipitation.

1.2.   Fundamental chemistry

Various models may be used to describe adsorption at the solid-solution interface, depending on whether the adsorbate is present in a diluted or concentrated solution, and on the nature of the adsorbate (non-electrolyte or electrolyte) and adsorbent (non-porous particle, ion-exchanger or zeolite). The picture that is most amenable to simple analysis (Adamson, 1990) is that of a monolayer of adsorbate molecules on the adsorbate surface, with solute-solid interactions decaying very rapidly with distance.

1.2.1. Adsorption isotherms

The moles of solute adsorbed per gram of adsorbent, n_2^s, is generally a function of the equilibrium solute concentration, C_2, and temperature, T, for a given system, i.e.,

$$n_2^s = f(C_2, T) \tag{1.1}$$

The adsorption is a function of concentration at a given temperature, i.e.,

$$n_2^s = f_T(C_2) \tag{1.2}$$

Various functional forms for f, or adsorption isotherms, have been proposed.

1.2.1.1.   The Langmuir and Freundlich isotherms

The functions proposed by Langmuir (1918) and Freundlich (1926) are the two most commonly employed isotherms. Although originally proposed for the adsorption of gaseous molecules, the Langmuir and Freundlich isotherms may be adapted to adsorption from solution as shown below in equations (1.3) and (1.4), respectively (Adamson, 1990):

$$(1/x) = (1/[x_m K])(1/c) + (1/x_m) \tag{1.3}$$

$$\log x = \log K + (1/n) \log c \tag{1.4}$$

where x is the mass of solute adsorbed per mass of adsorbent, x_m is the limiting mass of solute that can be taken up per mass of adsorbent, K, n are constants, and c is the concentration of the solute in the solution that is in equilibrium with the adsorbent.

1.2.1.2. The Frumkin isotherm

The basis of the Langmuir isotherm is that the energy of an adsorbed particle is the same at any site on the adsorbent surface, and is independent of the presence or absence of neighbouring adsorbed molecules. This is referred to as ideal adsorption. Non-ideal systems are commonly fitted to the Freundlich isotherm, where the amount adsorbed keeps increasing as the concentration of the solute increases. However, the Freundlich isotherm, although recognising surface heterogeneity, does not account for appreciable surface repulsion (Hayward and Trapnell, 1964).

An isotherm that explicitly accounts for the existence of finite lateral interactions among adsorbate molecules is one suggested by the Russian electrochemist Frumkin (1925). The general expression of the Frumkin isotherm is (Bockris and Khan, 1993):

$$\beta x = [\Phi/(1-\Phi)]\cdot\exp -2\alpha\Phi \qquad (1.6)$$

14

where $\Phi = M/M_{ads}$, M is the mass of solute adsorbed at equilibrium when the molar fraction in the solution is x, M_{ads} is the maximum mass of solute adsorbed at equilibrium, and β is a constant that describes the adsorption equilibrium ($\beta = \exp(-\Delta G^0{}_{ads}/RT)$, where $\Delta G^0{}_{ads}$ represents the standard free energy of adsorption). The term α is the lateral interaction coefficient. In terms of molar concentration, equation (1.6) may be rewritten in logarithm form (Brina and De Battisti, 1987) as:

$$\upsilon = \log(\beta/55.55) + 2\alpha\Phi/2.303 \qquad (1.7)$$

where $\upsilon = \log[\Phi/(1-\Phi)c]$, and c is the concentration of the solute that is in equilibrium with the adsorbent.

1.2.2. Adsorption kinetics

The kinetics and the equilibria of adsorption are the two important physicochemical factors for the evaluation of the adsorption process. For adsorption equilibria parameter evaluation, the experimental data is fitted to the appropriate adsorption isotherm. Adsorption kinetics describes the solute uptake rate from solution, and is an important contributory factor to the efficiency of adsorption.

15

The adsorption of solute from solution can be considered as a reversible reaction with equilibrium being established between the liquid phase (A) and the solid phase (B), i.e.,

$$A \Leftrightarrow B \qquad (1.8)$$
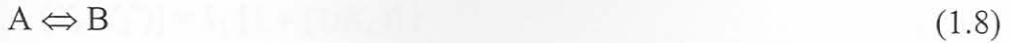
Assuming a first order reversible kinetics model, Bhattacharya and Venkobachar (1984) expressed the rate equation as:

$$dC_B/dt = - dC_A/dt = C_A{}^0(dX_A/dt) = k_1 C_A - k_2 C_B$$

$$= k_1(C_A{}^0 - C_A{}^0 X_A) - k_2(C_B{}^0 + C_A{}^0 X_A) \qquad (1.9)$$

where C_A and C_B are the concentrations of solute in solution and on the adsorbent, respectively, at time t, $C_A{}^0$ and $C_B{}^0$ are the initial concentrations of solute in solution and on adsorbent, respectively, X_A is the fractional conversion of solute at any time t, and k_1 and k_2 are the first order adsorption and desorption rate constants, respectively.

At equilibrium conditions $(dC_B/dt = dC_A/dt = 0)$ the rate equation in terms of equilibrium conversion is:

$$dX_A/dt = (k_1 + k_2)(X_A{}^e - X_A) \qquad (1.10)$$

16

where X_A^e is the fractional conversion of solute at equilibrium. Integration of equation 1.10 gives:

$$- \ln [1 - (X_A/X_A^e)] = k_1 [1 + (1/K_C)] t \qquad (1.11)$$

where K_C $(= k_1/k_2)$ is the equilibrium constant. Equation 1.11 can be rewritten in a different form as:

$$\ln [1 - U(t)] = - k' t \qquad (1.12)$$

where k' $(= k_1 + k_2)$ is the overall rate constant, and $U(t)$ $(=X_A/X_A^e)$ is the fractional attainment of equilibrium.

The overall rate constant k' (= the slope of the straight-line portion of the plot according to equation 1.12) can be correlated to diffusion coefficients as (Helfferich, 1962):

$$t_{\frac{1}{2}} = 0.03 \ r^2/D \qquad (1.13)$$

$$t_{\frac{1}{2}} = 0.23 \ r^2\delta \ C/(C^*D^*) \qquad (1.14)$$

where $t_{1/2}$ is the time at which $X/X_e = \frac{1}{2}$ (given by $(\ln 2)/k'$), r is the mean radius of adsorbent particles (assuming spherical geometry), D and D^* are the pore and film diffusion coefficients, respectively, C/C^* is the equilibrium loading of the adsorbent, and δ is the film thickness.

1.2.3. Estimation of adsorption capacity: Breakthrough curves

When a solution containing an adsorbate is passed through a fixed bed of a suitable adsorbent, the concentration of adsorbate in the effluent remains negligibly small until breakthrough occurs. Plotting effluent concentration versus effluent volume yields the breakthrough curve, as shown in Figure 1.1. *Breakthrough* is the term used to describe that point in the experiment (represented by V_E) after which there is a rapid, continuous increase in effluent concentration until the bed is exhausted.

For a fixed-bed unit operating at a steady liquor flow rate, and for which a symmetrical breakthrough S-curve has been obtained experimentally, the height of the mass transfer zone, h_Z, and the specific dynamic adsorption capacity, C_T, are given, respectively, by the relations (Michaels, 1952):

$$h_Z = h_T[\ V_Z/(V_T - 0.5\ V_Z)] \tag{1.15}$$

$$C_T = \int_0^{V_T} (X_0 - X)\, dV/m \tag{1.16}$$

18

where h_T is the bed height, V_T is the volume of effluent collected upon exhaustion of the bed, V_E is the volume of effluent collected up to breakthrough, $V_Z = V_T - V_E$, X_0 is the influent concentration, X is the effluent concentration, V is the effluent volume, and m is the mass of adsorbent.

Several workers (Kocirik et. al., 1982; Ko et. al., 2000; Chern and Chien, 2002) have used breakthrough curves to study and evaluate the sorption of various adsorbates on various adsorbents.
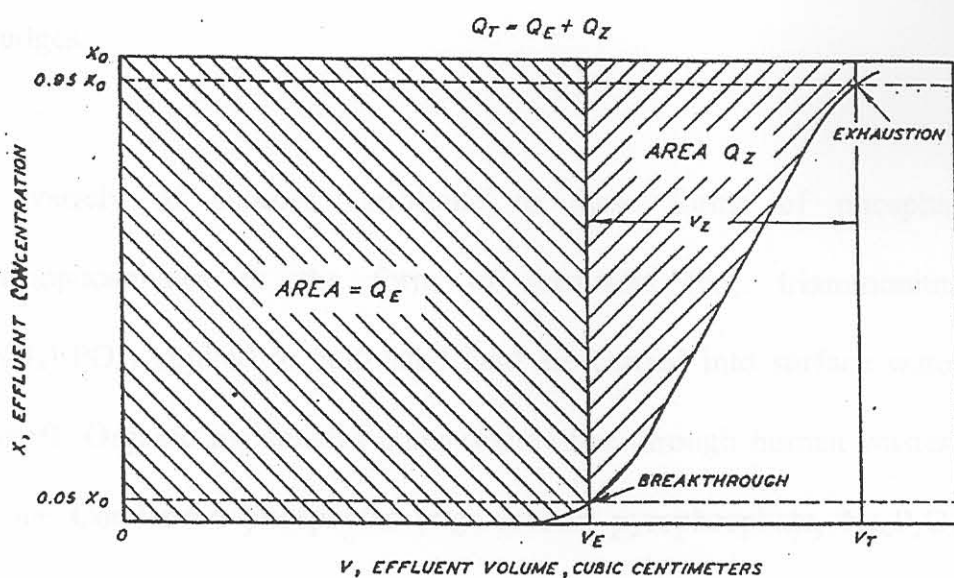
Figure 1.1. Idealised breakthrough curve for a fixed bed column (Michaels, 1952).

1.3. Phosphates in water

1.3.1. Forms and sources of phosphorus in water

Phosphorus occurs in natural waters and wastewater almost invariably as various forms of phosphates (Arnold, 1985). These are orthophosphates (PO_4^{3-}, HPO_4^{2-}, and PO_4^-), condensed phosphates (pyro-, meta-, and other polyphosphates, e.g. $P_2O_7^{4-}$, $P_3O_{10}^{5-}$, and $P_3O_9^{3-}$), and organically bound organic phosphates. They occur in solution, in particles, in aquatic organisms, in bottom sediments, and in biological sludges.

A variety of sources contribute to these forms of phosphate in water. Orthophosphates in the form of fertilisers (e.g. triammonium phosphate, $(NH_4)_3PO_4$) applied to cultivated land are carried into surface waters with storm runoff. Organic phosphates enter wastewater through human wastes, primarily as urine. Condensed phosphates (e.g. sodium pyrophosphate, $Na_4P_2O_7$ and sodium tripolyphosphate, $Na_5P_3O_{10}$) are used in the synthesis of commercial detergent formulations because they form soluble complexes with Ca^{2+} and Mg^{2+} ions in tap water, preventing the deposition of scum in the washing. These phosphates subsequently pass into the water used for laundering and cleaning (Sundstrom and Klei, 1979). Phosphates (e.g. Na_3PO_4) are also used extensively in the treatment of

boiler waters to remove hardness by precipitating Ca^{2+} and Mg^{2+} ions as the phosphates, preventing the formation of boiler scale, which can lead to the blocking of pipes.

1.3.2. Large-scale removal of phosphorus from wastewater and effluents

Eutrophication, the gradual increase in the levels of phosphorus, nitrogen, and other plant nutrients in an ageing aquatic ecosystem such as a lake, leads to an explosion in algae growth, which eventually results in a lack of light penetration and oxygen absorption that is necessary for underwater life (Britannica, 1989). Cultural or anthropogenic eutrophication, resulting from runoff containing excessive amounts of nutrients in the form of sewage, detergents, and fertilisers, is a well-known environmental concern. It is known that phosphorous is usually the limiting nutrient for the onset of eutrophication (Droste, 1997); therefore, the control of phosphorus concentrations in effluents is especially important.

Total phosphorus concentrations in raw wastewater are typically in the range of 4-10 mg/L, which must be reduced to 1 mg/L or less in order to meet environmental requirements (Eckenfelder, 1980). The majority of phosphorus compounds in wastewater are soluble, mostly orthophosphates (micro-organisms present in sewers slowly convert condensed phosphates into orthophosphates). They are not, therefore, adequately removed by plain sedimentation. Chemical precipitation and

21

microbiological treatment, usually in conjunction with each other, are the two commonly used processes for the large-scale removal of phosphate from wastewater.

Chemical agents used to precipitate phosphorus are compounds of calcium, iron, or aluminium, these being metals that form sparingly soluble salts with dissolved forms of phosphate. Examples of such coagulants are alum $(KAl(SO_4)_2 \cdot 12H_2O)$, $FeCl_3$, and lime, and the complex reactions involved may be simplified as (Droste, 1997):

$$3 \ KAl(SO_4)_2 \cdot 12H_2O + 4 \ PO_4^{3-} \Rightarrow 3 \ AlPO_4(s) + K_3PO_4 + 6 \ SO_4^{2-} + 12 \ H_2O \quad (1.17)$$

$$FeCl_3 + PO_4^{3-} \Rightarrow FePO_4(s) + 3 \ Cl^- \quad (1.18)$$

$$10 \ Ca^{2+} + 8 \ OH^- + 6 \ HPO_4^{2-} \Rightarrow Ca_{10}(OH)_2(PO_4)_6(s)(hydroxyapatite) + 6 \ H_2O \ (1.19)$$
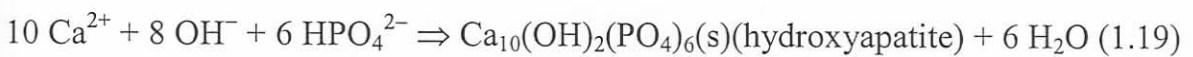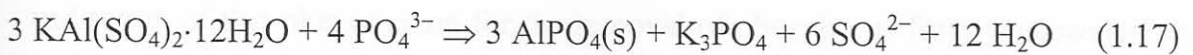
Apatites are highly insoluble, which makes lime the most efficient agent for phosphate precipitation. However, a high pH (ca 10) is required for apatite formation, and Ca^{2+} tends to consume additional lime and then precipitate as $CaCO_3$ in the presence of carbonate alkalinity:

$$Ca(OH)_2 + 2 \ HCO_3^- + 2 \ Ca^{2+} \Rightarrow 2 \ CaCO_3(s) + 2 \ H_2O \quad (1.20)$$
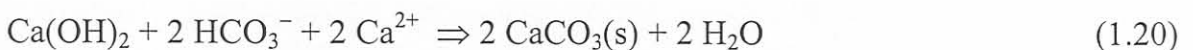
This means that very high doses of lime are required (Droste, 1997), which makes the process rather costly. The precipitates are subsequently physically removed by sedimentation, and the lime sludge produced may be dewatered and discarded or recalcined in a furnace to recover part of the lime.

When sludge containing certain microorganisms (e.g. Acinetobacter) is subjected to anaerobic conditions, phosphorus is released to solution; when the sludge is subsequently mixed with wastewater and then subjected to aerobic conditions, an immediate accumulation of phosphorus by the activated sludge occurs. Several workers (Bouck, 1978; Bark et. al., 1992; Rasmussen et. al., 1994) have studied the utilisation of this phenomenon for the removal of phosphorus from wastewater, and the process is used on a large scale.

CHAPTER 2

SORBENTS USED AND THE AIM OF THE STUDY

2.1. Fly ash

2.1.1. Production from the combustion of coal

Large quantities of pulverised coal are burned in coal-fired boilers in many parts of the world to raise steam from water, the steam then being used to drive turbines to produce electricity for domestic and industrial consumption. Fly ash is a by-product of this process of electric power generation.

Coal is formed by the decomposition of plant matter, without free access to air, under the influence of moisture, pressure and temperature (Vorres, 1979; Pettijohn, 1957). It is composed mainly of carbon, hydrogen and oxygen, with nitrogen and sulphur being lesser constituents. These elements account for the organic constituents of coal, mostly polycyclic aromatic hydrocarbons.

In addition, some mineral matter also becomes incorporated into coal during and after peat formation, the initial step of the coalification of plant matter. This includes the clay minerals (e.g. $[Al,Fe,Mg]_6[Si,Al]_4O_{10}[OH]_8$), quartz ($SiO_2$), feldspars ($KAlSi_3O_8$, $NaAlSi_3O_8$, $CaAl_2Si_2O_8$), garnets ($[R^{2+}]_3[R'^{3+}]_2[SiO_4]_3$; R= Ca,

24

Mg, Fe or Mn; R'= Al, Fe, Mn or Cr), kaolinite ($Al_4Si_4O_{10}[OH]_8$), calcite ($CaCO_3$) and pyrite (FeS_2) (Spackman et al., 1976; Nowacki, 1980). Smaller and trace amounts of many other elements are also present (Ray and Parker, 1977).

Two types of residual ash primarily result from the incombustible mineral constituents during the burning of coal. These are bottom ash, which is retained in the boiler as fused slag, and the fly ash, which leaves the furnace as dry ash carried in the flue gas (vapour). The bottom ash particles are much coarser than fly ash. The vapour is that part of the coal material which is volatilised during combustion.

The percentage of fly ash produced depends on the type of coal (lignite, anthracite, bituminous or sub-bituminous) and the type of boiler (and method of firing) used. The higher the ash fusion temperature of the coal, the lower the proportion of ash that is melted within the boiler and collects as bottom ash, and the higher the firing temperature in the boiler, the larger the proportion of bottom ash formed (Torrey, 1978). The electric utility industry generally uses three types of boilers, namely, dry-bottom boilers, wet-bottom boilers and cyclone furnaces (Babcock and Wilcox Co., 1978).

After leaving the combustion zone the ash particles are cooled rapidly (1500 °C to 200 °C in 4 seconds reported by Ray and Parker, 1977), leading to the formation of sub-micron particles from the inorganic vapours via nucleation and condensation on

25

existing particles. Ulrich et al. (1971 & 1976) proposed a mechanism to explain the growth in particle size. Finally, the ash is collected in a particulate control system, usually an electrostatic precipitator or a mechanical collector. The method of collection used also influences the characteristics of the final product.

In the year 2000, ca. 56.6 million metric tons of fly ash was produced in the United States alone (American Coal Ash Association, 2002). The corresponding figure for South Africa was 25 (Eskom 22, Sasol 3) million metric tons, the largest single source being the Lethabo power station near Vereeniging (Kruger, 2002).

2.1.2. Characterisation

2.1.2.1. Introduction

Fly ash is pozzolanic; that is, a siliceous and aluminous material which possesses little or no cementitious value in itself but will react with lime in the presence of water at ambient temperature to form compounds with cementitious properties (Diamond, 1981).

The hydraulicity that results from pozzolanic reactions is due to the formation of solid and water-insoluble masses consisting of hydrated compounds with C-S-H

bonds, such as tri-calcium silicate hydrate and tetra-calcium aluminate hydrate, from the reactions of reactive silica and alumina with lime (Turriziani, 1964):

$$2 S + 3 CH + 4 H \rightarrow C_3S_2H_4 \tag{2.1}$$

$$A + 4 CH + 15 H \rightarrow C_4AH_{19} \tag{2.2}$$
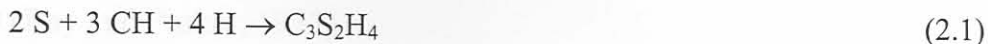
Because of the wide range of composition and characteristics of fly ashes, they are classified into two general types: Class F and Class C. Class F fly ash is produced from anthracite or bituminous coal and contains less than ca. 10 % CaO. Class C fly ash is produced from lignite or sub-bituminous coal, may contain as high as 30 or 40 % CaO, and possesses some cementitious properties in addition to being pozzolanic. Characterisation of fly ash requires the knowledge of chemical parameters such as mineralogical and chemical composition, as well as physical parameters such as fineness (granulometry, particle size distribution, and specific surface area) and density.

2.1.2.2. Mineralogical and chemical composition

The mineralogical and chemical composition of a fly ash depends on the characteristics and composition of the coal burned in the power plant. Due to the rapid cooling already mentioned in Section 2.1.1, the main (ca. 50-90 %) phase of fly ash is mineral matter in the form of glassy particles. The minor phase occurs in

the form of crystalline phases, together with particles of carbon resulting from unburned coal. The most common crystalline phases in Class F fly ash is magnetite (Fe_3O_4), hematite (Fe_2O_3), quartz (SiO_2), mullite $(Al_6Si_2O_{13})$, anhydrite $(CaSO_4)$, and free CaO (Ray and Parker, 1977).

Many workers have used X-ray diffraction (XRD) and light microscopic techniques such as Scanning Electron Microscopy (SEM) to identify and determine the quantities of glassy and other phases present in fly ash (Luke, 1961; Adams, 1980; Joshi et al., 1985). Watt and Thorne (1965) found by SEM and XRD examinations that most fly ashes, after extraction with water, contained mainly four crystalline phases: quartz, mullite, hematite, and magnetite. From the analyses for these minerals by X-ray methods and the chemically determined carbon content, the glass content was determined by difference, giving the results in Table 2.1. Then the composition of the glass phase was calculated from oxide chemical analysis, giving the results in Table 2.2.

Table 2.1 Mineralogical analysis of fly ash

Constituent	Quartz	Mullite	Hematite	Magnetite	Carbon	Glass
Mass percentage	2.2	6.5	1.1	0.8	0.9	88

Table 2.2 Calculated mean composition of glassy components of fly ash

Component	SiO_2	Al_2O_3	Fe_2O_3	CaO	MgO	Na_2O	K_2O	TiO_2
Mass percentage	52	27	10	0.8	2.4	1.8	4.6	1.1

The pozzolanicity is due to the glass phase; the crystalline phases influence the amount and composition of the glass phase, but they are not pozzolanic. Carbon is the most important component of ignition loss (LOI, 1000 °C). For cement and concrete applications low carbon content is desirable; this decreases the amount of water required to obtain a paste of normal consistency and produces higher strength concrete.

2.1.2.3. Physical properties

Fly ash consists of fine, powdery particles that are predominantly spherical in nature. The carbonaceous material in fly ash is composed of angular particles. The material usually has a light greyish colour, appearing darker as the Fe_2O_3 (brown) and unburned carbon (black) contents increase. The most important physical parameters that are determined for fly ash are density and fineness.

The mean density of the solid phases can be measured after grinding the ash to high fineness (ca. 1200 m^2/kg) to eliminate the bubbles and voids in agglomerates. Such values range from ca. 2.65 to 2.80 g/cm^3 (Jarrige, 1971). The bulk density

varies greatly with packing; without close compaction, values as low as 0.54 g/cm^3 have been reported (Berry and Malhotra, 1978).

Three measures of fineness are used, namely, granulometry, particle size distribution and specific surface area (Helmuth, 1987). Granulometry (ASTM 618) involves dry or wet sieve analysis; it measures the percentages retained on various size sieves. For fly ash to be used as a mineral additive in Portland cement concrete, the residue on a 45-μm sieve should not be more than 34 % (ASTM 618-87). For South African fly ashes this is usually less than 12 % (Mantel, 1991). A cumulative particle size distribution curve shows the percentage finer (or coarser) than any particular size over the entire range of sizes. Fly ash particles typically range in size from ca. 2 to over 300 μm, with mean particle diameters of the order of 20 μm.

Specific surface area is determined by the Blaine air permeability method (ASTM C204), the BET technique, where nitrogen adsorption isotherms are measured, the Wagner turbidimeter method (ASTM C115), and the hydrometer method (ASTM D422). Unfortunately, these standard methods yield widely different values for the same fly ash sample (Cabrera and Gray, 1973), indicating significant systematic errors. Automated particle size analysis instruments are also available which use

the scattering of a laser beam by the particles to measure parameters such as specific surface area, mean particle diameter, and particle size distribution.

2.1.3. Utilisation

Due to its pozzolanic reactivity with lime (a hydration product of Portland cement), fly ash has been used extensively in the cement and concrete industry, as an admixture, as a raw feed material in the manufacture of Portland cement, and as a component of Portland-pozzolan blended cement. The largest single use of fly ash is as a mineral admixture in Portland cement mortar and concrete. Reasons for fly ash addition include economy and enhancement of certain properties of fresh concrete and hardened concrete, as mentioned later in Section 2.4.

Other important uses of fly ash include use as a structural fill material, stabilised bases or sub-bases for road and pavement substructure, flowable fill, mineral filler in asphalt paving mixtures, and for waste stabilisation and solidification.

Table 2.3 lists figures for the production and use of fly ash for the year 2000 in the U.S. (ACAA, 2000). The corresponding figures for South Africa were 25 million metric tons produced and 1.2 (0.9 for cement and concrete, 0.3 for bricks and blocks) million tons used.

31

Table 2.3. Production and use of coal fly ash in 2000 in the USA

Use	
Cement/Concrete/Grout	9 527 551
Raw feed for cement clinker	1 020 520
Flowable fill	627 008
Structural fills	2 349 949
Road base/Sub-base	1 086 975
Soil modification	100 706
Mineral filler	107 110
Snow and ice control	2 768
Mining applications	1 036 382
Waste stabilization	1 787 649
Agriculture	12 581
Miscellaneous	410 018
Total usage	18 069 217
Total production	56 649 358
Percentage usage	31.9 %

2.1.4. Disposal: environmental considerations

The burning of coal for electricity production around the world generates enormous quantities of solid wastes, in the form of fly ash, flue gas de-sulphurisation (FGD) material, bottom ash and boiler slag. In the year 2000, some 97.2 million metric tons of coal conversion solid wastes was generated in the United States alone; less that 30 % of this was put to practical use, the rest being land-filled or stockpiled near power stations ACAA, 2000). South Africa (Eskom and Sasol) generated 34 million metric tons of solid waste from coal combustion

32

(Kruger, 2002). A common method of disposal is placement of the solid wastes in worked surface mines and back filling with overburden. The main environmental concern associated with the landfilling of fly ash is its leachability in the presence of groundwater flowing in the surrounding area, especially the leaching of potentially toxic trace metals.

Although the levels of toxic metals in the leachates studied by several workers reportedly falls within government regulated standards, research is ongoing. Groenewold et al. (1985) found that the levels of As, Se, Mo and Cd in a fly ash disposal site leachate under study did not pose long-term environmental problems. This was attributed to the self-cementing property of buried fly ash, which leads to decreased leachability over time. Similarly, Garcez and Tittlebaum (1985) reported a decrease in the concentration of Al, As and Mo in the leachate after fly ash was stabilised with soil for use as a road base.

2.2. Slag

2.2.1. Origin

Iron ore, scrap iron, and fluxes (limestone and dolomite) are charged into a blast furnace, along with coke for fuel in the manufacturing of iron. The coke undergoes combustion to produce carbon monoxide, which reduces the iron ore to a molten iron product. Slag is a non-metallic by-product of the process, formed by the

33

combination of the earthy (silica and alumina) constituents of the iron ore with lime and magnesia in the flux. About 14 million metric tons of blast furnace slag is produced annually in the United States (USDI, 1993).

The slag, which floats on the molten iron at the bottom, is tapped from the blast furnace as a molten stream (ca. 1450 °C). Widely different forms of slag are produced depending on the method used to cool the molten slag. These include air-cooled slag, expanded or foamed slag, pelletised slag, and granulated slag.

Granulated slag is produced when the molten slag is chilled, by spraying jets of water on the red-hot liquid. The slag is cooled so rapidly that crystallisation is prevented and it solidifies as a glass (Lea, 1970). The quenching also breaks up the material into small particles. Ground (to ca. 350 m^2/kg) granulated blast furnace slag (GGBFS) is sold in South Africa under the trade name Slagment (Mantel, 1991). This is the form of slag used for this study.

2.2.2. Properties

GGBFS is a latent hydraulic binder, that is, it hardens slowly in water by itself to form cementitious hydration products, but on addition of an activator (e.g. lime) its rate of hardening is greatly enhanced. The latency is due to the slow release of

calcium ions out of the glass and the subsequent formation of a protective layer of hydrates.

The composition of slag can vary over a wide range depending on the nature of the iron ore, the composition of the flux, the coke consumption, and the kind of iron being manufactured (Lea, 1970). The four major constituents are lime, silica, alumina and magnesia, with sulphur in the form of sulphide, and ferrous and manganese oxides as minor components. Table 2.4 shows the oxide chemical analysis of a typical South African slag (Mantel, 1991).

Table 2.4 Composition of a typical South African slag

Constituent	Mass percentage
SiO_2	36.6
Al_2O_3	13.2
Fe_2O_3	0.6
Mn_2O_3	1.2
TiO_2	1.9
CaO	33.0
MgO	10.7
SO_3	2.5
Na_2O	0.2
K_2O	0.9
LOI	0.6

There can be considerable variability in the physical and mechanical properties of blast furnace slag, depending on the iron production process. Emery (1980) reported specific gravity and compacted unit weight values of 2.0-2.5 and 1120-

1360 kg/m^3, respectively, for an air-cooled blast furnace slag (ACBFS); this is the slag type that is most commonly used as an aggregate material. This is due to favourable mechanical properties such as good abrasion resistance, good soundness characteristics, and high bearing strength (Noureldin, 1990).

2.2.3. Utilisation

GBFS is used as a mineral admixture for Portland cement concrete, as well as a hydraulic cement when ground to cement fineness (ACI, 1990). The ground slag (GGBFS) is also used to produce slag/Portland cement blends, either by being introduced into and milled with the cement feedstock, or blended in after the cement clinker is ground to its required fineness (AASHTO, 1986). ACBFS has been used as an aggregate in Portland cement concrete, asphalt concrete, and road bases. Almost all the blast furnace slag generated in the United States is reportedly utilised, with less than 10 percent disposed of in landfills (RMRC, 2002).

2.3. Ordinary Portland cement (OPC)

2.3.1. Manufacture

The processes involved in the manufacture of Portland Cement have been described in several publications (Mantel, 1991; PCA, 2002). The sequence of processes may be represented as follows:

36

Quarrying $\Rightarrow$ Raw Milling $\Rightarrow$ Blending $\Rightarrow$ Burning $\Rightarrow$ Cement Milling

Most plants depend on a nearby quarry for the required calcareous- and argillaceous raw materials; commonly limestone (for calcium oxide) coupled with smaller quantities of clay or shale and sand (for silica, alumina, and iron oxide). Lumps of rock blasted from the quarry face are crushed down to particles smaller than 19 mm and then transported to the raw mill, where the material is ground to a fine powder. Layers of the various raw materials are laid down alternately in a blending silo and blended in the proper proportion (Ca: Si: Al: Fe). The meal then goes into a 4-stage pre-heater kiln, where they are heated to 800-900 °C by hot gases produced by burning finely ground coal.

As the temperature increases in the kiln, Al_2O_3 and Fe_2O_3 start to react with CaO to form molten calcium aluminates (mainly C_3A) and calcium aluminoferrite (C_4AF, ferrite). Then silicate reactions start to take place as the temperature rises further (up to 1500 °C in the burning zone), solid CaO and SiO_2 reacting in the liquid melt to form di-calcium silicate (C_2S, belite) and tri-calcium silicate (C_3S, alite). The material from the kiln, now called clinker, is air-cooled, a small quantity of gypsum ($CaSO_4 \cdot 2H_2O$) added (for set-retardation), then proceeds to the cement mill. Here, steel balls in a rotating steel tube grind the clinker to a fine powder with specific surface area in the range 300-350 m^2/kg, known as OPC

37

(S.A. CEM I 42,5; U.S.A. ASTM Type I).

2.3.2. Properties

Portland cements are hydraulic cements composed primarily of hydraulic calcium silicates. The main properties of interest of OPC may be divided into three groups, namely, composition- chemical analysis and compound composition, fineness-density and specific surface area, and quality- setting time, heat of hydration, compressive strength, workability, and soundness of the OPC-containing concrete mix.

The constitution of Portland cement has been studied by phase equilibria, optical microscopy and X-ray examination, and chemical analysis. Table 2.5 shows the chemical analysis of a typical OPC (Mantel, 1991), as well as the compound composition of the alite (C_3S), belite (C_2S), aluminate (C_3A) and ferrite (C_4AF) major phases.

Table 2.5. Constitution of a typical OPC

Constituent	Mass %
SiO_2	22.9
Al_2O_3	4.2
Fe_2O_3	3.8
Mn_2O_3	0.4
TiO_2	--
CaO	65.0
MgO	3.3
P_2O_5	--
SO_3	0.2
Na_2O	0.1
K_2O	0.6
LOI	--
C_3S	52.0
C_2S	26.0
C_3A	4.0
C_4AF	12.9

The most important property of OPC is the hydration reactions it undergoes when mixed with water, which leads to strength development in the concrete mix. The development of strength comes from the growth of a solid 3-D hydrated calcium silicate crystalline network, C-S-H, mainly from the hydration of C_3S. The reactions involved, which are very complex, may be approximated as (Mantel, 1991):

$$C_3S + 6\ H \rightarrow C_3S_2H_3 + 3\ CH \qquad (2.3)$$

$$2\ C_2S + 4\ H \rightarrow C_3S_2H_3 + CH \qquad (2.4)$$

39

Hydrated calcium aluminate also contributes to early strength, but the contribution of hydrated calcium aluminoferrite (hydrogarnet) is very small (due to the much lower heat of hydration involved):

$$C_3A + CH + 18\ H \rightarrow C_4AH_{19} \tag{2.5}$$

$$C_4AF + 2\ CH + 10\ H \rightarrow C_6AFH_{12} \tag{2.6}$$
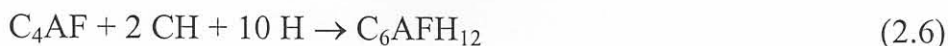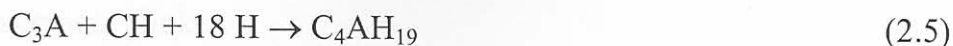
The reactions above are preceded by a period of slow reaction (the induction period) during which a protective film of micro-crystalline calcium sulphoaluminate (ettringite) forms around the individual C_3A crystals from the reaction of gypsum with the initial hydration products of C_3A:

$$C_3A + 3\ C\underline{S}H_2 + 29\ H \rightarrow C_3A3(C\underline{S})H_{35} \tag{2.7}$$

2.3.3. Utilisation

The use of Portland cement concrete in the construction of buildings, bridges, dams, pavements, etc. is well known. OPC has also been put to some lesser-known innovative uses. For example, it has recently been used in the environmental clean-up of old industrial sites in the United States (PCA, 2002) by binding waste (contaminated soil or sediment) for solidification and stabilisation.

2.4. OPC/Fly ash and OPC/Slag blends

As already mentioned in Sections 2.1.3 and 2.2.3, an important use of the by-product materials fly ash and slag is to produce blended cements, usually by inter-grinding with cement clinker.

The chief reason for the use of slag and fly ash as partial Portland cement replacement is to take advantage of the energy already invested in the slag making process. The production of Portland cement is an energy intensive process. In South Africa (Mantel, 1991), for example, ca. 15 tonnes of coal has to be burnt in order to produce 100 tonnes of clinker. Grinding slag for cement replacement, on the other hand, requires only about 25 percent of the energy required to manufacture Portland cement (RMRC, 2002).

In addition to the energy savings, the use of these blended cements has been found to improve the workability and durability of concrete. Slag and fly ash refine the pore structure by reacting with the CH liberated in the hydration of the C_3S and C_2S in the Portland cement (See equations 2.3 and 2.4), thereby forming additional or secondary C-S-H within the framework of the hardened cement paste. The improved durability has been largely attributed to reduced permeability (and reduced ion diffusion) that results from this pore structure refinement (Hooton, 1986). In addition, Montemor et al., reported improvements in concrete

carbonation rates (1995), passivation (1998), as well as induction and corrosion rates (2000).

2.5. The aim of the study

This study was focused on using fundamental research techniques to investigate the feasibility of utilizing OPC and its blends with slag and fly ash for phosphate removal from aqueous solution. This would involve establishing whether these materials remove significant amounts of phosphate and investigating the factors that can be expected to influence the rate and efficiency of phosphate removal. Such factors would include the particle size of the solid material, concentration of dissolved phosphate, contact time, pH and temperature. Adsorption capacities would also be measured as a measure for quantifying the capabilities of these materials for immobilizing dissolved phosphate.

OPC was considered to be a good candidate for the sorption of phosphate due to its fineness and porosity, coupled with the large amount of Ca it contains (elements such as Al, Mg, Mn, Fe and Ti are also present and can be expected to contribute). It was logical to extend the study to OPC/slag and OPC/fly ash (and slag and fly ash) because these blends are utilized for certain applications in the construction industry to take advantage of some important desirable properties that the industrial by-products slag and fly ash impart to the concrete.

42

If these materials do remove phosphate from aqueous solution, it would definitely add value to the process if the spent phosphate medium could be utilized in some beneficial way. To explore this, it was also envisaged that bricks would be manufactured from the materials after exposure to phosphate-containing water. Their compressive strengths would then be measured in order to assess whether they meet the national standard for strength that is required for masonry units.

The study was also motivated by certain economic and environmental considerations.

Firstly, commercial activated carbon recommended for liquid phase adsorption systems is marketed in South Africa at a cost of 73 euros for a packet of 2 kg (Aldrich, 2003-2004), which translates to more than R 300/kg. On the other hand, a 50 kg bag of OPC costs about R 30; this makes OPC a potential low cost alternative for sorption studies. Blending it with slag or fly ash leads to a further reduction in cost, as both are by-products.

Secondly, there is an on-going search to find effective ways to utilise the huge amounts of fly ash and slag that is land filled or stockpiled every year. In the year 2000, only 18 out of the over 56 million metric tons of fly ash generated in the United States were utilised, i.e. 32 % usage (see Table 2.3); for South Africa the percent usage was even lower, at 1.2 out of 25 million metric tons production, i.e.

less than 5 % usage (Kruger, 2002). Slag presents somewhat less of a disposal problem; about 10 % of the 14 million metric tons of blast furnace slag produced annually in the United States is disposed of in landfills (RMRC, 2002).

Thirdly, if OPC, OPC/slag and OPC/fly ash do remove phosphate from aqueous solution then these materials, traditionally used almost exclusively in the construction industry, may have a potential use in reducing the effects of the well-known environmental problem of eutrophication, caused by excessive amounts of phosphate (and nitrate) in bodies of water.

CHAPTER 3

PRINCIPAL INSTRUMENTAL TECHNIQUES USED

3.1. Particle size analysis by FDPA

3.1.1. Theory

Particle size distribution in fly ash (Goodwin and Mitchner, 1989) and powders produced by grinding processes (Washington, 1992) fit a log-normal distribution. The log-normal distribution is given by (Allen, 1974):

$$y = [1/(\sigma_z \sqrt{2\pi})] \exp [-(z-\bar{z})^2/2\sigma_z^2] \qquad (3.1)$$

where $y = d\Phi/dz$, Φ is the number, surface or weight distribution, $z = \ln D$, D represents the individual particle sizes, σ_z is the standard deviation of z, and $\bar{z}$ is the mean of the distribution (from which the mean particle size $\bar{D}$ can be calculated).

When a particle scatters light, the measured scattered light intensity may be related to the particle size; several theories are used to describe this relationship. These include the Lorentz-Mie theory (van de Hulst, 1957), the Generalised Lorentz-Mie

45

theory (Gouesbet et al., 1991), Geometric optics (Borhen and Huffman, 1983) and Fraunhofer diffraction.

Fraunhofer diffraction theory represents the large particle limit of the Lorentz-Mie theory for scattered light in the near forward direction. For visible incident laser light (e.g. $\lambda = 0.6328$ μm) in the near forward direction (scattering angles $\theta < 11°$) the particle size distribution may be related to the particle diameter in the 1-200 μm size range ($D > 10$ λ/π) (Bayvel and Jones, 1981). Under these conditions, diffraction (termed *Fraunhofer* diffraction) predominates over reflection and refraction, and the particle size distribution is independent of the optical properties of the sample (e.g. refractive index). The instrumental technique of Fraunhofer Diffraction Pattern Analysis (FDPA) was first introduced by Swithenbank et al. in 1977.

For a sample consisting of an ensemble of particles suspended (polydispersed) in a liquid or gas, the composite diffraction pattern produced is described mathematically by (Hirleman et al., 1984):

$$I(\theta) = I_{inc} \int_0^\infty (\pi^2 D^4/16\lambda^2)\,[2J_1(\chi)\,/(\chi)]^2\,n(D)\,d(D) \qquad (3.2)$$

46

where $I(\theta)$ is the scattered intensity at the angle θ measured from the laser beam, I_{inc} is the intensity of the incident beam, $n(D)$ is the particle size (number) distribution, and $n(D)$ $d(D)$ is the number of particles with sizes between D and $D+dD$.

In the Malvern instrument for FDPA the detector consists of a series of concentric rings. The energy within any detector element of inner radius s_1 and outer radius s_2 is given by (Annapragada and Adjei, 1996):

$$E(s_1, s_2) = \int_0^\infty A(D)[(J_0^2 + J_1^2)\,|\,s_1 - (J_0^2 + J_1^2)\,|\,s_2]\,d(D) \qquad (3.3)$$

where $J_n\,|\,s_i = J_n\,(\pi D s_i/\lambda)$ is the Bessel function of the n th order and first kind with argument $\pi D s_i/\lambda$, and $A(D)$ is the area fraction distribution of the particles in the sample.

Each of the detector elements exhibits a measurable response (usually a voltage) that is directly proportional to the incident energy:

$$V(s_1, s_2) = c'(s_1, s_2)\,E(s_1, s_2) \qquad (3.4)$$

where $c'(s_1, s_2)$ is a proportionality constant that can be obtained by calibrating the instrument. To obtain the actual particle size distribution the instrument must

incorporate some method (usually a software algorithm for numerical minimization) to invert the relationship between the scattered intensity pattern and the size distribution. Bayvel and Jones (1981) and Knight et al. (1991) have described their formulation of such methods.

3.1.2. Optical set-up

FDPA instrumentation, such as the Malvern Mastersizer used for this study, is based on a combination of optical analog and digital microprocessor computation. Figure 3.1 (a) shows the general optical set-up of a laser diffraction-based sizing system, and the diffraction set-up is shown in greater detail in Figure 3.1 (b).

The sample is dispersed in a suitable liquid or gas medium. In the Malvern instrument the light source comprises a 1 mW He-Ne laser (Allen, 1974). The laser is passed through the sample and the diffraction pattern produced is refracted by a Fourier transform lens and then focused onto a multi-element detector. The angle of incidence of scattered light on a Fourier lens corresponds to a particular annular position in the focal plane of the lens, regardless of the actual position of the scattering particle.
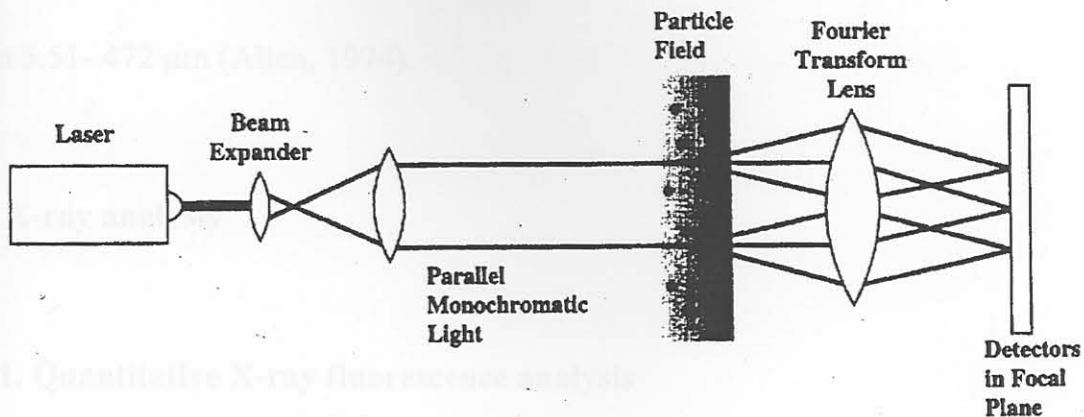
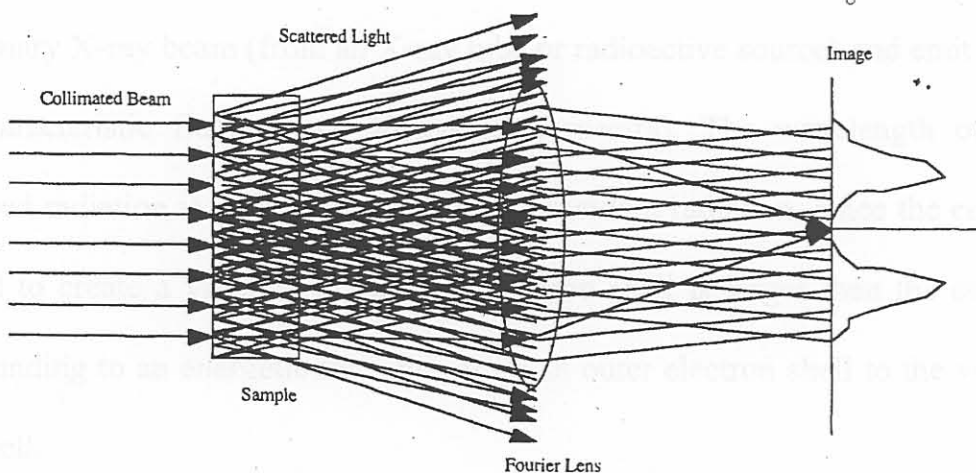Figure 3.1 (a). Optical set-up for FDPA (Black et al., 1996).

Figure 3.1 (b). Typical Fraunhofer diffraction set-up (Annapragada and Adjei, 1996).

The position of the maximum in the diffraction pattern for a given particle is determined by size so that the light intensities at different radii from the optical axis are size-dependent. The photodiode array detector in a Malvern instrument consists of a series of 31 semi-circular concentric annular detectors positioned at

49

the maxima of certain diffraction patterns, typically rings with diameters ranging from 5.51- 472 μm (Allen, 1974).

3.2. X-ray analysis

3.2.1. Quantitative X-ray fluorescence analysis

3.2.1.1. Theory

In X-ray fluorescence (XRF) the elements in the sample are excited by absorption of a primary X-ray beam (from an X-ray tube or radioactive source) and emit their own characteristic fluorescence X-rays (line spectra). The wavelength of the fluoresced radiation is greater than that of the incident radiation, since the energy required to create a vacancy in an inner electron shell is larger than the energy corresponding to an energetic transition from an outer electron shell to the vacant inner shell.

The intensity of the fluorescent radiation is directly proportional to the concentration of the fluorescing substance in the sample, and is also influenced by the amount of incident radiation absorbed by the sample as well as the portion of the fluorescent radiation which can be self-absorbed by the sample.

Typically, the incident radiation only penetrates a small distance relative to the thickness of the sample. The intensity I of the fluoresced radiation is given (Campbell, 1978) by:

$$I = kW/(\mu_i + \mu_f) \qquad\qquad (3.5)$$

where k is a proportionality constant, W is the weight fraction of the analysed element, and μ_i and μ_f are the averaged linear absorptive coefficients for the *whole* sample at the wavelength of the incident and fluorescent radiation, respectively. I is independent of the distance penetrated into the sample since all of the incident radiation is absorbed.

If a sample x and a standard s are analysed under the same conditions, then the concentration of analyte in the sample can be calculated from:

$$C_x = C_s \,(I_x/I_s) \qquad\qquad (3.6)$$

It is important to note that equation 3.10 is only useful if the sample and standard have similar composition. Generally, significant errors can occur in quantitative XRF analysis unless steps are taken to correct for matrix effects.

3.2.1.2. Instrumentation

There are two main types of XRF spectrometers in use, namely, wavelength-dispersive instruments, which use crystals to disperse the component wavelengths of the fluorescent radiation, and energy-dispersive instruments, which use electronic gates in the output circuit of the detector to discriminate between incident radiation of different wavelengths.

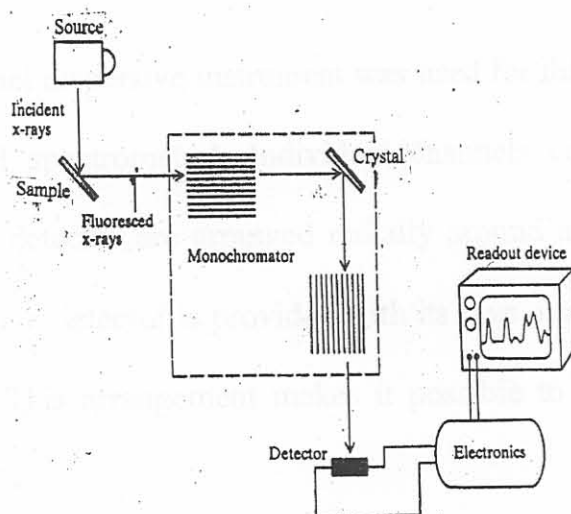A block diagram of a wavelength-dispersive instrument is shown in Figure 3.2.

Figure 3.2. Diagram of a wavelength-dispersive XRF spectrometer (Braun, 1987).

The source is usually an X-ray tube, with a Cr or W target for long and short wavelength analysis, respectively. The sample can be solid, liquid or gas. The crystal is used to render the fluoresced radiation monochromatic by Bragg

reflection (see Section 3.2.4.1.) prior to being measured with the detector. The instrument is equipped with a detector that converts radiant energy into an electrical signal. Three types of detectors are commonly used: gas-filled detectors, scintillation counters, and semiconductor detectors (Campbell, 1978).

The detector is usually operated as a photon counter in which the individual pulse of electricity produced by a quantum of radiation is counted, and the power of the beam is recorded digitally as number of counts per unit time. The electronics amplify the pulses and select a narrow range of pulse heights for display.

A multi-channel dispersive instrument was used for this study (Figure 3.2 shows a single-channel spectrometer). Individual channels consisting of an appropriate crystal and a detector are arranged radially around an X-ray source and sample holder, and each detector is provided with its own amplifier, pulse-height selector and counter. This arrangement makes it possible to determine several elements simultaneously.

3.2.2. Qualitative X-ray diffraction analysis

3.2.2.1. Theory: Bragg's law

Bragg's law in 3-dimensional reciprocal space is given (for first-order reflections, $n = 1$) by (Stout and Jensen, 1989):

$$\sin \theta = \lambda/(2d_{hkl}) = \lambda/[2(h^2a^{*2} + k^2b^{*2} + l^2c^{*2} + 2hka^*b^*\cos \gamma^*$$

$$+ 2hla^*c^*\cos \beta^* + 2klb^*c^*\cos \alpha^*)^{1/2}] \qquad (3.7)$$

where λ is the wavelength of the incident X-radiation, θ is the scattering angle, d_{hkl} is the perpendicular distance between direct lattice planes of the set with Miller indices (hkl), a^*, b^* and c^* are the mutually perpendicular axes of the reciprocal lattice, and α^*, β^* and γ^* are the angles between the axes of the reciprocal lattice.

It is evident from Bragg's law that, in principle, the interplanar spacing (and hence the identity of the crystal structure) can be determined from the measured diffraction angle if the wavelength of the incident X-ray radiation is known. The basis of qualitative XRD analysis is that an X-ray diffraction pattern is unique for each crystalline substance. Therefore, chemical identity can be assumed if an exact match can be found between the pattern of an unknown and that of an authentic sample.

3.2.4.2. Instrumentation

A diagram of a modern instrument for XRD analysis, such as the one used for this study, is shown in Figure 3.3.
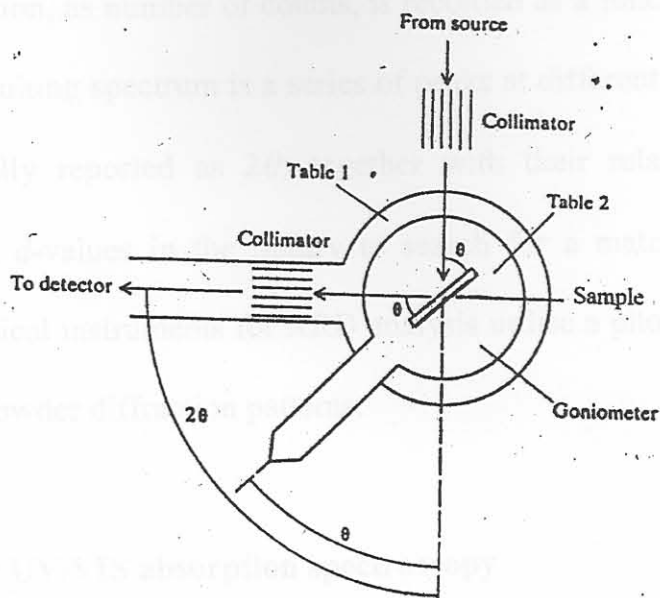
Figure 3.3. Set-up for XRD analysis (Braun, 1987).

The sample is used in the form of a fine homogeneous powder. Collimated radiation from an X-ray tube is reflected from the sample and passes through the exit collimator into the detector, which is usually a scintillation counter. The wavelength of radiation entering the detector is altered by simultaneously rotating the sample, exit collimator and detector relative to the incident radiation. A goniometer is used for this rotation. When the sample is rotated through an angle θ, the exit collimator and detector must be rotated through 2θ in order to maintain alignment. Two separate tables are used to achieve this.

Powdering the sample produces an enormous number of small crystallites oriented in every possible direction, so that a significant number will satisfy the Bragg condition for reflection from all possible interplanar spacing. The intensity of

diffracted radiation, as number of counts, is recorded as a function of the angle of rotation; the resulting spectrum is a series of peaks at different angles. These peak positions (usually reported as 2θ) together with their relative intensities are correlated with d-values in the library to search for a match for identification purposes. Classical instruments for XRD analysis utilise a photographic technique for recording powder diffraction patterns.

3.3. Molecular UV/VIS absorption spectroscopy

3.3.1. Theory: The Bouguer-Lambert-Beer (BLB) law

The BLB law is a statement to the effect that the absorbance A of a solution is directly proportional to the path length b through the solution and the concentration c of the absorbing species:

$$A = \varepsilon_\lambda bc \tag{3.8}$$

where ε_λ is a wavelength-dependent proportionality constant. Absorption of UV/VIS radiation (ca. 200-800 nm) generally results from excitation of bonding electrons. For the analysis of phosphate ion the most important transitions types are expected to be $n \rightarrow \pi^*$ and $\pi \rightarrow \pi^*$. For quantitative analysis ε_λ is usually

evaluated from the slope of the linear calibration plot of A versus c (concentration of analyte in several laboratory standard solutions) using regression analysis.

3.3.2. Instrumentation

A schematic diagram of the optical system of the UV/VIS instrument used for this study, a Shimadzu UV-150 digital double-beam spectrophotometer, is shown in Figure 3.4 (a). The light beam is selected between the W (325–1000 nm) and D_2 (200–325 nm) lamps for the visible and ultraviolet regions respectively by the light source selecting mirror M_1, forms an image on the entrance slit S_1, and is led into the monochromator. The Czerny-Turner grating monochromator consists of S_1, M_2, G, M_3, M_4 and S_2, and a monochromatic light with 5 nm band width is taken out from the exit slit S_2. The monochromatic light is divided into the sample and reference beams by the half-mirror M_6, passes through the cell holder and strikes the silicon photocell detector.

Figure 3.4 (b) shows the electronic system of the instrument. The difference between the photo currents i_S from the sample detector and i_R from the reference detector is taken by the subtracter after individual logarithmic conversion. The output from the subtracter is multiplied by a factor k to become $-k \log (i_S/i_R)$, where k is chosen in such a way that an output voltage of 1 V corresponds to a unit

57
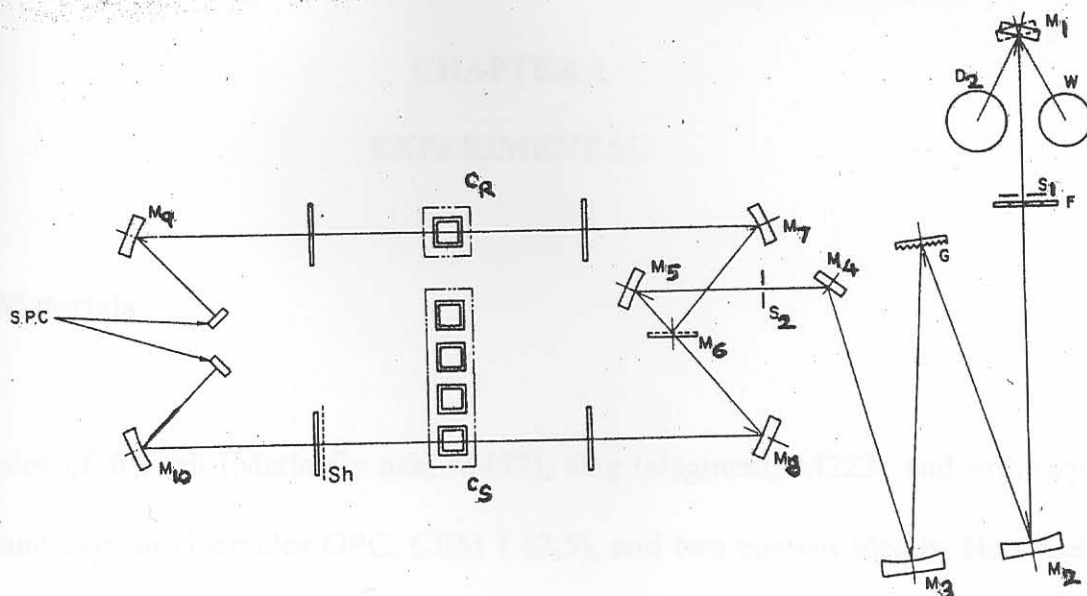
W:	Tungsten lamp	G:	Diffraction Grating
D$_2$:	Deuterium lamp	F:	Filters
M$_1$~M$_{10}$	Mirrors	C$_R$, C$_S$:	Reference cell, Sample cell
M$_6$:	Half-mirror	SPC:	Silicon photo cell
S$_1$, S$_2$:	Slit	Sh:	Shutter

Figure 3.4 (a). Schematic diagram of the Shimadzu UV-150 optical system (Shimadzu, 1994).
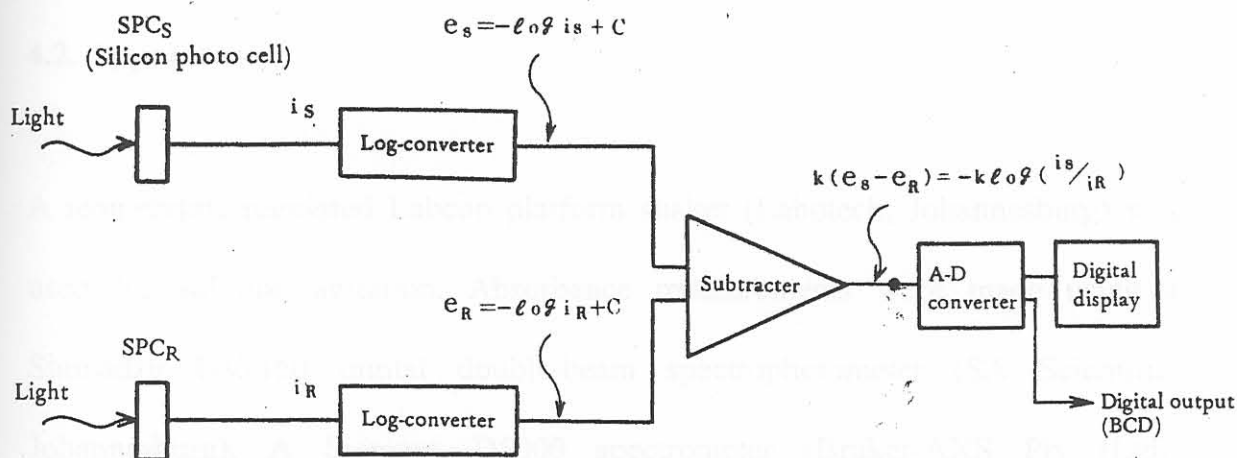

Figure 3.4 (b). Schematic of the Shimadzu UV-150 electronic system (Shimadzu, 1994).

absorbance, i.e. $i_S/i_R = 1/10$. The output signal is displayed on the digital meter after A-D (analogue-to-digital) conversion.

58

CHAPTER 4

EXPERIMENTAL

4.1. Materials

Samples of fly ash (Matla fly ash, M432), slag (slagment, M223) and ordinary Portland cement (Hercules OPC, CEM I 42,5), and two cement blends, Hercules OPC/Fly ash and De Hoek OPC/Slag, were obtained from PPC Technical Services (Germiston, South Africa). All the chemicals used were of analytical grade. De-ionised water from a Modulab system was used for preparing solutions for all the experiments.

4.2. Apparatus

A temperature-regulated Labcon platform shaker (Labotech, Johannesburg) was used for solution agitation. Absorbance measurements were made using a Shimadzu UV-150 digital double-beam spectrophotometer (SA Scientific, Johannesburg). A Siemens D5000 spectrometer (Bruker-AXS Pty (Ltd), Bryanston) was used for XRD analyses, and a Siemens SRS 3300 XRF spectrometer (Bruker-AXS Pty (Ltd), Bryanston) was used for chemical analysis. Particle size analysis was performed with a Malvern Mastersizer instrument

(Micron Scientific, Farramere). Particle fractionation was done using a sieving system from Labquip (SA Scientific, Johannesburg).

4.3. Procedures

4.3.1. Characterisation of the sorbents

The chemical oxide composition of the fly ash, slag and OPC samples was determined by XRF spectrometry after being prepared as fused disks according to standard procedures. XRD scans were performed using Cu K_α radiation ($\lambda = 0.154$ nm) at a speed of 0.2 degrees 2 theta/min. For particle size analysis, 1 g of material was suspended in water with sodium metaphosphate as dispersing agent and pumped past a laser beam. Laser Fraunhofer diffractometry principles were used and an algorithm software was applied to the data collected by computer to calculate parameters of interest such as specific surface area, mean particle diameter and density.

4.3.2. Composition of the cement blends

The percentage fly ash and percentage slag in the respective cement blends were calculated from values of CaO content of the fly ash, slag and each of the cement blends. These were determined experimentally as follows: An intimate mixture of 0.2 g sample and 0.8 g oven dried anhydrous lithium tetra-borate ($Li_2B_4O_7$) was

made and placed in a platinum crucible and then fused at 850°C in a muffle furnace for 15 minutes. The glassy product was dissolved by boiling in 100 ml of 10 % HNO_3, transferred quantitatively to a 500-ml volumetric flask and made up to the mark with de-ionised water. 25-ml aliquots were titrated with 0.01 M standardised EDTA solution using HHSNNA (2-hydroxy-1-[2-hydroxy-4-sulpho-1-naphthylazo]-3-naphthoic acid) indicator. 8 M KOH solution was used to precipitate Mg^{2+} and triethanolamine to mask Fe^{3+}, Al^{3+} and Ti^{4+}.

4.3.3. Phosphate ion calibration curve

The procedure used was based on the yellow ($\lambda= 470$ nm) vanadomolybdo-phosphoric acid UV/VIS spectrophotometric method described by Arnold (1985).

Preparation of PO_4^{3-} stock solution and calibration standards

Anhydrous potassium di-hydrogen phosphate, KH_2PO_4, was oven dried overnight at 110°C and 2.1950 g was then dissolved and diluted to 1000 ml to obtain a 500 mg/l PO_4^{3-}(as P) solution. 1.0, 2.5, 5.0, 10, 20, 40, 50 and 60 mg/l PO_4^{3-}(as P) calibration standards were then prepared in 50-ml volumetric flasks by appropriate dilution of the stock solution.

Preparation of vanadate-molybdate reagent

25 g ammonium molybdate, $(NH_4)_6Mo_7O_{24}\cdot 4H_2O$, was dissolved in 300 ml de-ionised water to obtain Solution A. 1.25 g ammonium metavanadate, NH_4VO_3, was dissolved in 300 ml boiling de-ionised water, cooled, and 330 ml concentrated HCl added to obtain Solution B. Solution B was then cooled to room temperature. Solution A was poured into Solution B, mixed well, and then diluted to 1000 ml.

Preparation of calibration curve

35 ml of each calibration standard was placed in a 50-ml volumetric flask. 10 ml vanadate-molybdate reagent was added and diluted to the mark with de-ionised water. A blank was prepared in which 35 ml de-ionised water was substituted for the calibration standard. After the yellow colour had developed for at least 10 minutes, the absorbance of each calibration standard was measured in a 10-mm glass cuvette versus the blank at a wavelength of 470 nm. A plot of absorbance versus concentration was then constructed to obtain a least-squares calibration curve.

4.3.4. Kinetics of phosphate ion removal

2-g samples of sorbent were weighed accurately and placed in several 250-ml Erlenmeyer flasks, each containing 200 ml of 80 mg/l PO_4^{3-} (as P) solution at pH 9.0 and 25°C (anhydrous KH_2PO_4 was used to prepare a 500 mg/l PO_4^{3-} (as P)

stock solution). The flasks were then closed with rubber stoppers and continuously shaken on a mechanical platform shaker at a speed of 120 cycles per minute. The concentration of PO_4^{3-} was determined for the contents of one flask at a time at pre-determined time intervals.

The shaking was interrupted momentarily at the pre-determined time intervals for a flask to be removed. 50 ml of the supernatant solution was decanted, filtered (Whatman No. 42), and 35 ml of the filtrate transferred to a 50-ml volumetric flask. 10 ml of vanadate-molybdate reagent was then added and the solution made up to the mark with de-ionised water. After the yellow colour had developed for 10 minutes, the absorbance was measured at 470 nm. The phosphate monitoring was carried out at 10-minute intervals for the first 1 hour, then at longer intervals thereafter until the absorbance values levelled off. A graph of $[PO_4^{3-}]$ versus time was then constructed.

4.3.5. Factors influencing phosphate removal kinetics and efficiency

4.3.5.1. Effect of concentration

Solutions of different initial concentrations- 20, 40, 60, 80 mg/l PO_4^{3-} (as P)- were used to investigate the effect of concentration on the kinetics of phosphate removal

by 2 g sorbent at pH 9.0 and 25°C following the procedure described in Section 2.3.4.

4.3.5.2. Effect of particle size

400 g of sorbent was shaken mechanically for 20 minutes in a stack of sieves of various apertures to obtain fractions of different particle sizes. 2 g of 45-75, 75-90, 90-150, 150-300, and >300-μm fractions were placed in Erlenmeyer flasks, each containing 200 ml of 80 mg/l PO_4^{3-}(as P) solution at pH 9.0 and 25 °C. The flasks were then shaken continuously for 16 hours to attain equilibrium. The residual phosphate concentration in the supernatant solutions was determined.

4.3.5.3. Effect of temperature

2 g of sorbent were placed in Erlenmeyer flasks, each containing 200 ml of 80 mg/l PO_4^{3-} (as P) solution at pH 9.0. The flasks were shaken continuously for 16 hours to attain equilibrium, with the flasks surrounded by water set at various temperatures- 25, 40, 50 and 60°C- after which the residual concentration of phosphate in the supernatant solutions was determined.

4.3.5.4. Effect of pH

2 g of sorbent were placed in Erlenmeyer flasks, each containing 200 ml of 80 mg/l PO_4^{3-} (as P) solution at 25°C and at initial pH values of 3.0, 5.0, 7.0, 9.0 and 11.0 (adjusted to the required pH value using 0.1 M HCl and 0.1 M NaOH). The flasks were shaken continuously for 16 hours to attain equilibrium, after which the residual concentration of phosphate in the supernatant solutions was determined.

4.3.6. Adsorption isotherms

Various masses (0.5, 2, 3, 4 and 5 g) of sorbent were shaken continuously with 200 ml of 100 mg/l PO_4^{3-} (as P) solution at pH 9.0 and 25°C for 16 hours to attain equilibrium, after which the residual concentration of phosphate in the supernatant solutions was determined.

4.3.7. Breakthrough curves for the estimation of adsorption capacity

The set-up used for the breakthrough experiments is shown in Figure 4.1. A glass column (4 cm ID, 35 cm high) with a tap at one end was clamped vertically and a 10-mm layer of glass wool inserted near the bottom. The space above the plug was packed with a bed made by intricately mixing 5 g sorbent and 8 g inert sand (to improve porosity) and another layer of glass wool was placed at the top of the bed.

65

The space above the bed was filled with a 400 mg/l PO_4^{3-}(as P) solution (at pH 9.0, 25°C), which was then allowed to flow continuously through the bed at a steady velocity of 2.0 cm/min (volumetric flow rate of 25 cm^3/min). Figure 4.1 (not drawn to scale) illustrates the experimental set-up used.
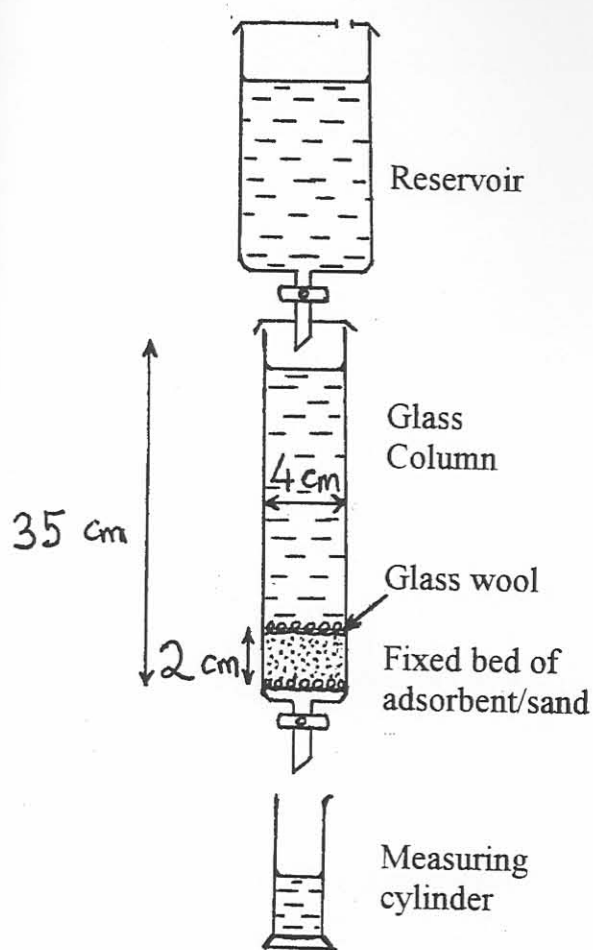

Figure 4.1. Schematic of the set-up used for the breakthrough experiments.

The concentration of phosphate in the effluent was monitored at half-minute intervals by collecting 5 cm^3 of it for analysis until the effluent concentration approached that of the influent. For practical purposes the breakthrough and

exhaustion times (see Section 1.4) were taken to be the times at which the effluent

concentration reached 5 and 95 %, respectively, of the influent concentration.

CHAPTER 5

RESULTS AND DISCUSSION: PHOSPHATE REMOVAL BY FLY ASH

5.1. Particle dimensions and chemical composition

Figure 5.1 shows the particle size distribution for the fly ash, obtained by Fraunhofer diffraction particle analysis as described in Experimental Section 4.3.1.
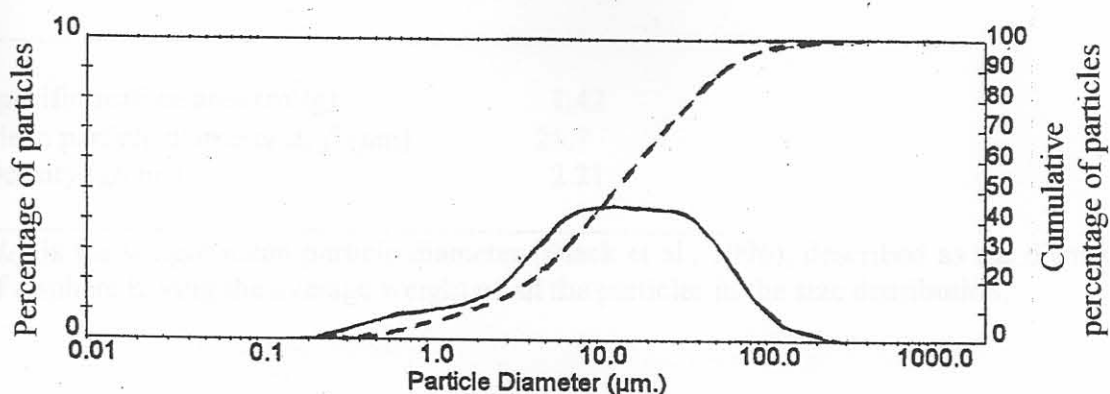

Figure 5.1. Particle size distribution for the FA sample.

The solid line represents the percentage of particles having a given diameter, the particle size distribution being a logarithmic function of the individual particle sizes (see equation (3.1)). The existence of the plateau indicates a slight deviation from a log-normal curve; this was probably influenced by factors such as the origin of the coal and the burning conditions in the boiler.

68

The broken line is a cumulative curve that represents the percentage of particles whose diameters are less than a given diameter. About 63 % of the particles were found to have diameters in the 5-50 μm size range.

Some important physical properties are summarised in Table 5.1.

Table 5.1. Physical properties of FA.

Characteristic	Value
Specific surface area (m^2/g)	1.42
Mean particle diameter $d_{4,3}{}^a$ (μm)	25.7
Density (g/cm^3)	2.21

[a]$d_{4,3}$ is the weight mean particle diameter (Black et al., 1996), described as the diameter of a sphere having the average weight of all the particles in the size distribution.

Figure 5.2 shows the XRD data accumulated over the 5-80° 2θ range. Fly ash typically contains over 50 % glass, which usually contains aluminium and silica. The glass hump can be seen clearly at ca 25° 2θ. The high background is due to the amorphous nature of the sample, i.e. mineral matter in the form of glassy particles.

Although the background was high, peaks for mullite (Al$_6$Si$_2$O$_{13}$) and quartz (SiO$_2$) (typical fly ash crystalline phases) were discernible in the diffractogram even without prior smoothing and background correction.
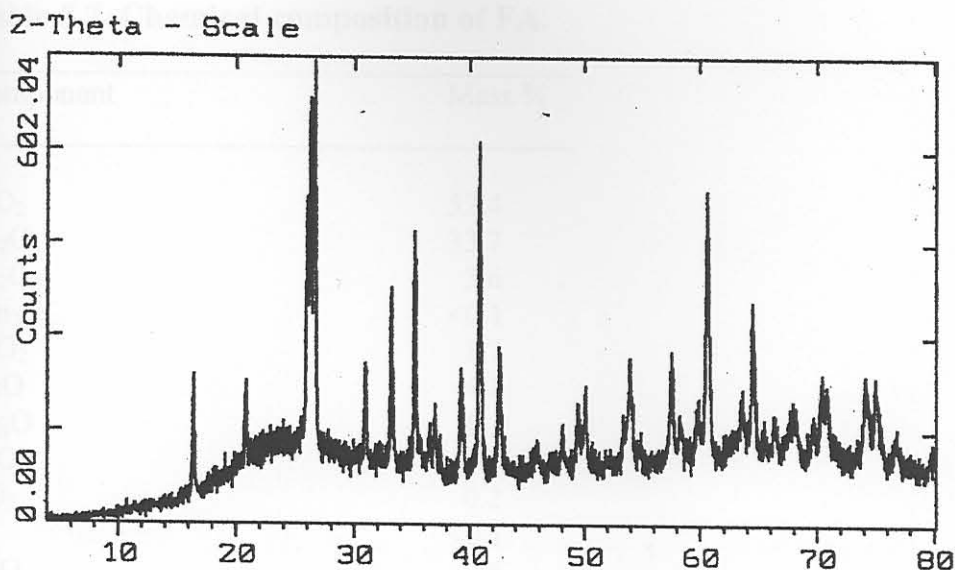
2-Theta - Scale

Figure 5.2. Diffractogram of the FA sample.

Characteristic peaks for mullite were identified at ca 16.5, 26.2, 35.3, 41, 60.5 and 64.5° 2θ. Quartz peaks were identified at ca 21, 26.5 and 50 2θ. Sillimanite (Al_2SiO_5), a member of the mullite family with less alumina, also appears to be present with peaks identified at 26 and 37.1° 2θ.

The chemical oxide composition obtained by XRF is shown in Table 5.2. The relatively low CaO content (4.1 %) typifies the Matla fly ash sample as a Class F fly ash.

70

Table 5.2. Chemical composition of FA.

Component	Mass %
SiO_2	52.4
Al_2O_3	33.7
Fe_2O_3	3.6
Mn_2O_3	<0.1
TiO_2	1.7
CaO	4.1
MgO	1.1
P_2O_5	0.3
SO_3	0.2
Cl	<0.1
K_2O	0.6
Na_2O	0.5
LOI @ 1000°C	0.8
Total	99.0

5.2. Calibration curve for UV/VIS analysis of PO_4^{3-} in aqueous solution

The calibration curve obtained is shown in Figure 5.3. Curvilinear regression (Miller and Miller, 1993) established the upper limit of linearity to be ca 55 mg/l PO_4^{3-} (as P), with a detection limit (3σ) of 0.2 mg/l and regression equation

$$y = 0.002948 + 0.01842\,x$$

over the linear range ($R^2 = 0.9998$), between $0 < [PO_4^{3-}] < 50$ mg/l.
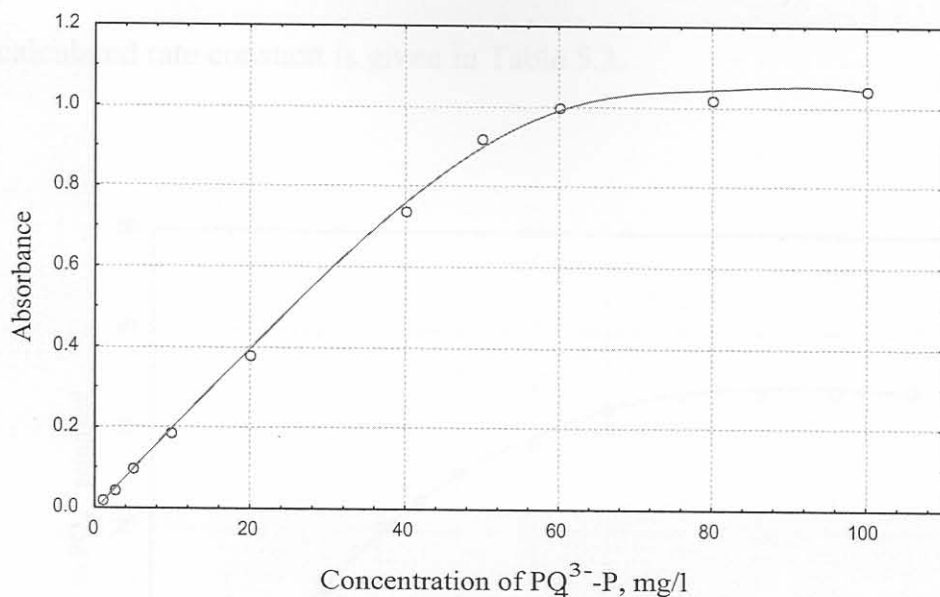
71

Figure 5.3. UV/VIS analysis calibration curve for PO_4^{3-}.

5.3. Kinetics

Figure 5.4 illustrates the percentage PO_4^{3-} removed with time, measured as described in Experimental Section 4.3.4. It can be seen that the uptake of PO_4^{3-} virtually ceased after a contact time of about 6 hrs; this is indicative of the onset of dynamic equilibrium.

The fractional attainment of equilibrium as a function of time, assuming a first order reversible kinetics model, is given by equation (1.12) as explained in Section 1.3. A plot according to equation (1.12) is shown in Figure 5.5. The good straight-line fit observed (linear correlation coefficient $R^2 = 0.991$) indicates that the

72

sorption reaction may be approximated by first order reversible kinetics. The calculated rate constant is given in Table 5.3.
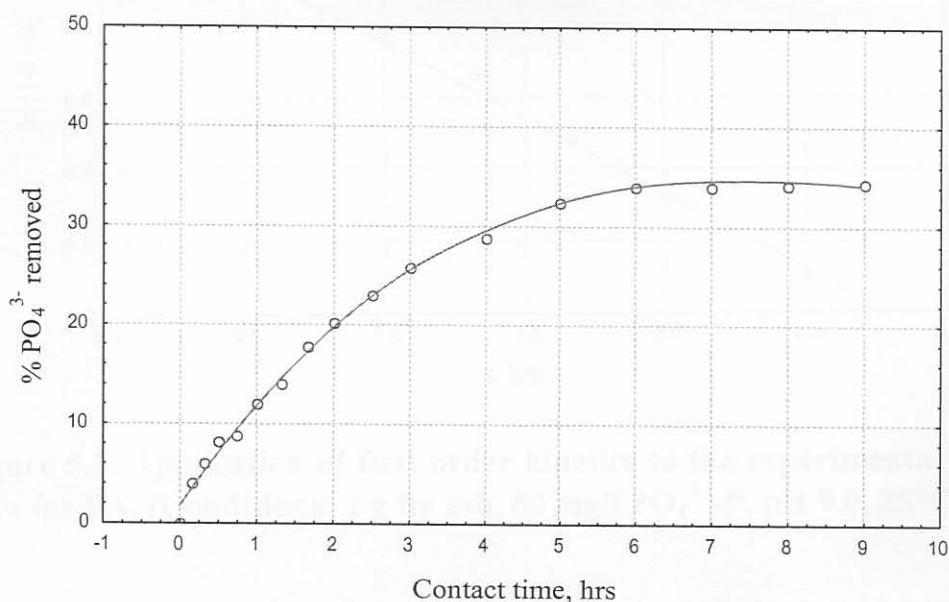

Figure 5.4. Kinetics of PO_4^{3-} removal by FA.
(Conditions: 2 g FA, 80 mg/l PO_4^{3-}-P, pH 9.0, 25°C)

Table 5.3. Values of first order reaction rate constant and intra-particle diffusion constant for PO_4^{3-} removal by FA.

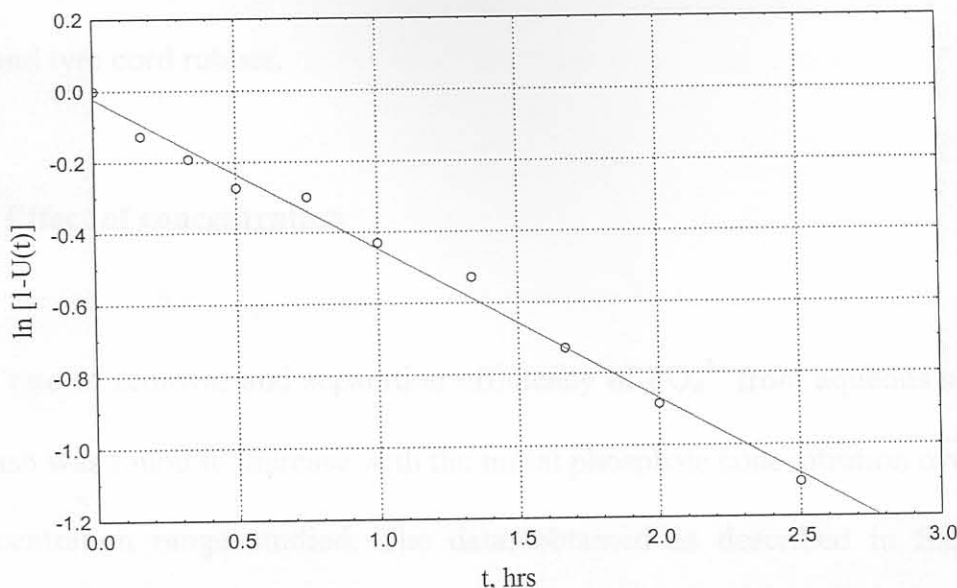| Parameter	Value
k' (per hour)	0.423
D (cm^2/s)	8.40×10^{-12}

73

Figure 5.5. Application of first order kinetics to the experimental adsorption data for FA. (Conditions: 2 g fly ash, 80 mg/l PO$_4^{3-}$-P, pH 9.0, 25°C)

Over the range of sorbent-solution agitation rates studied (100-140 cycles per minute horizontally) it was observed that the sorption rate was not affected by the rate of mixing. This suggests that diffusion in the pores of sorbent particles rather than diffusion through the film at the sorbent particle-aqueous solution interface is rate limiting, which would provide evidence that intra-particle diffusion is the controlling resistance rather than external diffusion.

The value of the intra-particle diffusion constant D calculated using equation (1.13) is given in Table 5.3. According to Michelsen et al. (1975), the value of D should be in the range 10^{-11}-10^{-13} cm^2/s for pore diffusion to be rate limiting; although it must be pointed out immediately that the system they studied involved

74

the removal of heavy metals such as Hg using ion-exchange products made from ground tyre cord rubber.

5.4. Effect of concentration

The rate of removal and separation efficiency of PO_4^{3-} from aqueous solution by fly ash was found to increase with the initial phosphate concentration over the concentration range studied. The data, obtained as described in Experimental Section 4.3.5.1, is represented in Figure 5.6.
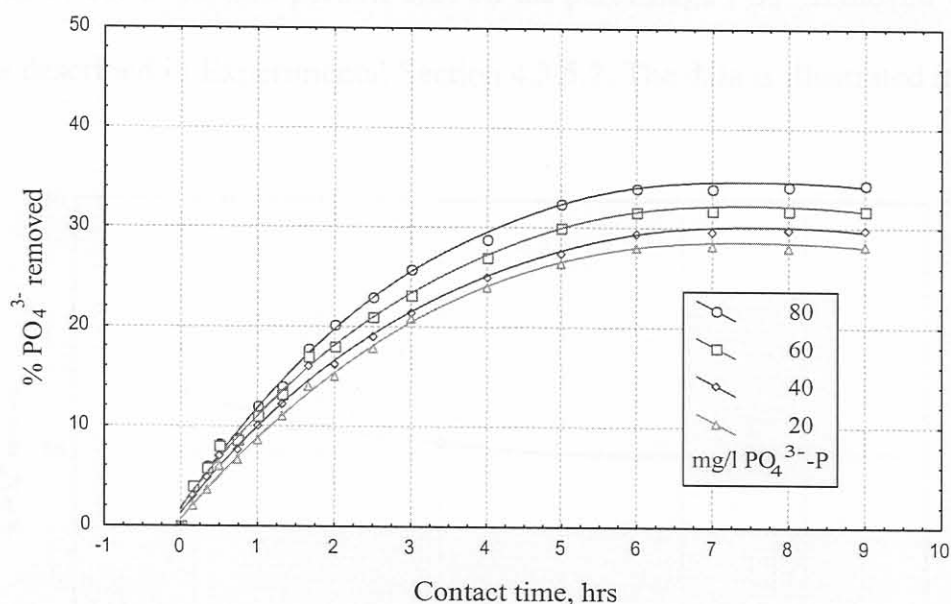

Figure 5.6. Effect of concentration on the kinetics of PO_4^{3-} removal by FA. (Conditions: 2 g FA, pH 9.0, 25°C)

The observed increase in the percentage PO_4^{3-} removed with increasing solute concentration (for the same amount of sorbent) is hardly surprising if the system

75

under study is non-ideal. As mentioned in Sections 1.2.1 and 1.2.2, for non-ideal systems the mass of solute adsorbed per mass of sorbent keeps increasing as the concentration of the solute increases. This has been ascribed to surface heterogeneity in such systems. Interestingly, the initial phosphate concentration does not appear to influence the time it takes (ca 6 hrs) for PO_4^{3-} removal to reach equilibrium.

5.5. Effect of particle size

The effect of sorbent particle size on the percentage PO_4^{3-} removed was measured as described in Experimental Section 4.3.5.2. The data is illustrated in Figure 5.7.
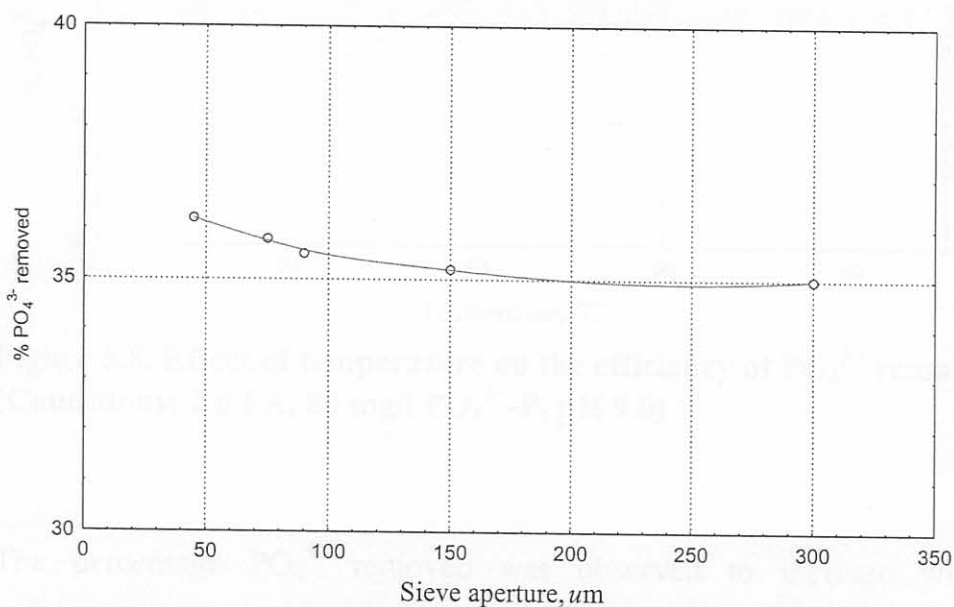

Figure 5.7. Effect of particle size on the efficiency of PO_4^{3-} removal by FA. (Conditions: 2 g fly ash, 80 mg/l PO_4^{3-}-P, pH 9.0, 25°C)

76

Although there was some increase in the percentage PO_4^{3-} removed as the particle size decreased, this increase does not appear to be proportional to the increased surface area.

5.6. Effect of temperature

The effect of temperature on the percentage PO_4^{3-} removed was measured as described in Experimental Section 4.3.5.3. The data is illustrated in Figure 5.8.
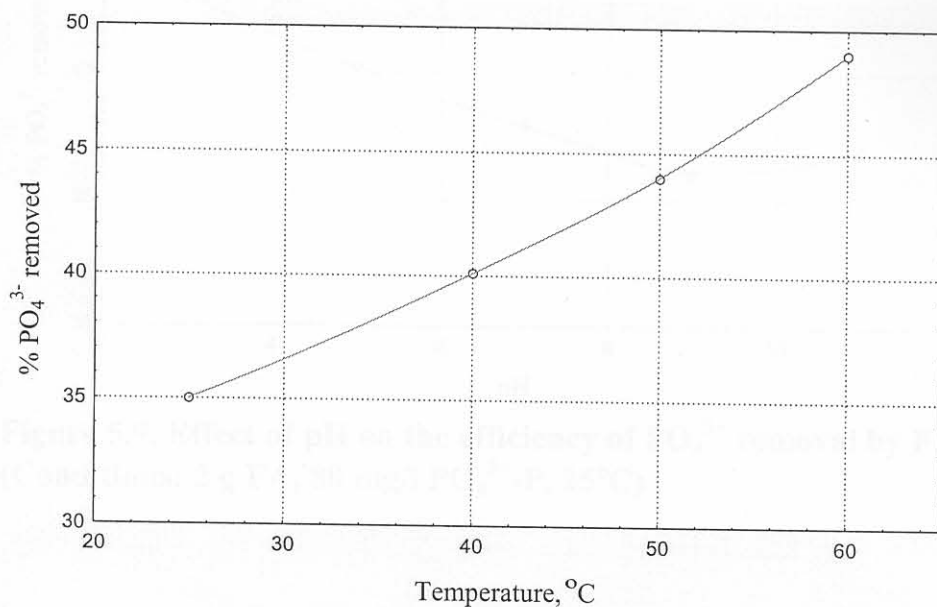

Figure 5.8. Effect of temperature on the efficiency of PO_4^{3-} removal by FA. (Conditions: 2 g FA, 80 mg/l PO_4^{3-}-P, pH 9.0)

The percentage PO_4^{3-} removed was observed to increase with increasing temperature. This is probably due to the resulting increase in diffusion rate.

5.7. Effect of pH

The variation of the percentage PO_4^{3-} removed with the initial pH of the aqueous solution was measured as described in Experimental Section 4.3.5.4. The data obtained is shown in Figure 5.9.
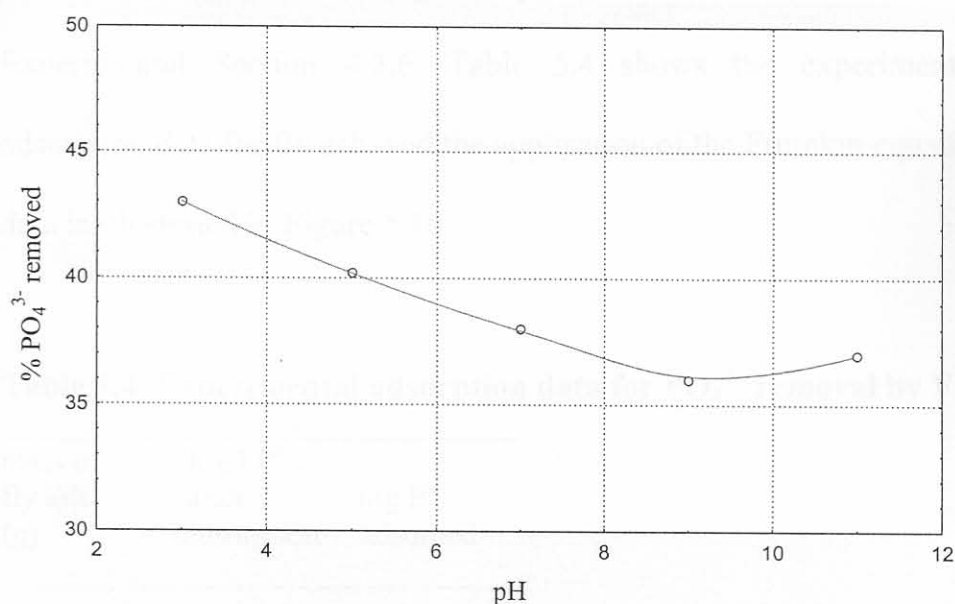
Figure 5.9. Effect of pH on the efficiency of PO_4^{3-} removal by FA. (Conditions: 2 g FA, 80 mg/l PO_4^{3-}-P, 25°C)

It can be seen from the figure that the efficiency of PO_4^{3-} removal increases steadily in acidic pH. This may be due to the accumulation of positive charge on the adsorbent surface that increases its affinity for the negatively charged phosphate ions. The observed slight increase in the efficiency of PO_4^{3-} removal beyond pH 9 could be due to the creation of favourable conditions for calcium

phosphate precipitation at high pH, thus enhancing the removal of PO_4^{3-} by some

dissolved calcium present in the fly ash.

5.8. Adsorption isotherms

Adsorption data for modelling adsorption isotherms was obtained as described in

Experimental Section 4.3.6. Table 5.4 shows the experimentally obtained

adsorption data for fly ash, and the application of the Frumkin equation (1.7) to the

data is illustrated in Figure 5.10.

Table 5.4. Experimental adsorption data for PO_4^{3-} removal by FA.

mass of fly ash (g)	mg/l P^a after adsorption	mg P^a adsorbed
0.5	72.8	5.4
2	71.9	5.6
3	71.4	5.7
3.5	70.2	6.4
4	65.0	7.0
5	58.7	8.3

$^a PO_4^{3-}$(as P)

Attempts to fit the data to the Langmuir (equation 1.3) and Freundlich (equation

1.4) isotherms yielded non-linear plots with values of $R^2 < 0.4$. It is evident that the

Frumkin isotherm (see equations 1.6 & 1.7) is the appropriate one for fitting the data, which is indicative of a non-ideal system with finite lateral interactions among adsorbate particles. The Frumkin constants were calculated and are shown in Table 5.5.

Table 5.5. Isotherm linear correlation coefficients and Frumkin constants for PO_4^{3-} adsorption by FA.

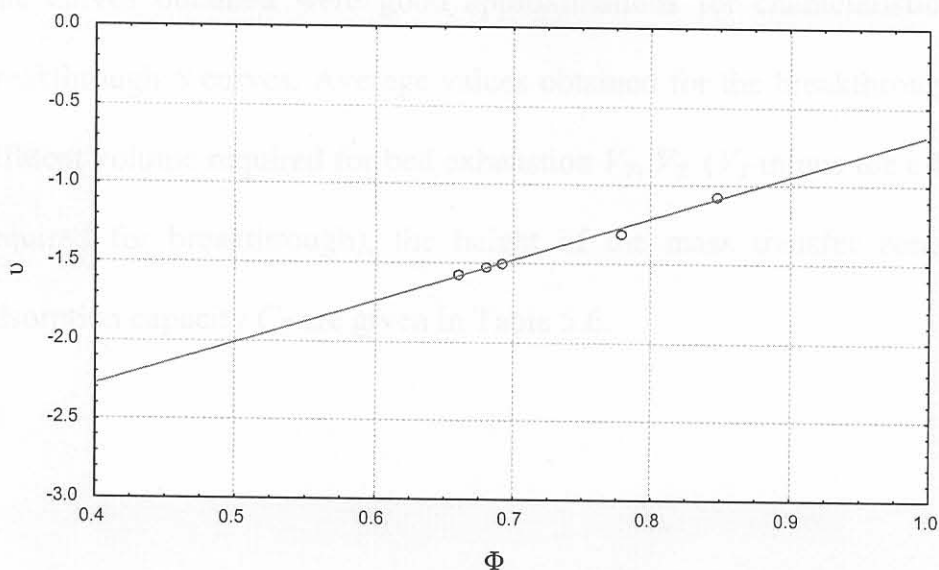| Isotherm	R^2	α	β
Frumkin	0.992	3.061	0.025
Langmuir	0.376		
Freundlich	0.279		

Figure 5.10. Application of the Frumkin equation to the experimental adsorption data (given in Table 5.4) for FA.

80

5.9. Breakthrough curves

Data for constructing breakthrough curves was obtained as described in Experimental Section 4.3.7. The data obtained for the breakthrough experiments (see equations 1.15 and 1.16) for fly ash are shown in Table 5.6, and a representative breakthrough curve is illustrated in Figure 5.11.

Table 5.6. Breakthrough data for FA.

t_E (min)	V_T (cm^3)	V_Z (cm^3)	h_Z (cm)	C_T (mg PO$_4{}^{3-}$-P/g)
2.8	187	116	1.742	32

The curves obtained were good approximations for characteristic symmetrical breakthrough S curves. Average values obtained for the breakthrough time t_E, the effluent volume required for bed exhaustion V_T, V_Z (V_T minus the effluent volume required for breakthrough), the height of the mass transfer zone h_Z, and the adsorption capacity C_T are given in Table 5.6.
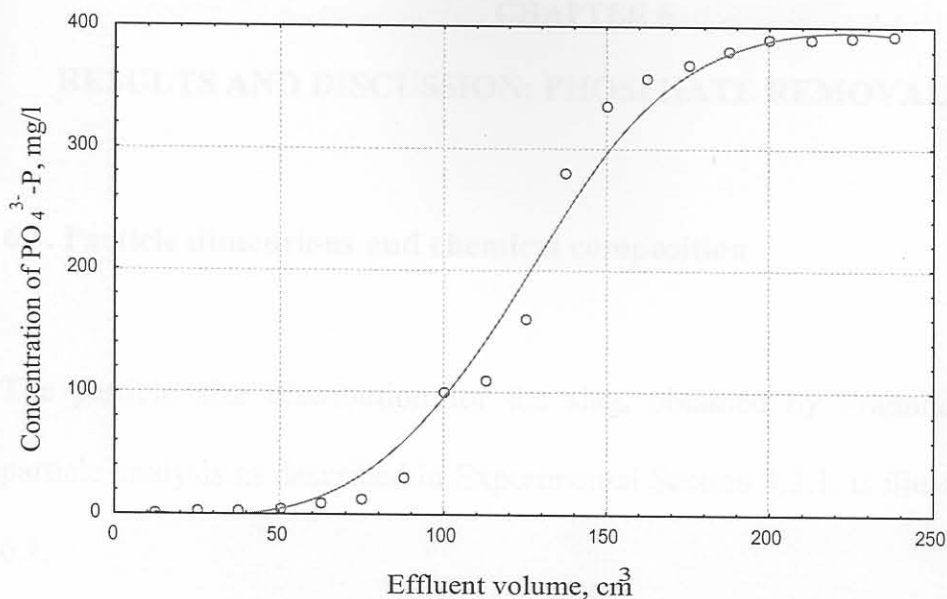
81

Figure 5.11. Breakthrough curve for PO_4^{3-} removal by FA.

An average C_T value of 32 mg PO_4^{3-}-P/g was obtained for fly ash.

CHAPTER 6

RESULTS AND DISCUSSION: PHOSPHATE REMOVAL BY SLAG

6.1. Particle dimensions and chemical composition

The particle size distribution for the slag, obtained by Fraunhofer diffraction

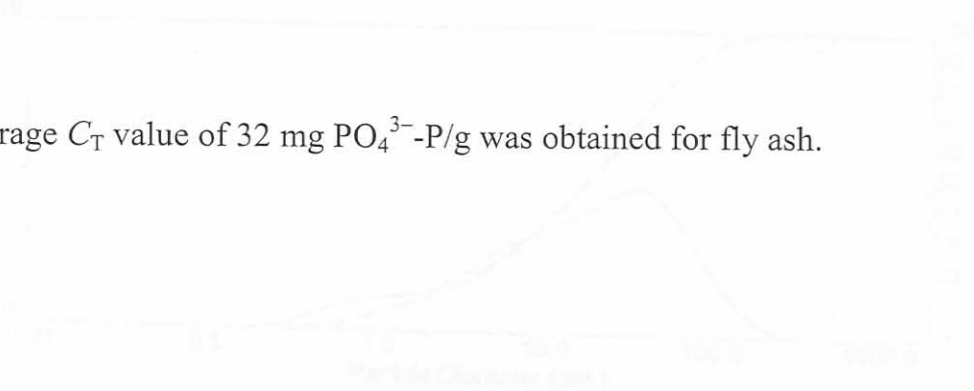particle analysis as described in Experimental Section 4.3.1, is illustrated in Figure

6.1.
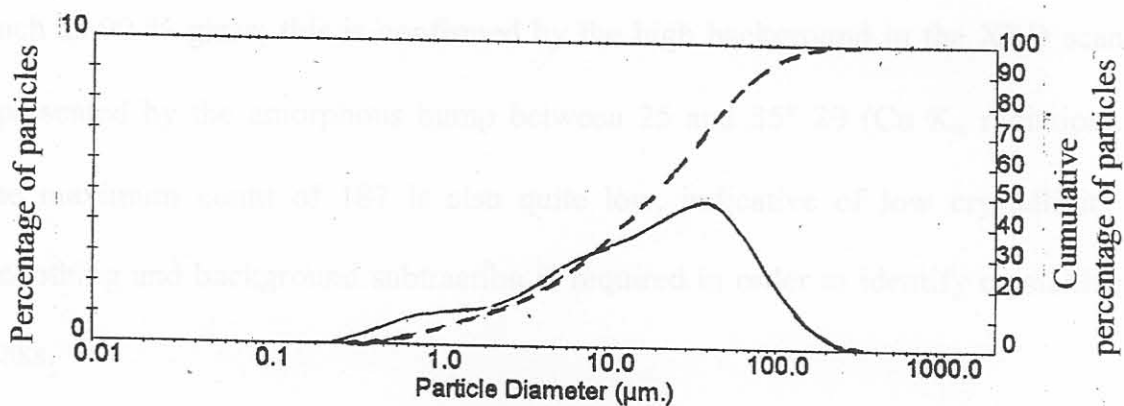
Figure 6.1. Particle size distribution for the slag sample.

The solid line represents the percentage of particles having a given diameter, the

particle size distribution being a logarithmic function of the individual particle

sizes (see equation (3.1)). The broken line is a cumulative curve that represents the

percentage of particles whose diameters are less than a given diameter. About 57%

of the particles were found to have diameters in the 5-50 μm size range.

83

Table 6.1 represents a summary of some important physical characteristics.

Table 6.1. Physical properties of slag.

Characteristic	Value
Specific surface area (m^2/g)	1.29
Mean particle diameter $d_{4,3}$ (μm)	31.4
Density (g/cm^3)	2.82

The raw XRD pattern is shown in Figure 6.2(a). Slags are known to contain as much as 90 % glass; this is confirmed by the high background in the XRD scan represented by the amorphous hump between 25 and 35° 2θ (Cu K$_\alpha$ radiation). The maximum count of 187 is also quite low, indicative of low crystallinity. Smoothing and background subtraction is required in order to identify crystalline peaks.

Figure 6.2(b) shows the smoothed and background-subtracted pattern. The main crystalline phase appears to be tricalcium silicate (C$_3$S) with relatively prominent peaks at 29.5, 34.5, 41.5, and 52° 2θ, synonymous with the main phase in OPC.

The chemical oxide composition obtained by XRF is shown in Table 6.2. Lime, silica, alumina and magnesia are evident as the four major constituents of the slag sample used.

84
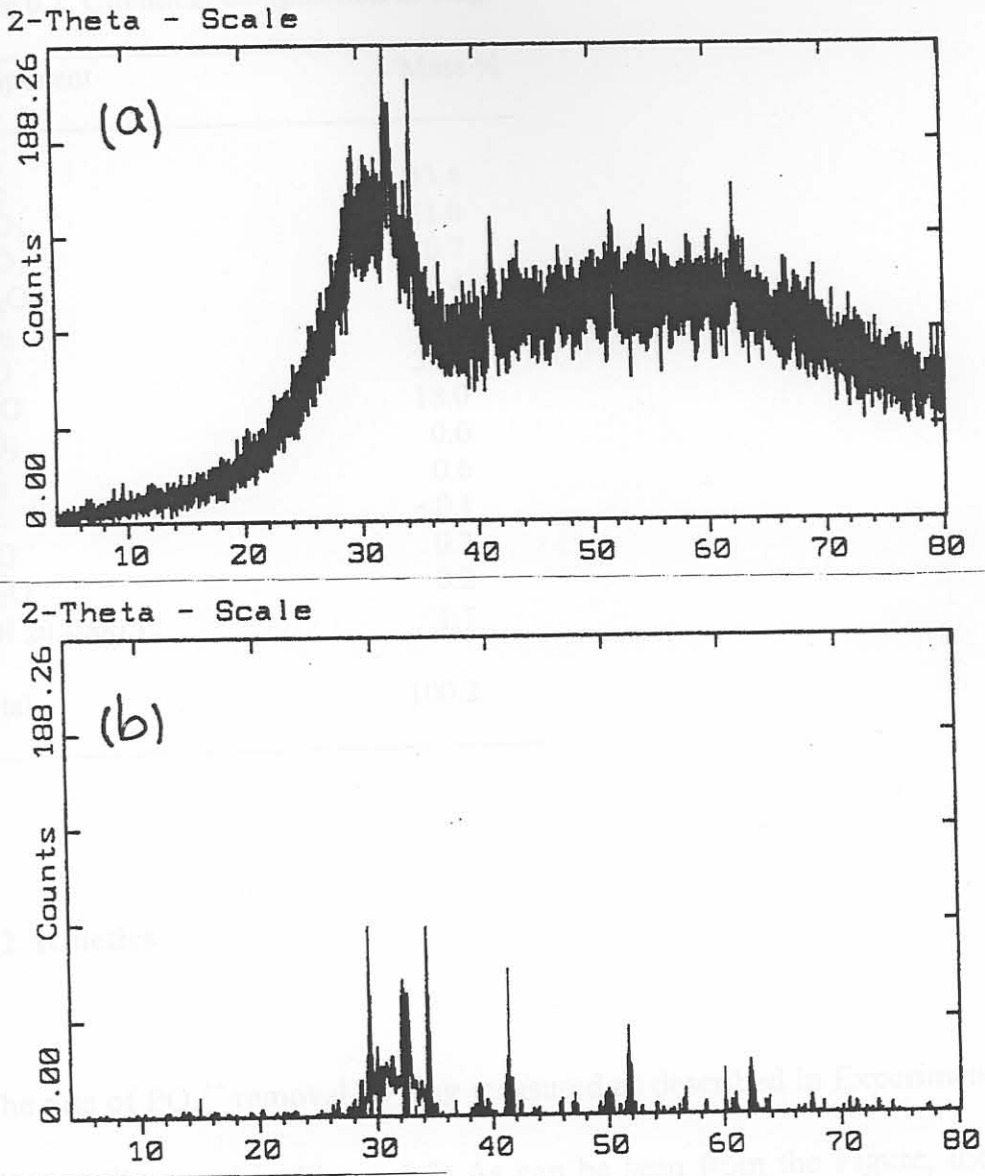
Figure 6.2. Diffractogram of the slag sample: (a) raw pattern (b) smoothed and background subtracted pattern.

Table 6.2. Chemical composition of slag.

Component	Mass %
SiO_2	33.4
Al_2O_3	11.0
Fe_2O_3	0.7
Mn_2O_3	0.4
TiO_2	0.6
CaO	33.3
MgO	18.0
P_2O_5	0.0
SO_3	0.6
Cl	<0.1
K_2O	0.3
Na_2O	0.2
LOI @ 1000°C	1.7
Total	100.2

6.2. Kinetics

The rate of PO_4^{3-} removal by slag measured as described in Experimental Section 4.3.4 is illustrated in Figure 6.3. As can be seen from the Figure, the uptake of PO_4^{3-} approaches a limiting value of ca 65 % after a contact time of ca 4 hrs, signalling the attainment of dynamic equilibrium conditions. The fractional attainment of equilibrium as a function of time, assuming a first order reversible kinetics model, is given by equation (1.12) as explained in Section 1.3.

A plot according to equation (1.12) is shown in Figure 6.4.

86
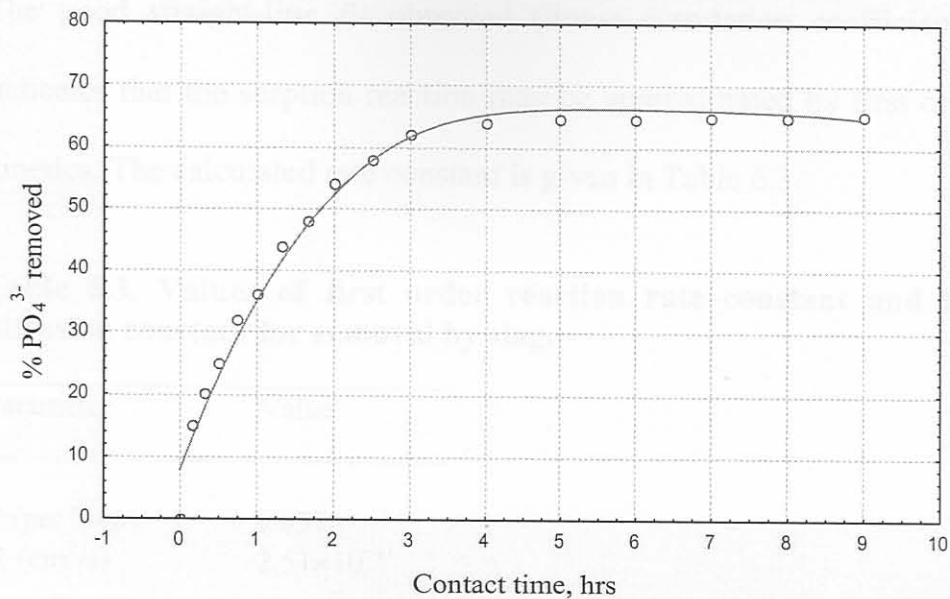
Figure 6.3. Kinetics of PO$_4^{3-}$ removal by slag.
(Conditions: 2 g slag, 80 mg/l PO$_4^{3-}$-P, pH 9.0, 25°C)
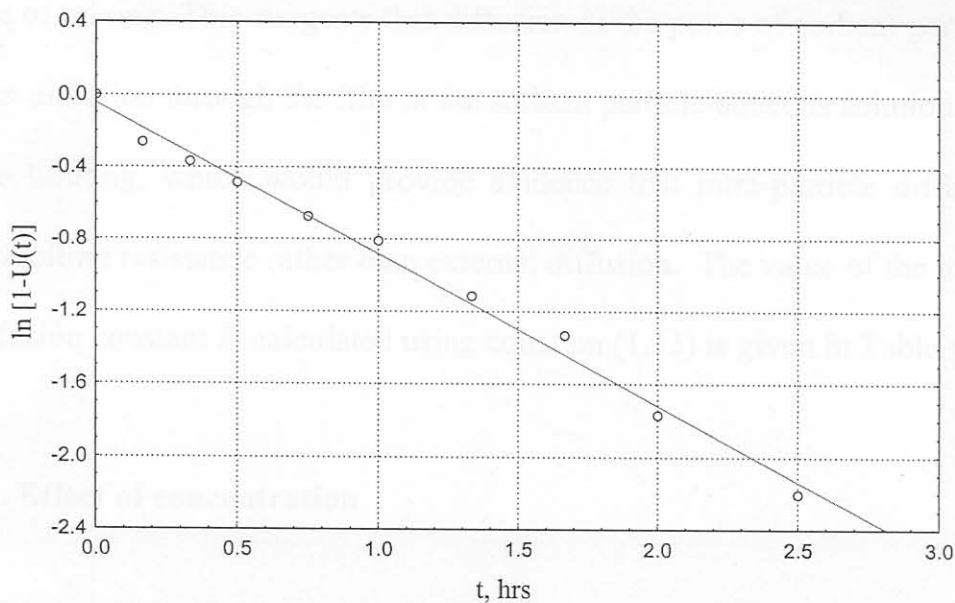

Figure 6.4. Application of first order kinetics to the experimental adsorption data for slag. (Conditions: 2 g slag, 80 mg/l PO$_4^{3-}$-P, pH 9.0, 25°C)

The good straight-line fit observed (linear correlation coefficient R^2= 0.992) indicates that the sorption reaction may be approximated by first order reversible kinetics. The calculated rate constant is given in Table 6.3.

Table 6.3. Values of first order reaction rate constant and intra-particle diffusion constant for removal by slag.

Parameter	Value
k' (per hour)	0.837
D (cm^2/s)	2.51×10^{-11}

Over the range of sorbent-solution agitation rates studied (100-140 cycles per minute horizontally) it was observed that the sorption rate was not affected by the rate of mixing. This suggests that diffusion in the pores of sorbent particles rather than diffusion through the film at the sorbent particle-aqueous solution interface is rate limiting, which would provide evidence that intra-particle diffusion is the controlling resistance rather than external diffusion. The value of the intra-particle diffusion constant D calculated using equation (1.13) is given in Table 6.3.

6.3. Effect of concentration

Figure 6.5 illustrates the effect of concentration on the efficiency of PO_4^{3-} removal, measured as described in Experimental Section 4.3.5.1.
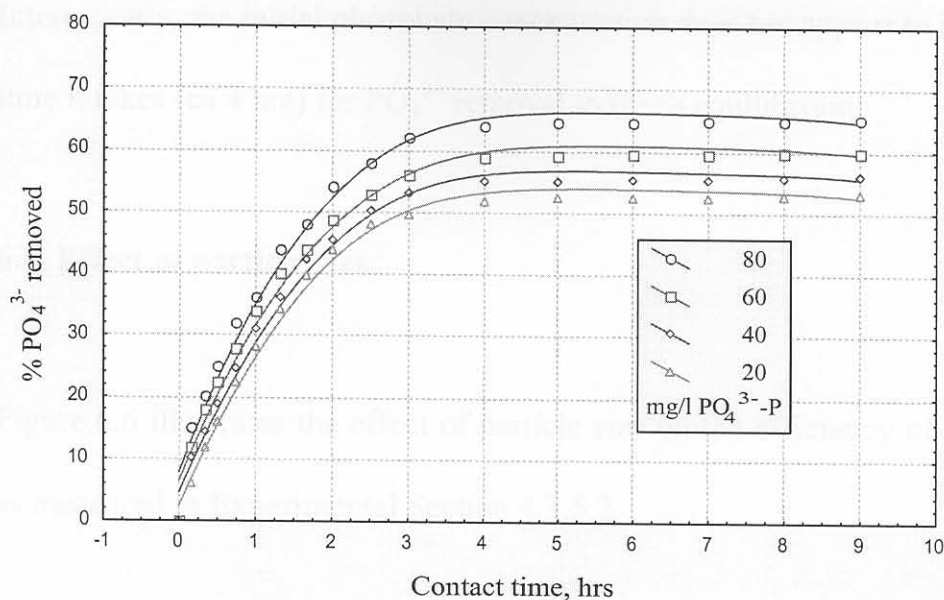
Figure 6.5. Effect of concentration on the kinetics of PO_4^{3-} removal by slag. (Conditions: 2 g slag, pH 9.0, 25°C)

The rate of removal and separation efficiency of PO_4^{3-} from aqueous solution by slag was found to increase with the initial phosphate concentration over the concentration range studied.

The observed increase in the percentage PO_4^{3-} removed with increasing solute concentration (for the same amount of slag) is hardly surprising if the system under study is non-ideal. As mentioned in Sections 1.2.1 and 1.2.2, for non-ideal systems the mass of solute adsorbed per mass of sorbent keeps increasing as the concentration of the solute increases. This has been ascribed to surface heterogeneity in such systems.

Interestingly, the initial phosphate concentration does not appear to influence the time it takes (ca 4 hrs) for PO_4^{3-} removal to reach equilibrium.

6.4. Effect of particle size

Figure 6.6 illustrates the effect of particle size on the efficiency of PO_4^{3-} removal as measured in Experimental Section 4.3.5.2.

Figure 6.6. Effect of particle size on the efficiency of PO_4^{3-} removal by slag. (Conditions: 2 g slag, 80 mg/l PO_4^{3-}-P, pH 9.0, 25°C)

Although there was some increase in the percentage PO_4^{3-} removed as the particle size decreased, this increase does not appear to be proportional to the increased surface area.

6.5. Effect of temperature

The effect of temperature on the efficiency of PO_4^{3-} removal measured as described in Experimental Section 4.3.5.3 is illustrated in Figure 6.7.
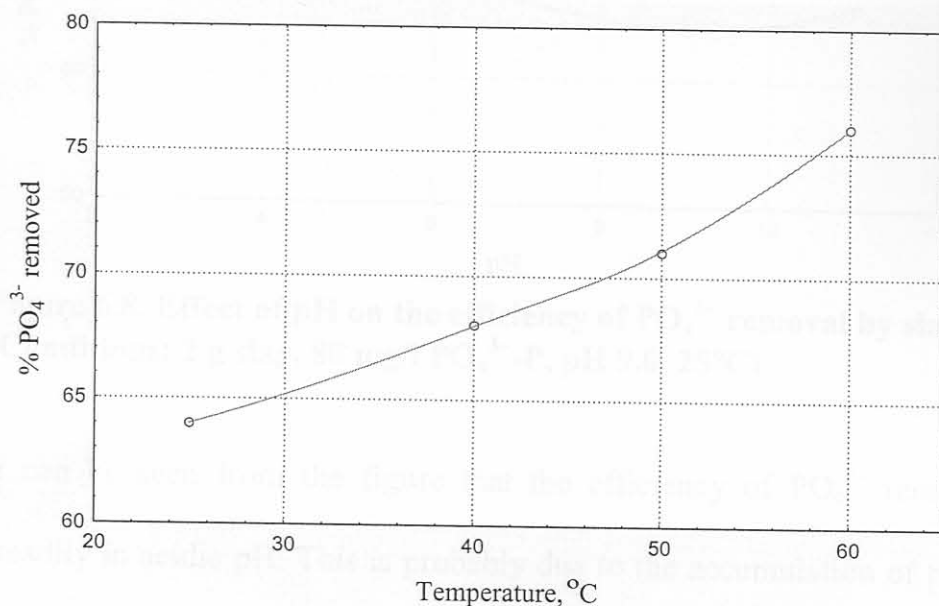
Figure 6.7. Effect of temperature on the efficiency of PO_4^{3-} removal by slag. (Conditions: 2 g slag, 80 mg/l PO_4^{3-}-P, pH 9.0, 25°C)

The percent PO_4^{3-} removed was observed to increase with temperature. This may be ascribed to an expected increase in diffusion coefficient with increasing temperature.

6.6. Effect of pH

Figure 6.8 illustrates the variation of percent PO_4^{3-} removed with the initial pH of the aqueous solution, measured as described in experimental Section 4.3.5.4.
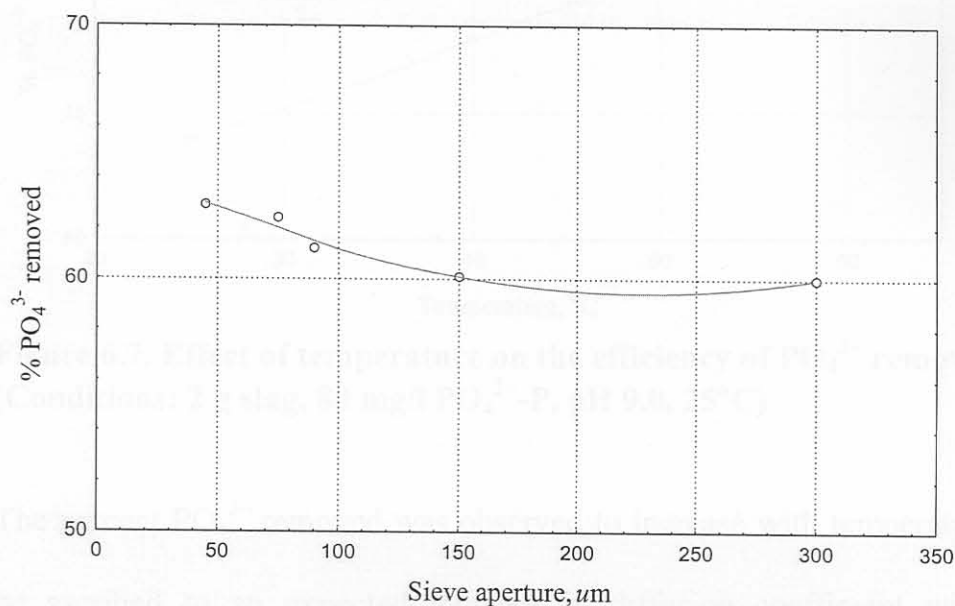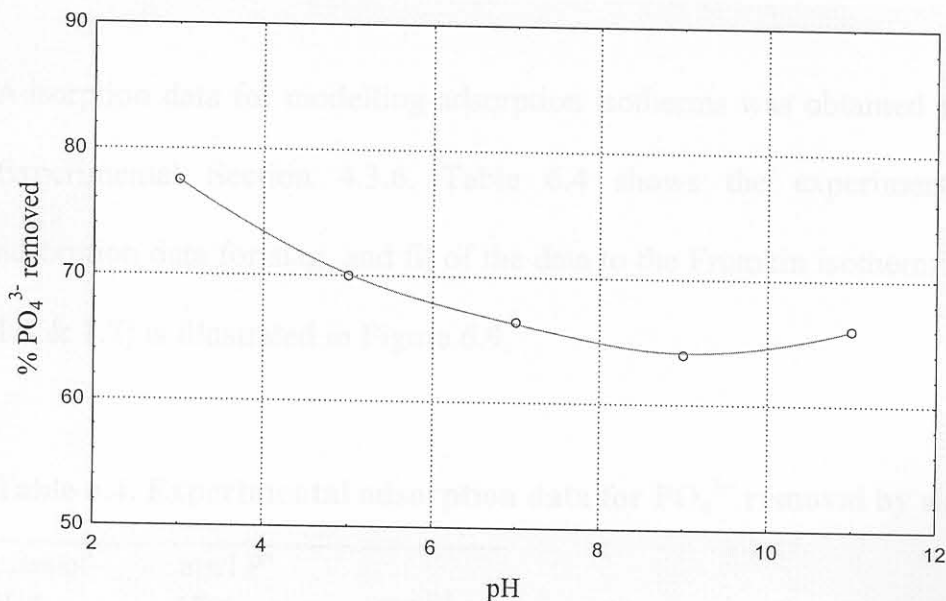
Figure 6.8. Effect of pH on the efficiency of PO$_4^{3-}$ removal by slag. (Conditions: 2 g slag, 80 mg/l PO$_4^{3-}$-P, pH 9.0, 25°C)

It can be seen from the figure that the efficiency of PO$_4^{3-}$ removal increases steadily in acidic pH. This is probably due to the accumulation of positive charge on the adsorbent surface that increases its affinity for the negatively charged phosphate ions. The observed slight increase in the efficiency of PO$_4^{3-}$ removal beyond pH 9 could be due to the creation of favourable conditions for calcium phosphate precipitation at high pH, thus enhancing the removal of PO$_4^{3-}$ by some dissolved calcium formed by hydration of slag, or being present in the slag as free lime.

6.7. Adsorption isotherms

Adsorption data for modelling adsorption isotherms was obtained as described in Experimental Section 4.3.6. Table 6.4 shows the experimentally obtained adsorption data for slag, and fit of the data to the Frumkin isotherm (see equations 1.6 & 1.7) is illustrated in Figure 6.9.

Table 6.4. Experimental adsorption data for PO_4^{3-} removal by slag.

mass of slag (g)	mg/l P^a after adsorption	mg P^a adsorbed
0.5	48.5	10.3
2	46.7	10.6
3	45.8	10.8
3.5	43.5	11.3
4	33.7	13.3
5	21.7	15.7

$^aPO_4^{3-}$(as P)
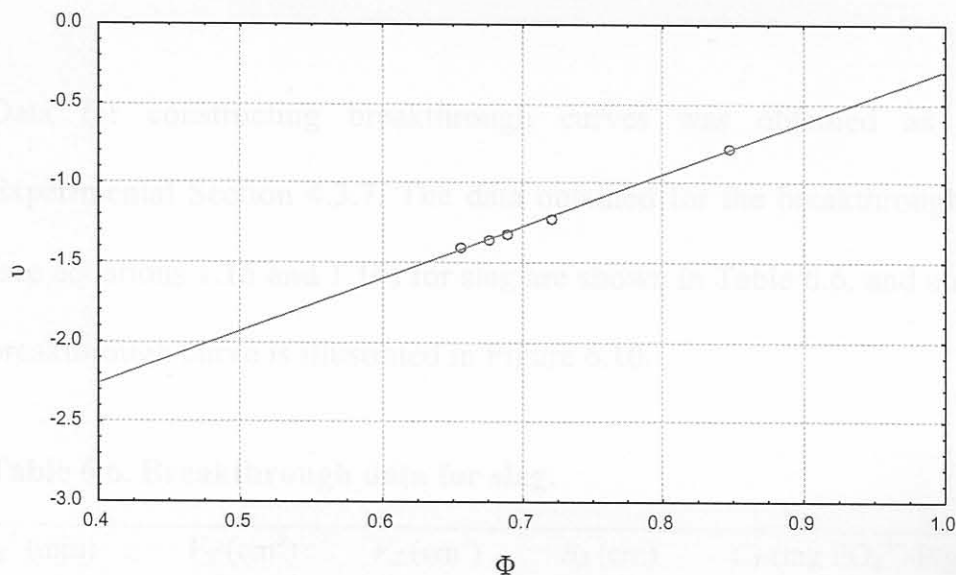
Figure 6.9. Application of the Frumkin equation to the experimental adsorption data (given in Table 6.4) for slag.

Attempts to fit the data to the Langmuir (equation 1.3) and Freundlich (equation 1.4) isotherms yielded non-linear plots with values of $R^2 < 0.3$. It is evident that the Frumkin isotherm (equation 1.7) is the appropriate one for fitting the data, which is indicative of a non-ideal system with finite lateral interactions among adsorbate particles. The Frumkin constants were calculated and are shown in Table 6.5.

Table 6.5. Isotherm linear correlation coefficients and Frumkin constants for PO_4^{3-} adsorption by slag.

Isotherm	R^2	α	β
Frumkin	0.997	3.780	0.015
Langmuir	0.270		
Freundlich	0.233		

94

6.8. Breakthrough curves

Data for constructing breakthrough curves was obtained as described in Experimental Section 4.3.7. The data obtained for the breakthrough experiments (see equations 1.15 and 1.16) for slag are shown in Table 6.6, and a representative breakthrough curve is illustrated in Figure 6.10.

Table 6.6. Breakthrough data for slag.

$t_E{}^a$ (min)	V_T (cm^3)	V_Z (cm^3)	h_Z (cm)	C_T (mg PO$_4{}^{3-}$-P/g)
7.0	312	138	1.133	60

^{a}Breakthrough time

The curves obtained were good approximations for characteristic symmetrical breakthrough S curves. Average values obtained for the breakthrough time t_E, the effluent volume required for bed exhaustion V_T, V_Z (V_T minus the effluent volume required for breakthrough), the height of the mass transfer zone h_Z, and the adsorption capacity C_T are given in Table 6.6.

An average capacity value C_T of 60 mg PO$_4{}^{3-}$-P/g slag was obtained.

95
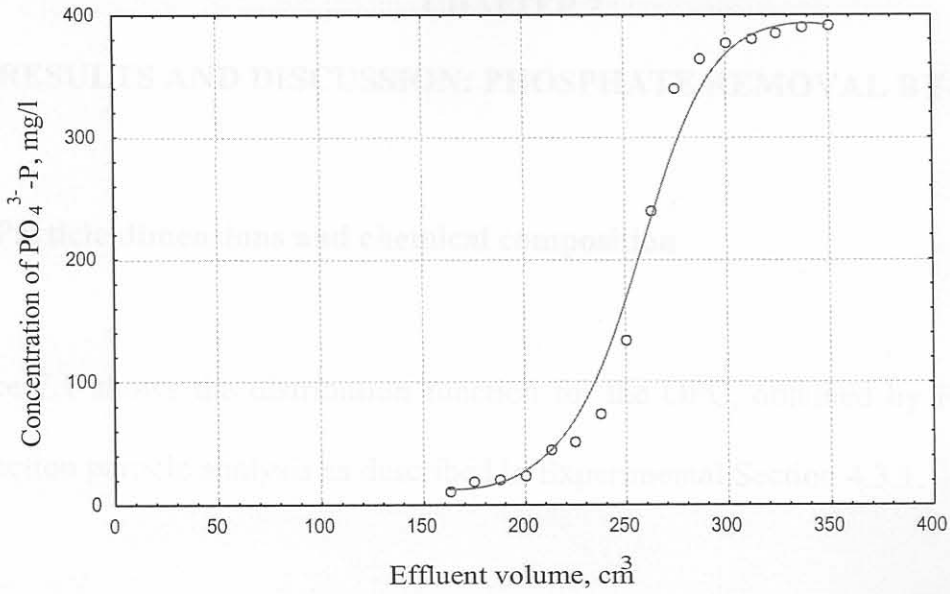
Figure 6.10. Breakthrough curve for removal by slag.

CHAPTER 7

RESULTS AND DISCUSSION: PHOSPHATE REMOVAL BY OPC

7.1. Particle dimensions and chemical composition

Figure 7.1 shows the distribution function for the OPC, obtained by Fraunhofer diffraction particle analysis as described in Experimental Section 4.3.1.
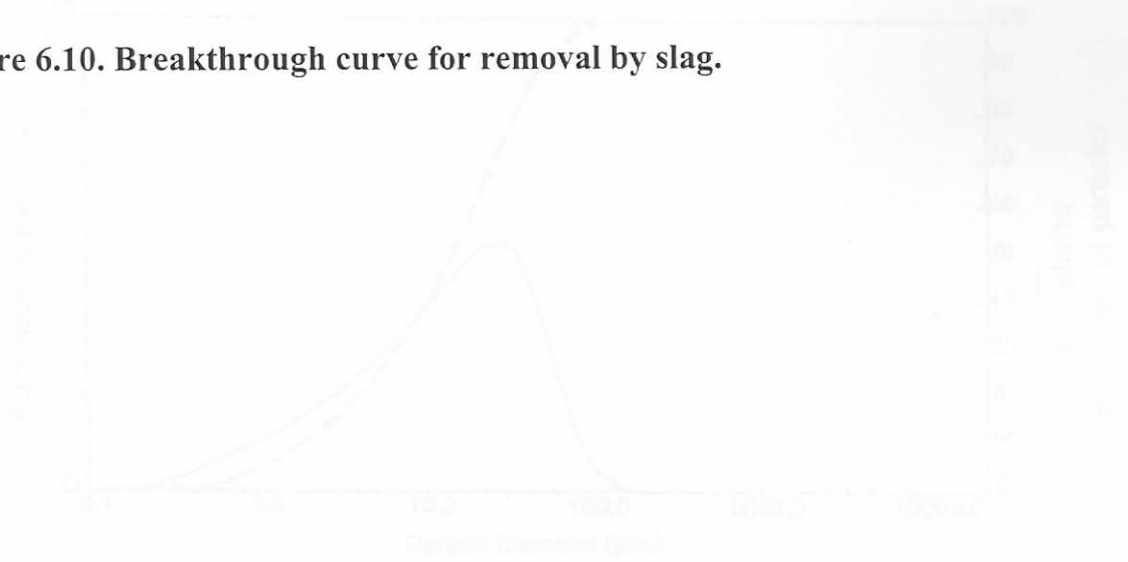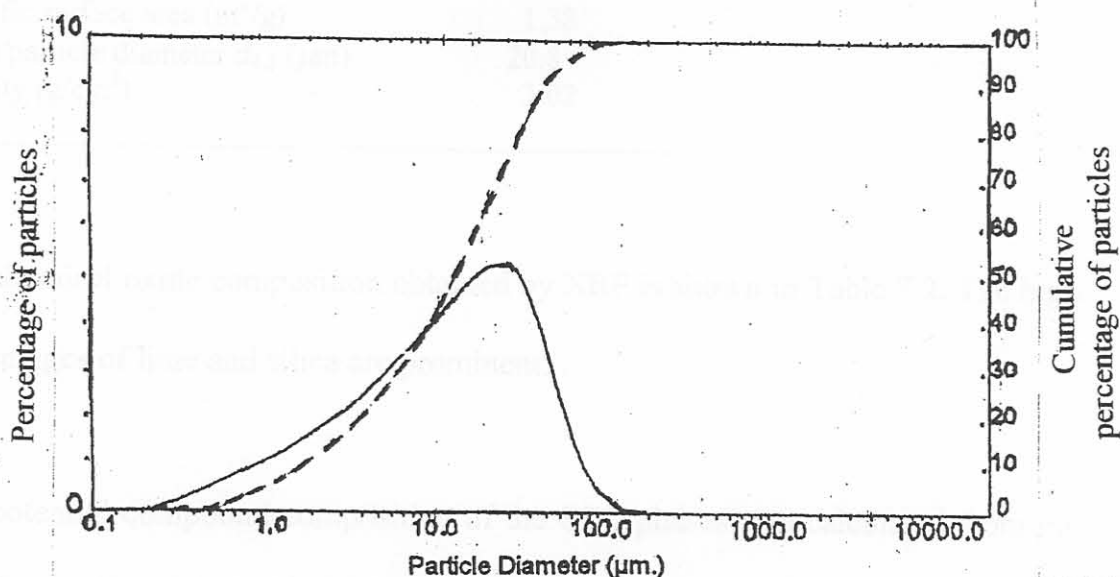
Figure 7.1. Particle size distribution for the OPC sample.

The solid line represents the percentage of particles having a given diameter, the particle size distribution being a logarithmic function of the individual particle sizes (see equation (3.1)). Its shape approximates a log-normal curve, albeit slightly skewed towards lower particle sizes. The broken line is a cumulative curve that represents the percentage of particles whose diameters are less than a

97

given diameter. About 65 % of the particles were found to have diameters in the 5-50 μm size range.

Some important physical properties are summarised in Table 7.1.

Table 7.1. Physical properties of OPC.

Characteristic	Value
Specific surface area (m^2/g)	1.38
Mean particle diameter $d_{4,3}$ (μm)	20.8
Density (g/cm^3)	3.02

The chemical oxide composition obtained by XRF is shown in Table 7.2. The high percentages of lime and silica are prominent.

The potential compound composition of the OPC phases was calculated from the experimental chemical oxide composition data using the Bogue (1955) equations. The values obtained for the major phases, namely, alite (C_3S), belite (C_2S), aluminate (C_3A) and ferrite (C_4AF) are given in Table 7.3.

Table 7.2. Chemical oxide composition of OPC.

Component	Mass %
SiO_2	22.5
Al_2O_3	4.5
Fe_2O_3	1.4
Mn_2O_3	0.9
TiO_2	0.2
CaO	63.2
MgO	3.6
P_2O_5	0.2
SO_3	2.4
Cl	<0.1
K_2O	0.8
Na_2O	0.1
LOI @ 1000°C	1.0
Total	100.8

Table 7.3. Potential compound composition of OPC.

Phase	Mass %
C_3S	54.0
C_2S	23.8
C_3A	9.6
C_4AF	4.3

7.2. Kinetics

Figure 7.2 illustrates the percentage PO_4^{3-} removed with time, measured as described in Experimental Section 4.3.4. It can be seen that the uptake of PO_4^{3-}

virtually ceased after a contact time of about 3 hrs, indicating the establishment of dynamic equilibrium. The fractional attainment of equilibrium as a function of time, assuming a first order reversible kinetics model, is given by equation (1.12) as explained in Section 1.3.

A plot according to equation (1.12) is shown in Figure 7.3.
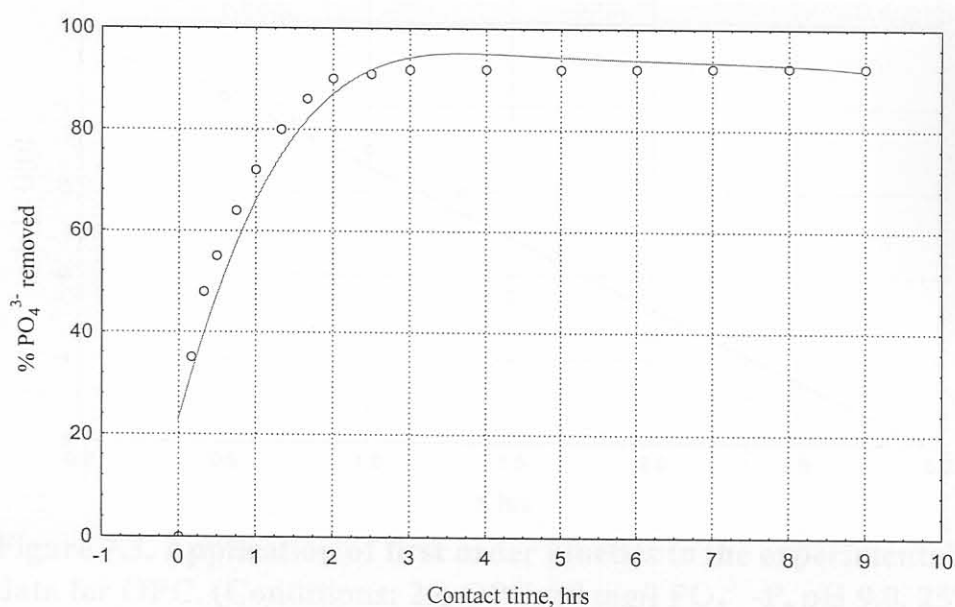
Figure 7.2. Kinetics of PO_4^{3-} removal by OPC.
(Conditions: 2 g OPC, 80 mg/l PO_4^{3-}-P, pH 9.0, 25°C)

The reasonably good straight-line fit observed (R^2= 0.994) indicates that the sorption reaction may be approximated by first order reversible kinetics; the calculated rate constant is given in Table 7.4.

Table 7.4. Values of first order reaction rate constant and intra-particle diffusion constant for removal by OPC.

Parameter	Value
k' (per hour)	1.682
D (cm^2/s)	8.72×10^{-11}
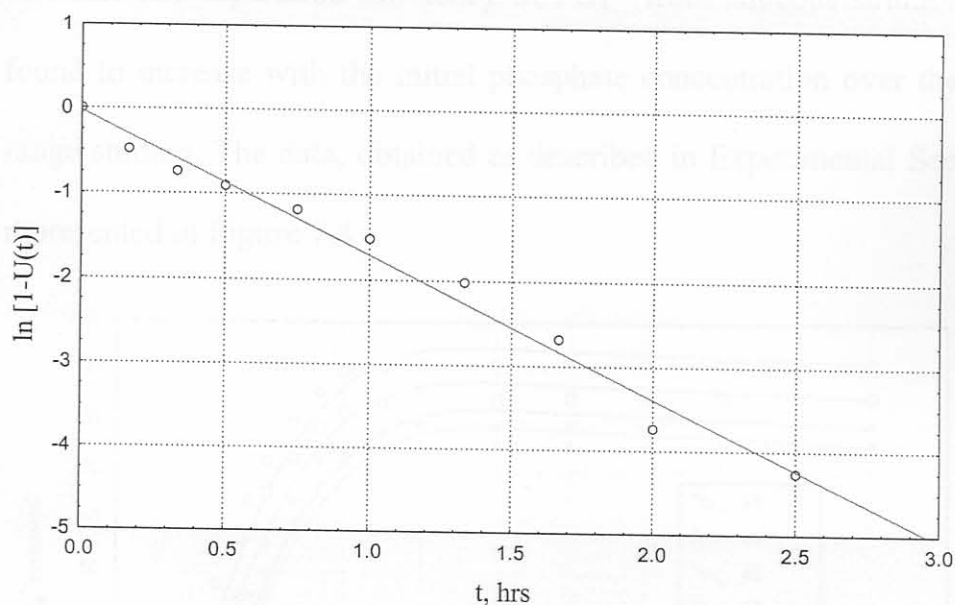
Figure 7.3. Application of first order kinetics to the experimental adsorption data for OPC. (Conditions: 2 g OPC, 80 mg/l PO$_4^{3-}$-P, pH 9.0, 25°C)

Over the range of sorbent-solution agitation rates studied (100-140 cycles per minute horizontally) it was observed that the sorption rate was not affected by the rate of mixing. This suggests that diffusion in the pores of sorbent particles rather than diffusion through the film at the sorbent particle-aqueous solution interface is rate limiting, which would provide evidence that intra-particle diffusion is the controlling resistance rather than external diffusion.

The value of the intra-particle diffusion constant D calculated using equation (1.13) is given in Table 7.3.

7.3. Effect of concentration

The rate and separation efficiency of PO_4^{3-} from aqueous solution by OPC was found to increase with the initial phosphate concentration over the concentration range studied. The data, obtained as described in Experimental Section 4.3.5.1, is represented in Figure 7.4.
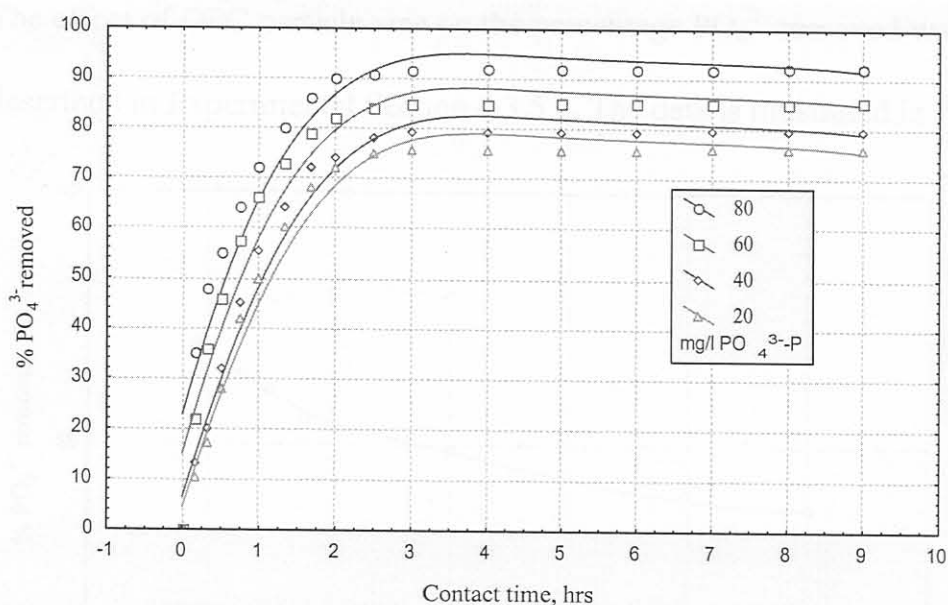
Figure 7.4. Effect of concentration on the kinetics of PO_4^{3-} removal by OPC. (Conditions: 2 g OPC, pH 9.0, 25°C)

The observed increase in the percentage PO_4^{3-} removed with increasing solute concentration (for the same amount of sorbent) is hardly surprising if the system

under study is non-ideal. As mentioned in Sections 1.2.1 and 1.2.2, for non-ideal systems the mass of solute adsorbed per mass of sorbent keeps increasing as the concentration of the solute increases. This has been ascribed to surface heterogeneity in such systems. Interestingly, the initial phosphate concentration does not appear to influence the time it takes (ca 3 hrs) for PO_4^{3-} removal to reach equilibrium.

7.4. Effect of particle size

The effect of OPC particle size on the percentage PO_4^{3-} removed was measured as described in Experimental Section 4.3.5.2. The data is illustrated in Figure 7.5.
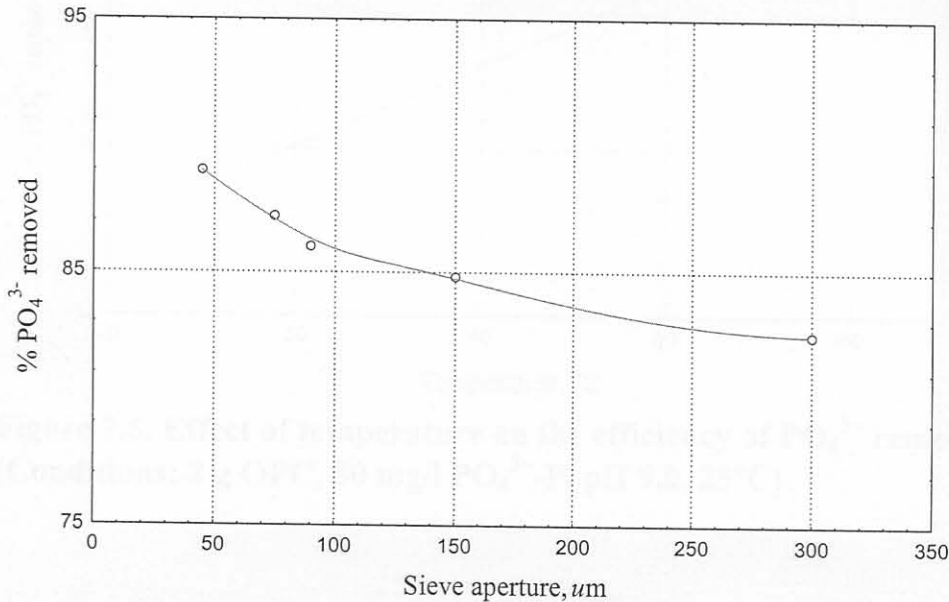
Figure 7.5. Effect of particle size on the efficiency of PO_4^{3-} removal by OPC. (Conditions: 2 g OPC, 80 mg/l PO_4^{3-}-P, pH 9.0, 25°C)

103

Although there was some increase in the percentage PO_4^{3-} removed as the particle size decreased, this increase does not appear to be proportional to the increased surface area.

7.5. Effect of temperature

The effect of temperature on the efficiency of PO_4^{3-} removal was measured as described in Experimental Section 4.3.5.3, and the data is illustrated in Figure 7.6.
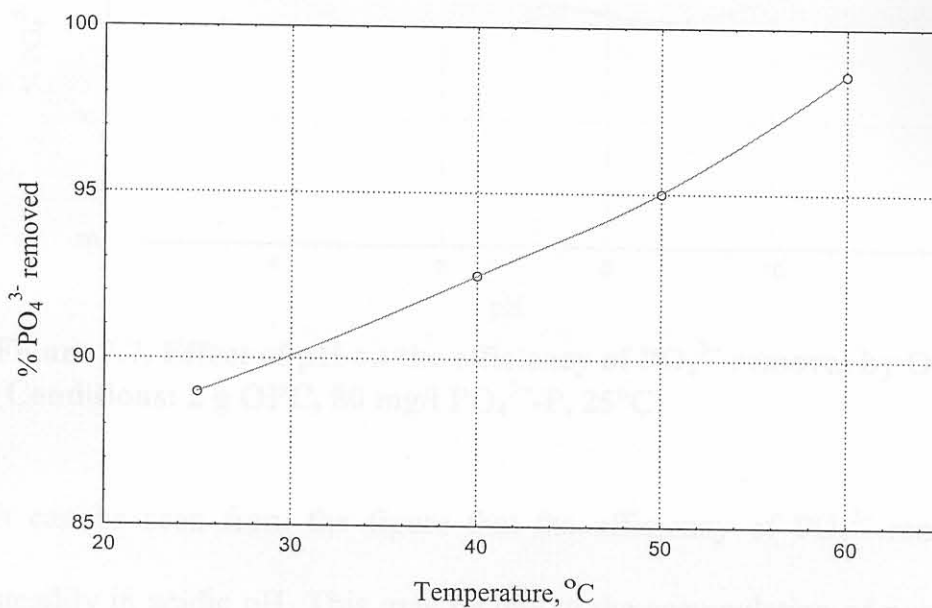
Figure 7.6. Effect of temperature on the efficiency of PO_4^{3-} removal by OPC. (Conditions: 2 g OPC, 80 mg/l PO_4^{3-}-P, pH 9.0, 25°C)

The percent PO_4^{3-} removed was observed to increase with temperature, which is to be expected as the rate of diffusion increases with increasing temperature.

7.6. Effect of pH

The variation of the percentage PO_4^{3-} removed with the initial pH of the aqueous solution was measured as described in Experimental Section 4.3.5.4. The data obtained for OPC is shown in Figure 7.7.
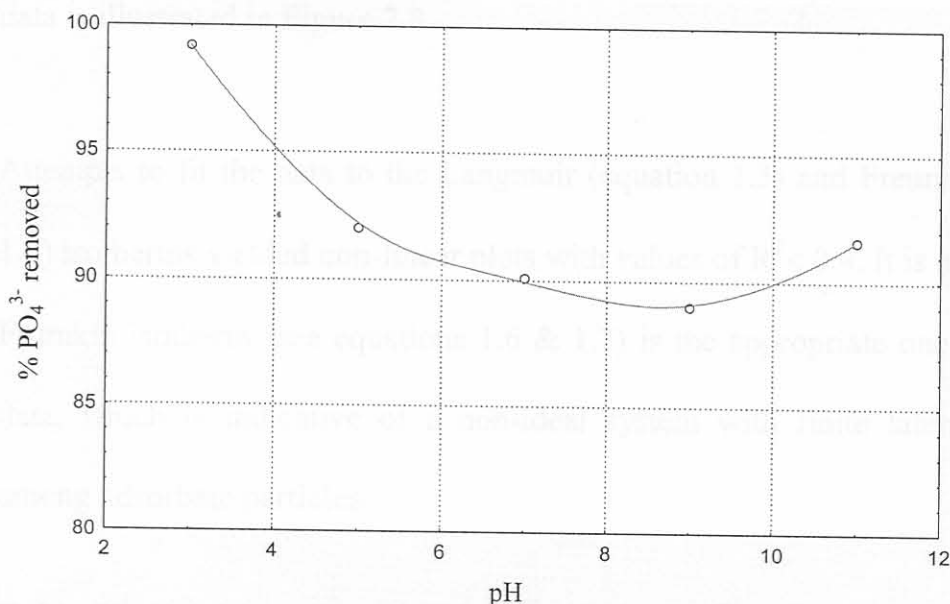
Figure 7.7. Effect of pH on the efficiency of PO_4^{3-} removal by OPC. (Conditions: 2 g OPC, 80 mg/l PO_4^{3-}-P, 25°C)

It can be seen from the figure that the efficiency of PO_4^{3-} removal increases steadily in acidic pH. This may be due to the accumulation of positive charge on the adsorbent surface that increases its affinity for the negatively charged phosphate ions. The observed slight increase in the efficiency of PO_4^{3-} removal beyond pH 9 could be due to the creation of favourable conditions for calcium phosphate precipitation at high pH, thus enhancing the removal of PO_4^{3-} by some dissolved calcium formed by hydration of OPC.

7.7. Adsorption isotherms

Adsorption data for modelling adsorption isotherms was obtained as described in Experimental Section 4.3.6. Table 7.5 shows the experimentally obtained adsorption data for fly ash, and the application of the Frumkin equation (1.7) to the data is illustrated in Figure 7.8.

Attempts to fit the data to the Langmuir (equation 1.3) and Freundlich (equation 1.4) isotherms yielded non-linear plots with values of $R^2 < 0.4$. It is evident that the Frumkin isotherm (see equations 1.6 & 1.7) is the appropriate one for fitting the data, which is indicative of a non-ideal system with finite lateral interactions among adsorbate particles.

Table 7.5. Experimental adsorption data for PO_4^{3-} removal by OPC.

mass of fly ash (g)	mg/l P^a after adsorption	mg P^a adsorbed
0.5	34.4	13.1
2	32.2	13.6
3	31.1	13.8
3.5	28.2	14.4
4	15.6	16.9
5	0.4	19.9

$^a PO_4^{3-}$ (as P)

The Frumkin constants were calculated and are shown in Table 7.6.

106

Table 7.6. Isotherm linear correlation coefficients and Frumkin constants for PO_4^{3-} adsorption by OPC.

Isotherm	R^2	α	β
Frumkin	0.995	4.976	0.004
Langmuir	0.269		
Freundlich	0.139		
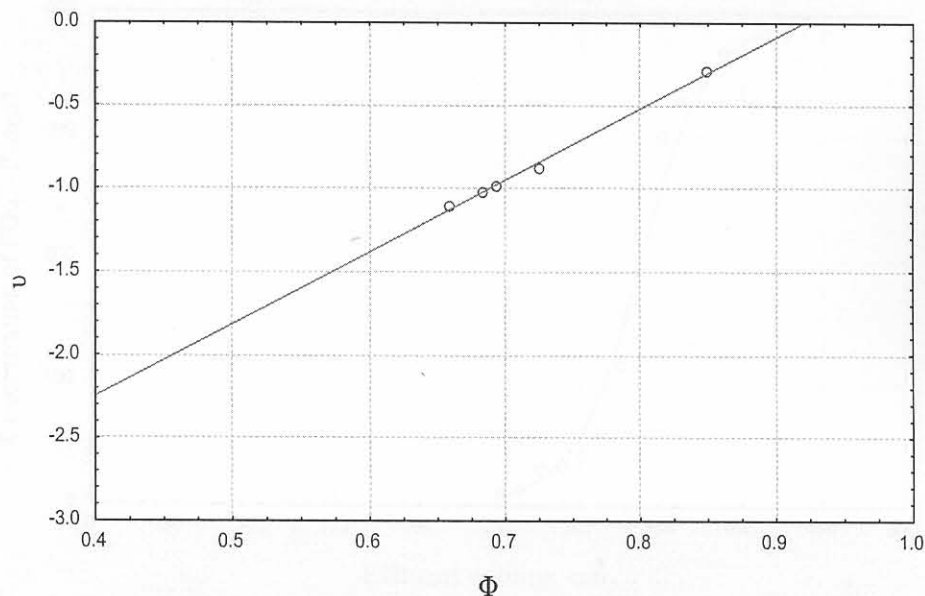
Figure 7.8. Application of the Frumkin equation to the experimental adsorption data (given in Table 7.4) for OPC.

7.8. Breakthrough curves

Data for constructing breakthrough curves was obtained as described in Experimental Section 4.3.7. The data obtained from the breakthrough experiments (see equations 1.15 and 1.16) for OPC are shown in Table 7.7, and a representative breakthrough curve is illustrated in Figure 7.9.

Table 7.7. Breakthrough data for OPC.

t_E^a (min)	V_T (cm^3)	V_Z (cm^3)	h_Z (cm)	C_T (mg PO$_4^{3-}$-P/g)
10.8	412	1142	0.833	83

[a]Breakthrough time
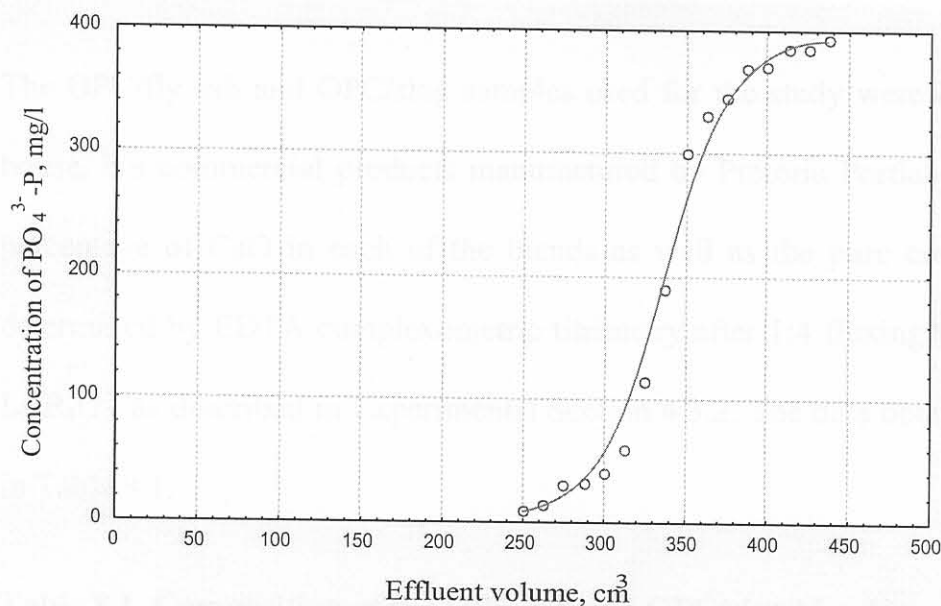
Figure 7.9. Breakthrough curve for PO$_4^{3-}$ removal by OPC.

The curves obtained were good approximations for characteristic symmetrical breakthrough S curves. Average values obtained for the breakthrough time t_E, the effluent volume required for bed exhaustion V_T, V_Z (V_T minus the effluent volume required for breakthrough), the height of the mass transfer zone h_Z, and the adsorption capacity C_T are given in Table 7.7.

An average C_T value of 83 mg PO$_4^{3-}$-P/g was obtained for the OPC.

CHAPTER 8

RESULTS AND DISCUSSION: PHOSPHATE REMOVAL BY

OPC/FA AND OPC/SLAG

8.1. Composition of the cement blends

The OPC/fly ash and OPC/slag samples used for the study were not blended in-house, but commercial products manufactured by Pretoria Portland Cement. The percentage of CaO in each of the blends as well as the pure constituents were determined by EDTA complexometric titrimetry after 1:4 fluxing with anhydrous $Li_2B_4O_7$, as described in Experimental Section 4.3.2. The data obtained are shown in Table 8.1.

Table 8.1. Composition of the OPC/FA and OPC/slag blends.

Adsorbent	% CaO	Calculated composition of blend
FA	4.5	
Slag	34.1	
OPC	63.8	
OPC/FA	57.3	OPC + 11 % FA
OPC/Slag	58.2	OPC + 19 % Slag

The experimentally obtained % CaO values were then used to calculate the composition of the blends using the expression (derived from first principles):

109

$$X \times \% \text{ CaO in FA (or slag)} + (100 - X) \times \% \text{ CaO in OPC}$$
$$= 100 \times \% \text{ CaO in OPC/FA (or OPC/slag) blend}$$

where X is the % FA (or slag) in the blend. The data are given in Table 8.1.

8.2. Kinetics

Figures 8.1 and 8.2 illustrate the percentage PO_4^{3-} removed with time by OPC/FA and OPC/slag respectively, measured as described in Experimental Section 4.3.4.
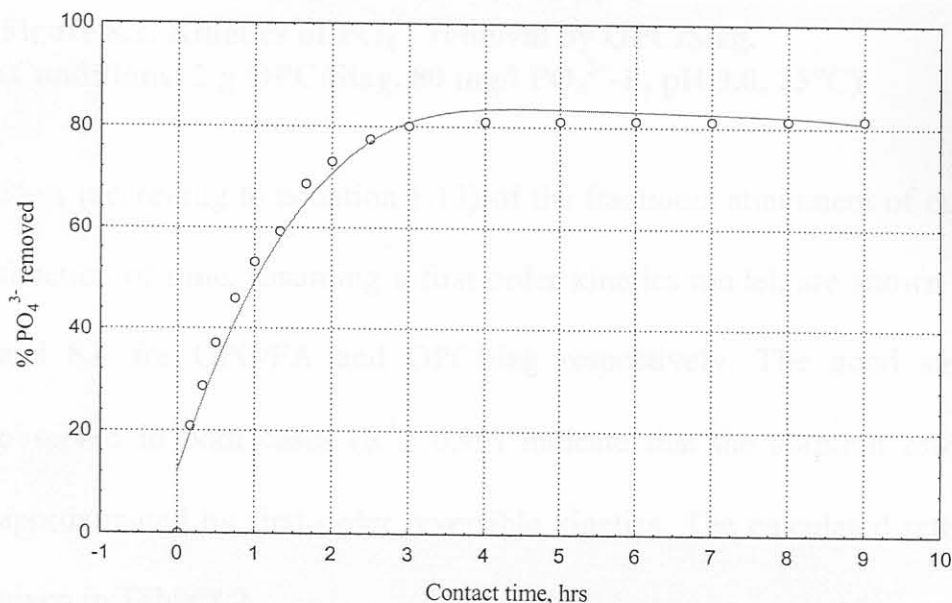
Figure 8.1. Kinetics of PO_4^{3-} removal by OPC/FA.
(Conditions: 2 g OPC/Fly ash, 80 mg/l PO_4^{3-}-P, pH 9.0, 25°C)

It can be seen that for both blends the uptake of PO_4^{3-} practically ceased after a contact time of about 3½ hrs, indicating the onset of dynamic equilibrium.

110
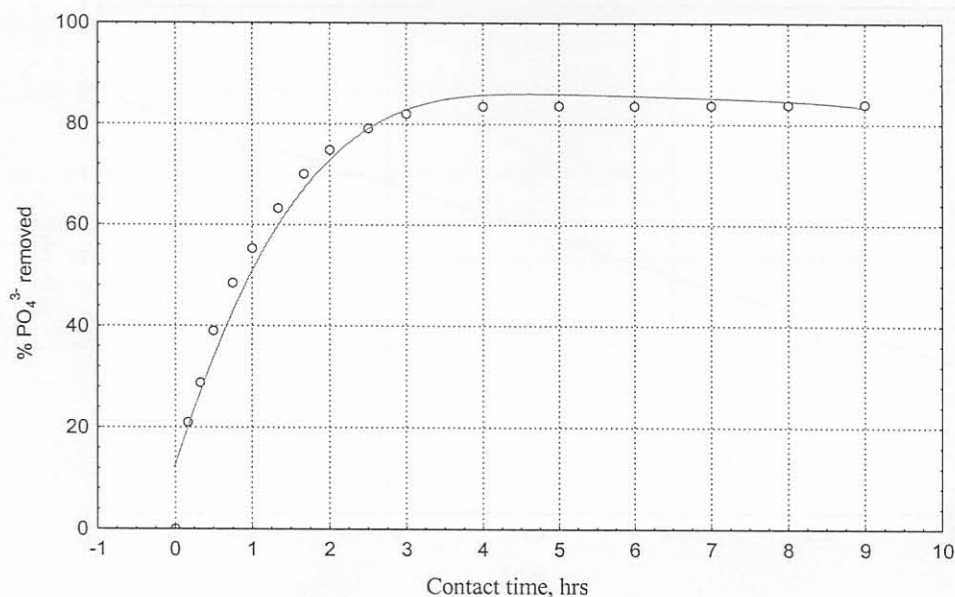
Figure 8.2. Kinetics of PO$_4^{3-}$ removal by OPC/Slag.
(Conditions: 2 g OPC/Slag, 80 mg/l PO$_4^{3-}$-P, pH 9.0, 25°C)

Plots (according to equation 1.12) of the fractional attainment of equilibrium as a function of time, assuming a first order kinetics model, are shown in Figures 8.3 and 8.4 for OPC/FA and OPC/slag respectively. The good straight-line fits observed in both cases (R^2≅ 0.99) indicate that the sorption reactions may be approximated by first order reversible kinetics. The calculated rate constants are given in Table 8.2.

Table 8.2. Values of first order reaction rate constants for PO$_4^{3-}$ removal by OPC/FA and OPC/slag.

Adsorbent	k' (per hour)
OPC + 11 % FA	1.082
OPC + 19 % Slag	1.136

111
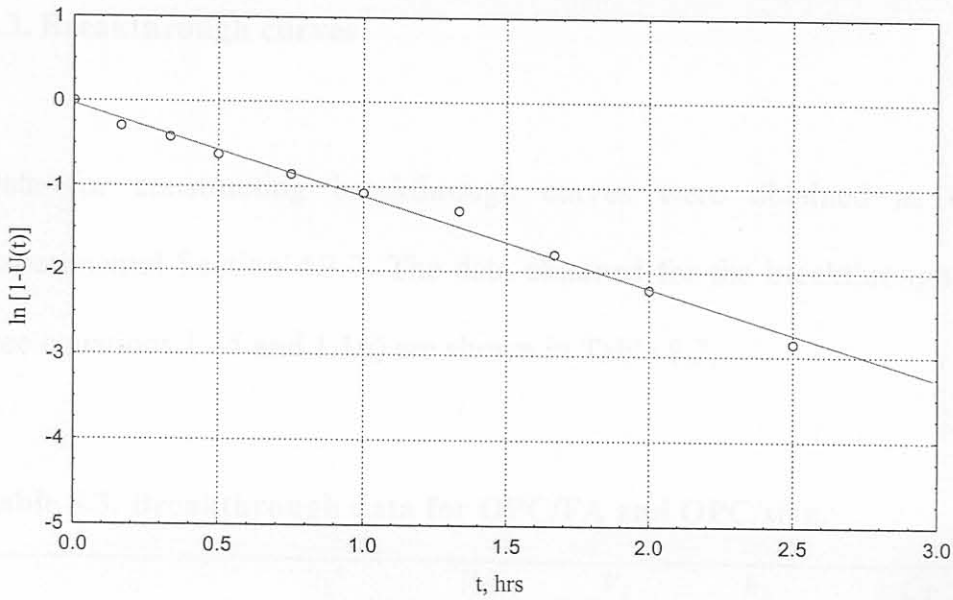
Figure 8.3. Application of first order kinetics to the experimental adsorption data for OPC/FA. (Conditions: 2 g OPC/FA, 80 mg/l PO_4^{3-}-P, pH 9.0, 25°C)
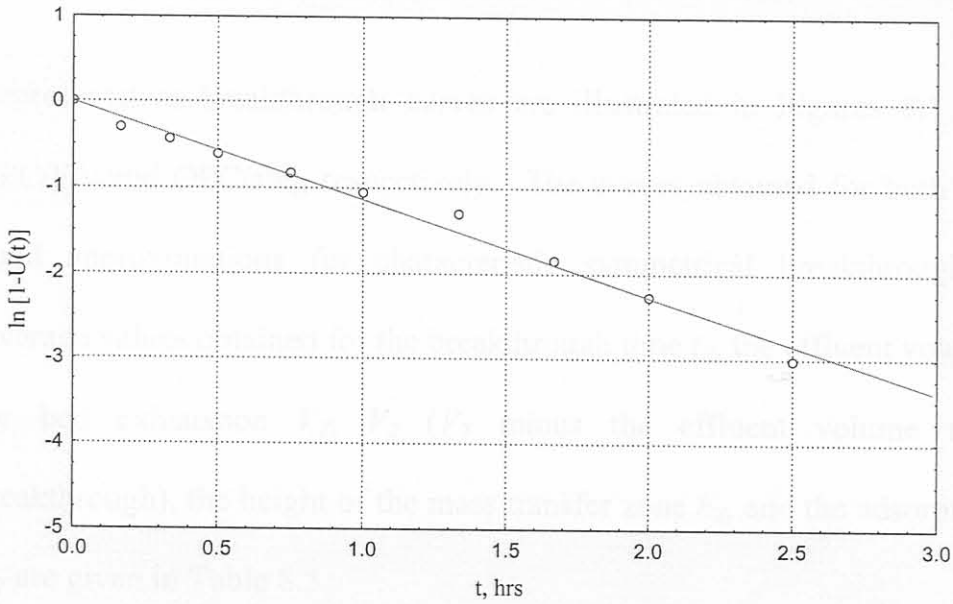
Figure 8.4. Application of first order kinetics to the experimental adsorption data for OPC/Slag. (Conditions: 2 g OPC/Fly ash, 80 mg/l PO_4^{3-}-P, pH 9.0, 25°C)

112

8.3. Breakthrough curves

Data for constructing breakthrough curves were obtained as described in Experimental Section 4.3.7. The data obtained for the breakthrough experiments (see equations 1.15 and 1.16) are shown in Table 8.3.

Table 8.3. Breakthrough data for OPC/FA and OPC/slag.

Adsorbent	$t_E{}^a$ (min)	V_T (cm^3)	V_Z (cm^3)	h_Z (cm)	C_T (mg PO$_4{}^{3-}$-P/g)
OPC + 11 % FA	9.4	375	139	0.910	75
OPC + 19 % Slag	9.9	388	140	0.881	78

[a]Breakthrough time

Representative breakthrough curves are illustrated in Figures 8.5 and 8.6 for OPC/FA and OPC/slag respectively. The curves obtained for both blends were good approximations for characteristic symmetrical breakthrough S curves. Average values obtained for the breakthrough time t_E, the effluent volume required for bed exhaustion V_T, V_Z (V_T minus the effluent volume required for breakthrough), the height of the mass transfer zone h_Z, and the adsorption capacity C_T are given in Table 8.3.

113
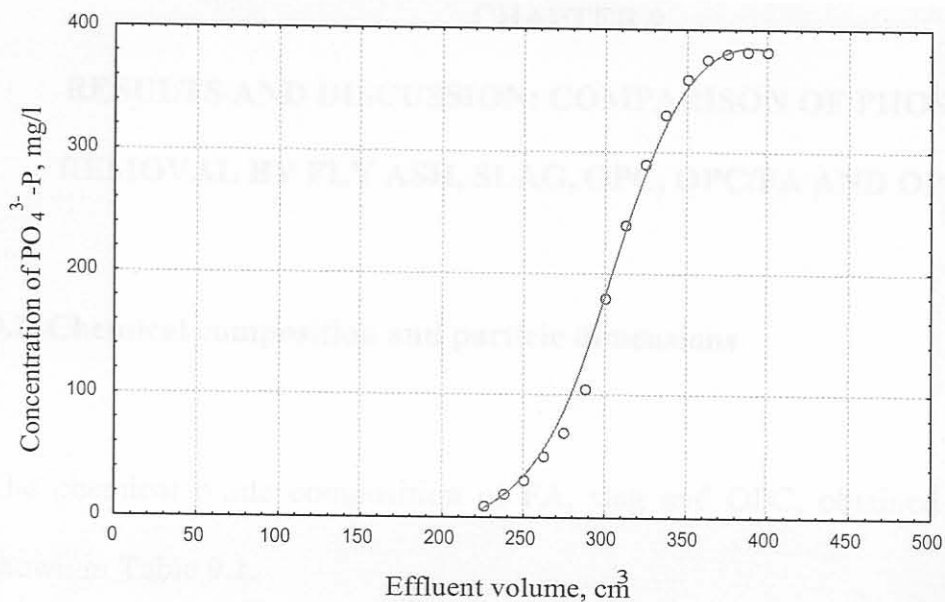
Figure 8.5. Breakthrough curve for PO$_4^{3-}$ removal by OPC/FA.
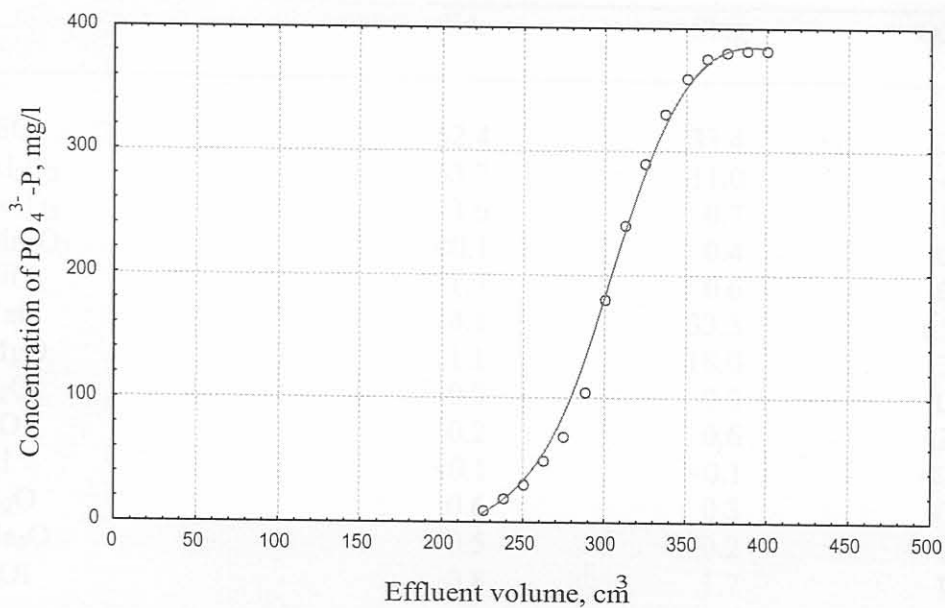
Figure 8.6. Breakthrough curve for PO$_4^{3-}$ removal by OPC/Slag.

114

CHAPTER 9

RESULTS AND DISCUSSION: COMPARISON OF PHOSPHATE REMOVAL BY FLY ASH, SLAG, OPC, OPC/FA AND OPC/SLAG

9.1. Chemical composition and particle dimensions

The chemical oxide composition of FA, slag and OPC, obtained by XRF, are shown in Table 9.1.

Table 9.1. Chemical composition of FA, slag and OPC.

	Mass %		
	FA	Slag	OPC
SiO_2	52.4	33.4	22.5
Al_2O_3	33.7	11.0	4.5
Fe_2O_3	3.6	0.7	1.4
Mn_2O_3	<0.1	0.4	0.9
TiO_2	1.7	0.6	0.2
CaO	4.1	33.3	63.2
MgO	1.1	18.0	3.6
P_2O_5	0.3	0.0	0.2
SO_3	0.2	0.6	2.4
Cl	<0.1	<0.1	<0.1
K_2O	0.6	0.3	0.8
Na_2O	0.5	0.2	0.1
LOI	0.8	1.7	1.0
Total	99.0	100.2	100.8
CaO/SiO_2	0.08	1.00	2.81

The theoretical total is 100 % and the difference between this and the actual total reported is an indication of both the accuracy of the analysis and the possible existence of elements in the sample that had not been analysed for. LOI (loss on ignition) is the mass loss caused by materials vaporised during the heating of the sample to a temperature of 1000 °C for a period of about 30 minutes. Calculated values for lime-silica ratios (CaO/SiO_2) are included in Table 9.1. The high CaO/SiO_2 ratio for OPC compared to slag and fly ash reflects the greater tendency for the former to undergo cementitious reactions (e.g. hydration).

Table 9.2 contains a summary of some important physical properties obtained by Fraunhofer particle diffraction analysis.

Table 9.2. Physical characteristics of FA, slag and OPC.

Characteristic	Value		
	FA	Slag	OPC
Specific surface area (m^2/g)	1.42	1.29	1.38
Mean particle diameter (μm)	25.7	31.4	20.8
Density (g/cm^3)	2.21	2.82	3.02

It can be seen from Table 9.2 that the specific surface areas (1.4, 1.3 and 1.4 m^2/g respectively) of the fly ash, slag and OPC samples used for the study are quite similar. One would therefore expect them to exhibit somewhat similar adsorption

116

capacities if physical adsorption at the surface of the sorbent particles is the sole or principal contributory phenomenon to solute removal, other factors being equal.

9.2. Kinetics

Figure 9.1 illustrates the variation of percentage removal of PO_4^{3-} with time for the different adsorbents. It can be seen that OPC removed PO_4^{3-} at the fastest rate and fly ash the slowest. The uptake of PO_4^{3-} by OPC virtually ceased after a contact time of about 3 h, compared to about 6 h for fly ash, with 84 and 34 percent PO_4^{3-} removal at equilibrium, respectively.
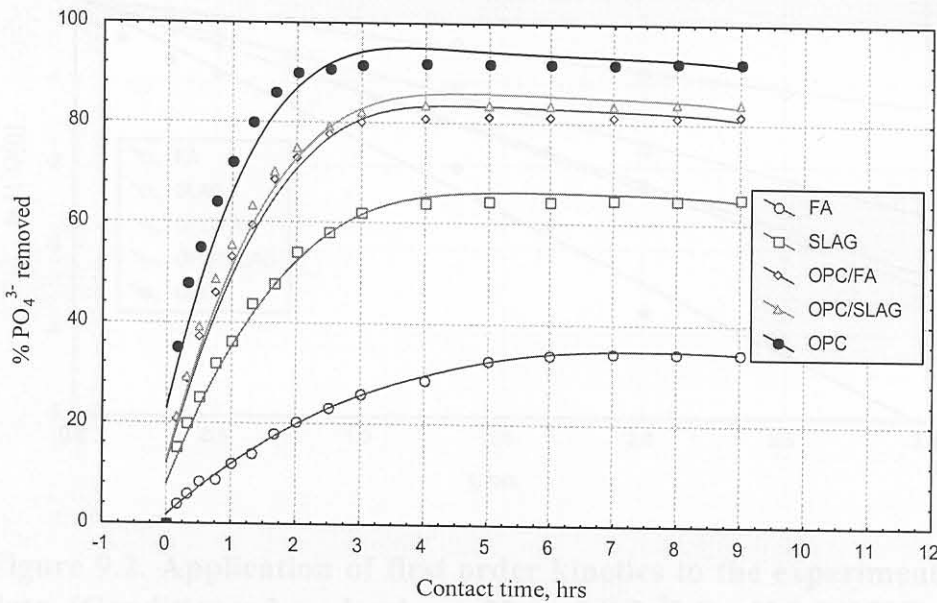
Figure 9.1. Kinetics of PO_4^{3-} removal by the adsorbents.
(Conditions: 2 g adsorbent, 80 mg/l PO_4^{3-}-P, pH 9.0, 25°C)

Blending of OPC with fly ash or slag was observed to lead to an overall decrease in the rate and efficiency of PO_4^{3-} removal. Although slag removes PO_4^{3-} better than fly ash, 19 % replacement of OPC with slag evidently results in a blend with a lower PO_4^{3-} removal efficiency than 11 % replacement with fly ash.

Curves plotted according to equation (1.12) are presented in Figure 9.2. The good straight-line fits observed (linear correlation coefficients $R^2 \geq 0.99$) indicates that the sorption reactions may be approximated by first-order reversible kinetics; the calculated rate constants are given in Table 9.3.
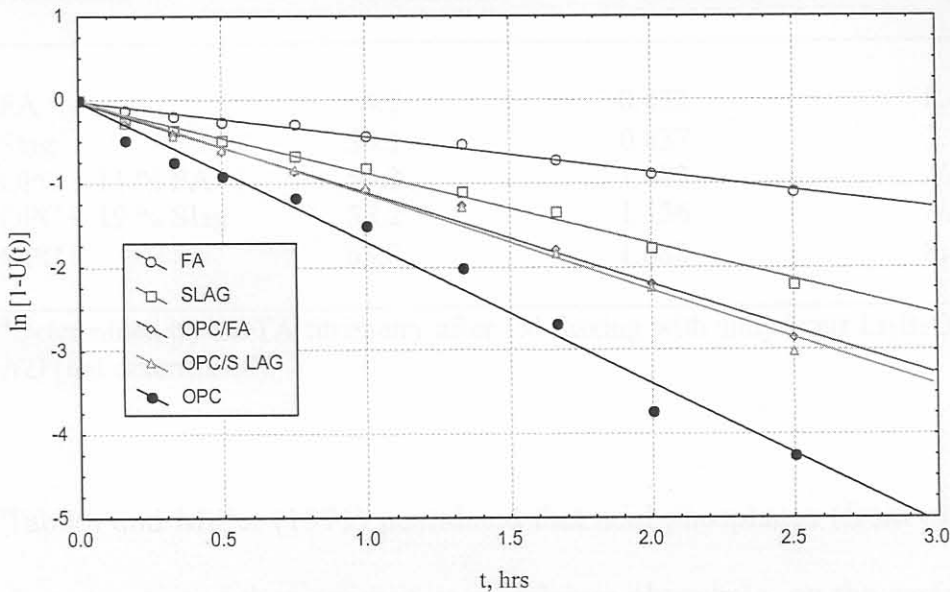
Figure 9.2. Application of first order kinetics to the experimental adsorption data. (Conditions: 2 g adsorbent, 80 mg/l PO_4^{3-}-P, pH 9.0, 25°C)

Over the range of sorbent-solution agitation rates studied (100-140 cycles per minute horizontally) it was observed that the sorption rate was not affected by the

118

rate of mixing. This suggests that diffusion through the pores of sorbent particles rather than diffusion to the film at the sorbent particle-aqueous solution interface were rate limiting, which would provide evidence that intra-particle diffusion is the controlling resistance rather than external diffusion. The values of intra-particle diffusion constants calculated using equation (1.13) are given in Table 9.3. The value obtained for OPC was an order of magnitude greater than that for fly ash.

Table 9.3. The values of first order reaction rate constants and intra-particle diffusion coefficients.

Adsorbent	% CaO[a]	k' (per hour)	D (cm^2/s)
FA	4.5	0.423	8.40×10^{-12}
Slag	34.1	0.837	2.51×10^{-11}
OPC + 11 % FA	57.3	1.082	ND
OPC + 19 % Slag	58.2	1.136	ND
OPC	63.8	1.682	8.72×10^{-11}

[a]Determined by EDTA titrimetry after 1:4 fluxing with anhydrous $Li_2B_4O_7$.
ND (not determined).

Tabikh and Miller (1971) postulated that acid phosphates (from phosphogypsum) deprotonate and then precipitate as calcium phosphate, on the surface of the grain in the alkaline region in the immediate vicinity of a hydrating particle. This provides a protective barrier against attack by water, resulting in the delayed setting times observed. Hence, the affinity of phosphate (the adsorbate, from the acid phosphate KH_2PO_4) for CaO (in the adsorbent) observed in this study is

119

hardly surprising. This would also explain the reason why pre-treatment of the phosphogypsum by washing with milk of lime (Erdogan et. al., 1994) was successful in minimising the effect on setting time extension.

9.3. Effect of concentration

The rate and separation efficiency of PO_4^{3-} from aqueous solution by these adsorbents was found to increase with the initial phosphate concentration over the concentration range studied (see Figures 5.6, 6.5 and 7.4); this is indicative of a non-ideal system, as explained in Section 5.4. Changes in concentration alone did not appear to significantly affect the time required for PO_4^{3-} adsorption to reach equilibrium.

9.4. Effect of particle size

Figure 9.3 shows the effect of particle size on the efficiency of PO_4^{3-} removal by fly ash, slag and OPC. Although there was some increase in the percentage PO_4^{3-} removed as the adsorbent particle size decreased, this increase was not proportional to the increased surface area. This diminished effect of increasing surface area on the percentage PO_4^{3-} removed is an indication that for these

120

adsorbents physical adsorption at the surface of the sorbent particles is probably not the sole phosphate removal mechanism.
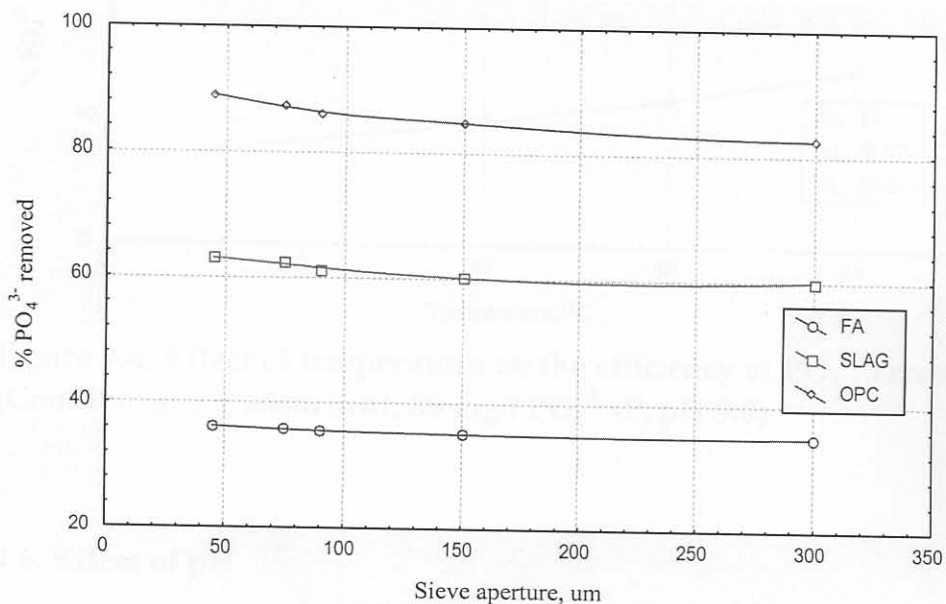
Figure 9.3. Effect of particle size on the efficiency of PO_4^{3-} removal. (Conditions: 2 g adsorbent, 80 mg/l PO_4^{3-}-P, pH 9.0, 25°C)

9.5. Effect of temperature

The effect of temperature on the efficiency of PO_4^{3-} removal by fly ash, slag and OPC is illustrated in Figure 9.4. The percentage PO_4^{3-} removed was observed to increase with increasing temperature. This is not surprising, since the rate of intra-particle diffusion (see Section 9.2) is expected to increase with increasing temperature.
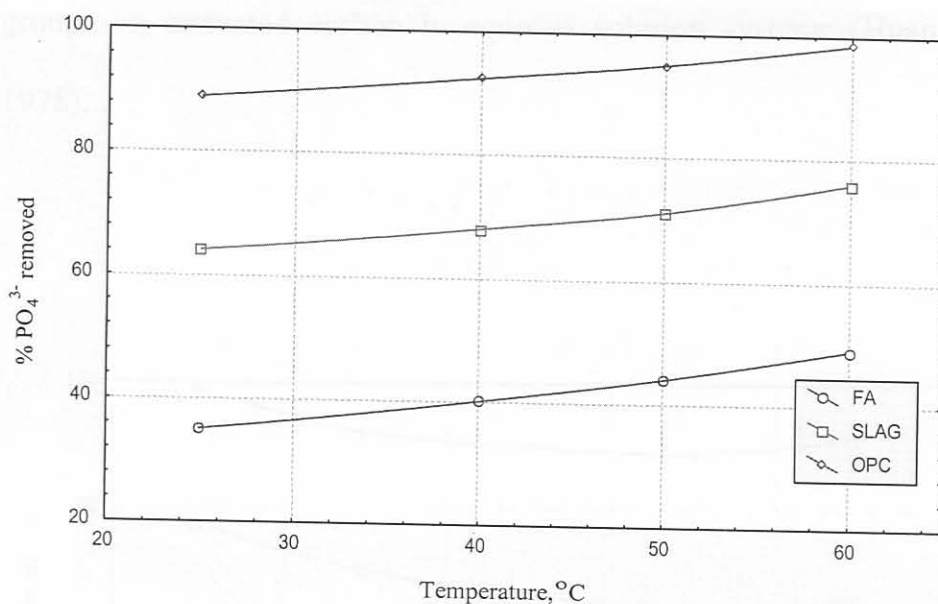
Figure 9.4. Effect of temperature on the efficiency of PO$_4^{3-}$ removal. (Conditions: 2 g adsorbent, 80 mg/l PO$_4^{3-}$-P, pH 9.0)

9.6. Effect of pH

Figure 9.5 illustrates the variation of percentage PO$_4^{3-}$ removed with the <u>initial</u> pH of the aqueous solution that was added to fly ash, slag and OPC. It can be seen from the figure the efficiency of PO$_4^{3-}$ removal increases steadily in acidic pH. This is probably due to the accumulation of positive charge on the adsorbent surface (at low pH) that increases its affinity for the negatively charged phosphate ions. Some of the oxides (especially those of Al and Si) in these sorbents can be expected to form hydroxide complexes in aqueous solution whose basic or acidic dissociation may lead to an accumulation of net positive or negative charge at the solid-solution interface. Similar behaviour has been reported for surface hydroxo

groups on activated carbon in aqueous solution systems (Huang and Ostovic, 1978).
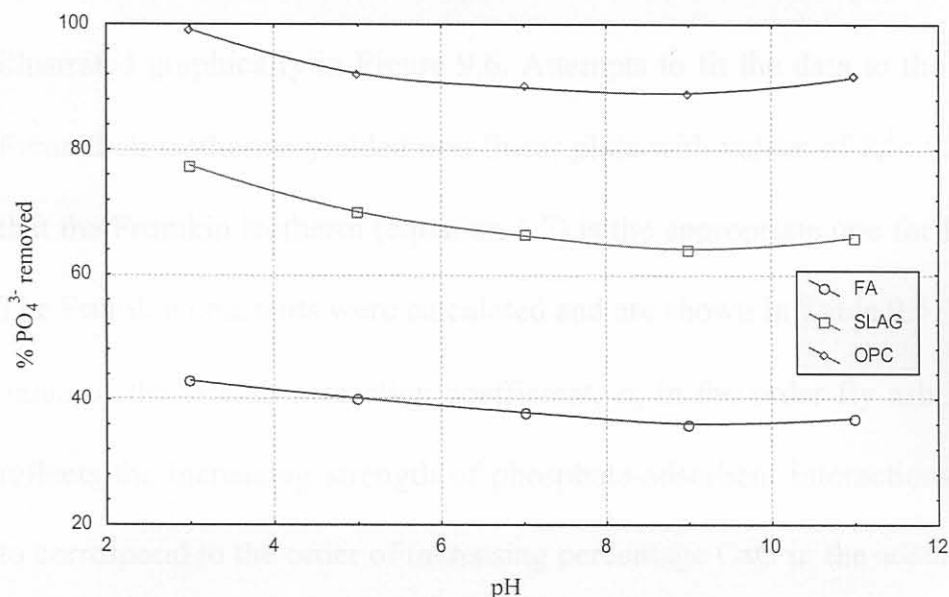
Figure 9.5. Effect of pH on the efficiency of PO_4^{3-} removal.
(Conditions: 2 g adsorbent, 80 mg/l PO_4^{3-}-P, 25°C)

The observed slight increase in the efficiency of PO_4^{3-} removal beyond pH 9 could be due to the creation of favourable conditions for calcium phosphate precipitation at high pH, thus enhancing the removal of PO_4^{3-} by dissolved calcium formed by hydration of the adsorbent.

123

9.7. Adsorption isotherms

Table 9.4 shows the experimentally obtained adsorption data for fly ash, slag and

OPC. The fit of these data to the Frumkin isotherm (see equations 1.6 & 1.7) are

shown in Table 9.5, and the application of the Frumkin equation to the data is

illustrated graphically in Figure 9.6. Attempts to fit the data to the Langmuir and

Freundlich isotherms yielded non-linear plots with values of $R^2 < 0.4$. It is evident

that the Frumkin isotherm (equation 1.7) is the appropriate one for fitting the data.

The Frumkin constants were calculated and are shown in Table 9.5. The increasing

value of the lateral interaction coefficient, α, in the order fly ash, slag and OPC

reflects the increasing strength of phosphate-adsorbent interactions. This appears

to correspond to the order of increasing percentage CaO in the adsorbents.

Table 9.4. Experimental adsorption data for FA, slag and OPC.

	FA		Slag		OPC	
Mass of adsorbent (g)	P^a after adsorption (mg/l)	P^a adsorbed (mg)	P^a after adsorption (mg/l)	P^a adsorbed (mg/l)	P^a after adsorption (mg/l)	P^a adsorbed (mg)
0.5	72.8	5.44	48.5	10.3	34.4	13.1
2	71.9	5.62	46.7	10.6	32.2	13.6
3	71.4	5.72	45.8	10.8	31.1	13.8
3.5	70.2	6.43	43.5	11.3	28.2	14.4
4	65.0	7.00	33.7	13.3	15.6	16.9
5	58.7	8.26	21.7	15.7	0.4	19.9

$^aPO_4^{3-}$(as P)

Table 9.5. Isotherm constants and linear correlation coefficients for FA, slag and OPC.

Adsorbent	Freundlich R^2	Langmuir R^2	Frumkin		
			R^2	α	β
FA	0.2793	0.3763	0.9918	3.061	0.0254
Slag	0.2333	0.2687	0.9974	3.780	0.0149
OPC	0.1385	0.2699	0.9945	4.976	0.0042
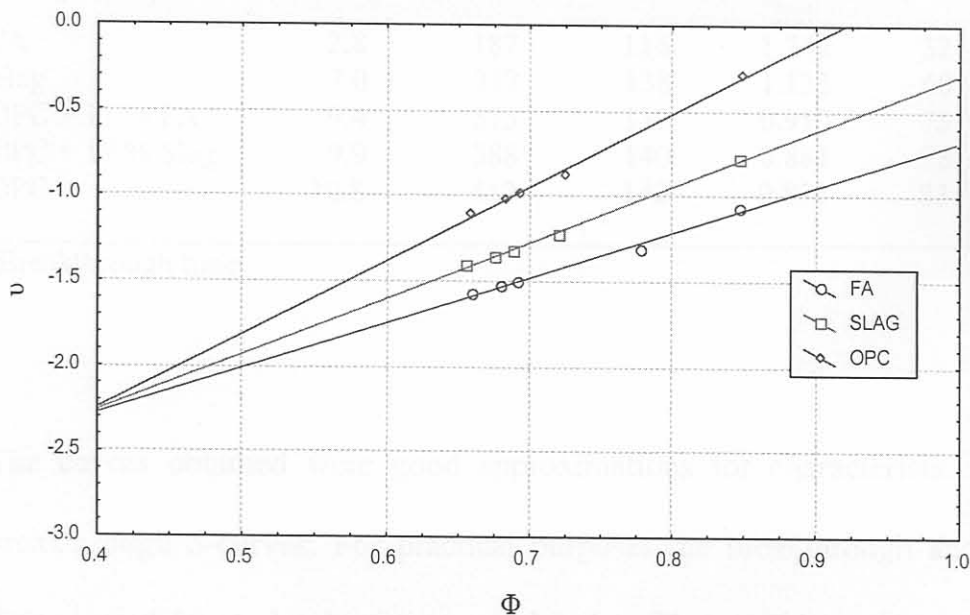
Figure 9.6. Application of the Frumkin equation to the experimental adsorption data (given in Table 9.4) for FA, slag and OPC.

It must be pointed out that magnesium, like calcium, will also dissolve to a certain extent and contribute to the observed PO_4^{3-} removal. However, this contribution appears to be relatively minor, considering the fact that slag contains nearly six times as much MgO as OPC (see Table 9.3).

9.8. Breakthrough curves

The data obtained for the breakthrough experiments for the various adsorbents are shown in Table 9.6, and typical breakthrough curves are represented in Figure 9.7.

Table 9.6. Breakthrough data for FA, slag, OPC, OPC/FA and OPC/slag.

Adsorbent	t_E[a] (min)	V_T (cm^3)	V_Z (cm^3)	h_Z (cm)	C_T (mg PO$_4^{3-}$-P/g)
FA	2.8	187	116	1.742	32
Slag	7.0	312	138	1.133	60
OPC + 11 % FA	9.4	375	139	0.910	75
OPC + 19 % Slag	9.9	388	140	0.881	78
OPC	10.8	412	142	0.833	83

[a]Breakthrough time

The curves obtained were good approximations for characteristic symmetrical breakthrough *S*-curves. For practical purposes the breakthrough and exhaustion times were taken to be the times at which the effluent concentration reached 5 and 95 %, respectively, of the influent concentration.

The value of the height of the exchange zone h_Z decreases in the order: fly ash, slag, OPC/fly ash, OPC/slag, OPC. This is a measure of increasing rate of ion exchange and/or phosphate removal, while the increasing value of the breakthrough time t_E is indicative of increasing adsorption capacity. These

126

experimentally obtained (by graphical integration of Eq.(1.16) values may be extrapolated to estimate the capacity of a large-scale bed (Helfferich, 1962).
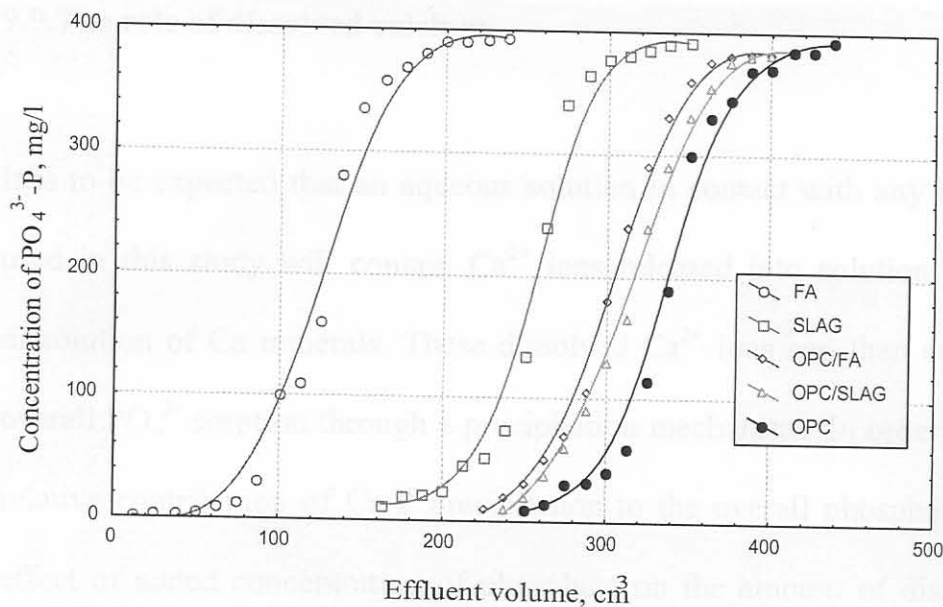
Figure 9.7. Breakthrough curves for PO$_4^{3-}$ removal by FA, slag, OPC, OPC/FA and OPC/slag.

The value of 32 mg/g obtained in this study for phosphate adsorption on fly ash is of the same order of magnitude as the 67 mg/g reported by Akgerman and Zardkoohi (1996) for the adsorption of phenol on an American fly ash. Sakadevan and Bavor (1998) reported a value of 44.2 mg/g for phosphate adsorption on slag, compared to the 60 mg/g obtained in this study. It must be pointed out that Sakadevan and Bavor (1998) followed the common practise of calculating adsorption capacity from the best-fit adsorption isotherm. The breakthrough

127

curves approach used in this study, although more time-consuming, offers a more direct experimental determination.

9.9. The role of dissolved calcium

It is to be expected that an aqueous solution in contact with any of the materials used in this study will contain Ca^{2+} ions released into solution through partial dissolution of Ca minerals. These dissolved Ca^{2+} ions can then contribute to the overall PO_4^{3-} sorption through a precipitation mechanism. In order to estimate the relative contribution of Ca-P precipitation to the overall phosphate sorption, the effect of added concentration of phosphate on the amount of dissolved calcium was investigated.

9.9.1. Procedure

2 g of sorbent were shaken continuously with 200 ml of 0, 20, 40, 60 and 80 mg/l PO_4^{3-}-P solution (initial pH 9.0, 25°C) for 10 hours, after which the concentration of calcium in the filtered (45-μm membrane) supernatant solution was measured by flame atomic absorption spectrometry. A Varian SpectrAA220 instrument supplied by SMM Instruments (Pty) Limited, Johannesburg, was used. The experimental conditions used were as follows: flame: N_2O-C_2H_2, lamp current: 10 mA, λ: 422.7 nm, slit width: 0.5 nm.

128

9.9.2. Results and discussion

The observed effect of added concentration of phosphate on the amount of
dissolved calcium is shown in Figure 9.8.
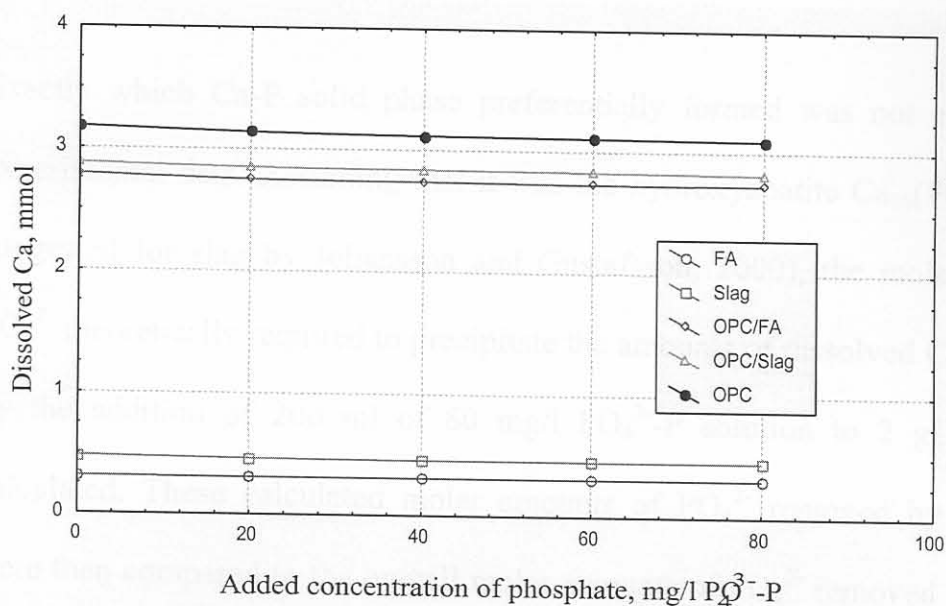
**Figure 9.8. Effect of added concentration of phosphate on the amount of
dissolved calcium.**

(Conditions: 2 g sorbent, 200 ml PO_4^{3-} solution, pH 9.0, 25°C)

The amount of dissolved calcium decreased as the initial concentration of the
added phosphate solution increased. This was taken as evidence for Ca-P
precipitation. This phenomenon appears to be relatively more pronounced for OPC

and its blends than it is for slag and FA, which is hardly surprising. OPC is expected to release more Ca^{2+} ions into solution via dissolution since it contains a larger amount of Ca to start with (see Table 9.1), and also has a greater tendency to undergo hydration, which releases additional into solution (see Equations 2.3 and 2.4).

Exactly which Ca-P solid phase preferentially formed was not clear from the experimental data. Assuming that it was the hydroxyapatite $Ca_{10}(PO_4)_6(OH)_2$ (as suggested for slag by Johansson and Gustafsson, 2000), the molar amounts of PO_4^{3-} theoretically required to precipitate the amounts of dissolved Ca^{2+} consumed by the addition of 200 ml of 80 mg/l PO_4^{3-}-P solution to 2 g sorbent were calculated. These calculated molar amounts of PO_4^{3-} removed by precipitation were then compared to the overall molar amounts of PO_4^{3-} removed when 200 ml of 80 mg/l PO_4^{3-}-P solution is added to 2 g sorbent (see Figure 9.1), to obtain estimates for the percentage of PO_4^{3-} removed by Ca-P precipitation. The results are shown in Table 9.7.

Table 9.7. Estimated relative contribution of Ca-P precipitation to the overall phosphate sorption.

Sorbent	Mol PO_4^{3-} removed		% PO_4^{3-} removal by Ca-P precipitation
	Overall	By Ca-P precipitation	
FA	1.8×10^{-4}	2.1×10^{-6}	1.2
Slag	3.3×10^{-4}	1.6×10^{-5}	4.8
OPC+11% FA	4.2×10^{-4}	3.6×10^{-5}	8.6
OPC+19% Slag	4.3×10^{-4}	3.8×10^{-5}	8.8
OPC	4.7×10^{-4}	4.6×10^{-5}	9.8

As can be seen from the entries in the table, the molar amounts of phosphate removed by Ca-P precipitation are one (two in the case of fly ash) order of magnitude smaller than the overall amounts sorbed. Similar results were obtained when the calculations were repeated for other known Ca-P solid phases, such as tricalcium phosphate $Ca_3(PO_4)_2$, amorphous calcium phosphate $Ca_4H(PO_4)_3$ and brushite $CaHPO_4.2H_2O$. The contribution of Ca-P precipitation appears to be only marginal for fly ash, and even for OPC is less than ca.10 %.

Adsorption is evidently the major contributing mechanism to the overall phosphate removal. There are other observations that would be difficult to explain if precipitation were the major contributing mechanism compared to adsorption. Firstly, the process follows first order kinetics and takes several hours to reach completion, whereas precipitation reactions are typically much faster. Secondly,

131

the experimental data fits the Frumkin adsorption isotherm very closely. Thirdly, phosphate removal efficiency increases with increasing temperature. If precipitation were dominant, an increase in temperature would probably result in re-dissolution of precipitate and hence decreased phosphate removal. Fourthly, more phosphate is removed at lower pH. The solubility of the Ca-P solid phase is expected to decrease at lower pH due to decreased concentration of phosphate, so less phosphate removal would be expected at low pH.

9.10. Report on production of bricks

The possibility of producing bricks from a bed of sand and OPC, OPC/slag or OPC/FA, after being used to remove phosphate from aqueous solution, was investigated as a possible added-value application.

9.10.1. Procedure

A 20-mg/l PO_4^{3-}-P aqueous solution, sand and OPC, OPC/FA or OPC/slag were weighed (the calculated amounts are shown in Table 9.8.) and mixed to uniform consistency. The mixtures were poured into 7 cm × 7 cm × 7 cm lubricated moulds and air bubbles removed by vibration. The moulds were placed in plastic containers under a water vapour saturated atmosphere for 1 day, after which they were removed and placed in water for specified curing periods. The bricks were

132

tested for their compressive strengths within 5 min of their removal from water, according to the standard method for concrete masonry units in South Africa (SABS, 1984). This involved placing the brick correctly on the testing machine, applying a pre-load of 5 kN (without shock) to the brick and then increasing the load at a uniform stress rate of about 15 MPa/min until the brick failed. The failure load was recorded and used to calculate the compressive strength. The testing machine used was a Farnell press (D. Kind laboratory Supplies, Johannesburg).

9.10.2. Data and calculations

The mix proportions and calculated amounts of constituents required for the mixtures used to produce the test bricks are shown in Table 9.8.

Table 9.8. Mix proportions used for producing test bricks.

Mixture	Sand : OPC	Amounts				
		Water (cm^3)	Sand (g)	OPC (g)	FA (g)	Slag (g)
1	1 : 2	214	237.4	474.8	-	-
2	1 : 2 + 15% FA	214	130.6	474.8	106.8	-
3	1 : 2 + 15% slag	214	130.6	474.8	-	106.8

Water to cement ratio, W/C = 0.3

9.10.3. Results and discussion

The strength of the bricks produced according to the mix proportions shown in Table 9.8 are given in Table 9.9.

Table 9.9. Brick compressive strength.

Mixture	Curing period (days)	Compressive Strength (kN)	(MPa)[a]
1	2	37	7.6
	7	80	16.3
	14	120	24.5
	28	180	36.7
2	2	35	7.1
	7	60	12.2
	14	90	18.4
	28	120	24.5
3	2	20	4.1
	7	35	7.1
	14	50	10.2
	28	95	19.4

[a] $1\ Pa = 1\ N/m^2$, Area of a brick $= 7\ cm \times 7\ cm = 0.0049\ m^2$

Figure 9.9 illustrates the strength development graphically. The compressive strengths of the water-cured bricks were found to increase in the order OPC/slag, OPC/fly ash, OPC. In South Africa bricks must meet a minimum compressive strength requirement of 7.0 MPa after 28 days (SABS, 1984) before they can be approved for building purposes. The results clearly show that the bricks produced

and tested in this study more than meet this requirement, even after just 7 days of curing.
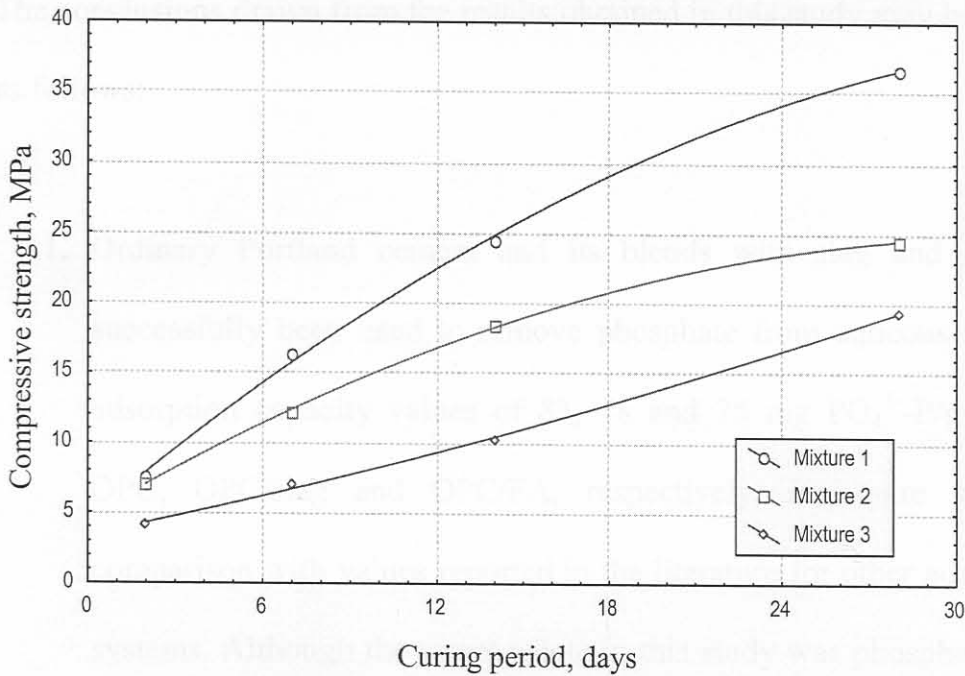
Figure 9.9. Strength development in the bricks produced.

135

CHAPTER 10

CONCLUSIONS

The conclusions drawn from the results obtained in this study may be summarised as follows:

1. Ordinary Portland cement and its blends with slag and fly ash have successfully been used to remove phosphate from aqueous solution. The adsorption capacity values of 83, 78 and 75 mg PO_4^{3-}-P/g obtained for OPC, OPC/slag and OPC/FA, respectively, are quite substantial in comparison with values reported in the literature for other adsorbent-solute systems. Although the target solute in this study was phosphate, it will not be surprising if, as reported for slag in the literature, these materials are also found to be capable of removing other pollutants such as heavy metals from aqueous solution. This study suggests a novel application for these traditional construction materials, namely, as low cost adsorbents for laboratory studies on the removal of impurities from aqueous solution.

2. Improved phosphate removal efficiency is obtainable at higher solute concentration, higher temperature, lower pH and smaller adsorbent particle size, albeit to varying degrees. Using OPC to illustrate this statement, the following improvements in phosphate removal efficiency were observed

136

(for 2 g adsorbent agitated with 200 ml of phosphate solution, 80 mg/l PO_4^{3-}-P at 25°C and initial pH 9.0 unless otherwise stated): 76 and 92 % for 20 and 80 mg/l PO_4^{3-}-P, 89 and 98 % at 25 and 60°C, 89 and 99 % at initial pH 9 and 3, and 82 and 89 % for >300 and 45-75 μm particle fractions, all respectively.

3. The predominant mechanism contributing to the removal of phosphate from aqueous solution is evidently adsorption. The rate of phosphate adsorption by these cementitious materials follows first order kinetics, and the experimental adsorption data may be modelled by the Frumkin isotherm. Precipitation of phosphate ions by dissolved calcium ions contributes to the overall phosphate removal. However, the contribution of the Ca-P mechanism is minor.

4. Due to environmental conditions that occur in the field. Care must be taken in trying to extrapolate the results of a laboratory study to the field situation. However, this study suggests that OPC, OPC/slag and OPC/FA may be capable of removing phosphate from wastewater. This concept, as a possible application, merits further investigation, probably on a pilot scale. Obviously the levels of heavy metal leachate from the materials into the water would have to be closely monitored.

5. Another important consideration related to the recommendation made in 4 above is the question of what to do with the phosphate-contaminated material once it has done its job. It must be pointed out that this issue is a challenge that also applies to the established method of using lime for removing phosphate from wastewater. In that method the spent lime sludge is dewatered and then simply discarded, or calcined in a furnace to recover part of the lime. Since the materials suggested involved in this study are used in the construction industry, it was logical to envisage the production of masonry bricks from the spent material. The results of this study suggest that high strengths are indeed attainable. As long as high compressive strengths are obtained, the actual cement to aggregate ratio required to produce this strength should not be of crucial importance, since this would be an added value process anyway. The possible long term effect of immobilized phosphate on the strength of the bricks will have to be investigated further.

APPENDIX 1

PUBLICATIONS & PRESENTATIONS ON THIS STUDY

An investigation of phosphate ion adsorption from aqueous solution by fly ash and slag, 2nd Young Cement and Concrete Engineers', Scientists' and Technologists' Conference, University of Cape Town, October 12, **1999**.

NM Agyei, CA Strydom, and JH Potgieter, *An investigation of phosphate ion adsorption from aqueous solution by fly ash and slag*, Cement and Concrete Research, 30(5), 823-826, **2000**.

An investigation of phosphate ion adsorption from aqueous solution by pozzolanic materials, 35th Convention of the South African Chemical Institute, Potchfestroom University for CHE, September 24-29, **2000**.

NM Agyei, CA Strydom, and JH Potgieter, *The removal of phosphate ions from aqueous solution by fly ash, slag, ordinary Portland cement and related blends*, Cement and Concrete Research, 32(12), 1889-1897, **2002**.

Estimation of the capacity of South African coal fly ash for phosphate ion removal from aqueous solution, 36th Convention of the South African Chemical Institute, University of Port Elizabeth, July 1-5, **2002**.

Utilization of South African coal fly ash for phosphate ion removal from aqueous solution, 11th International Congress of the Chemistry of Cement, ICC, Durban, May 11-16, **2003**.

NM Agyei, JH Potgieter, and CA Strydom, *A novel application of building materials in pre-treatment of wastewater*, Unpublished Manuscript.

APPENDIX 2

PREVIOUS PUBLICATIONS

AM Stalcup and NM Agyei, *Heparin: a chiral mobile phase additive for capillary zone electrophoresis*, Analytical Chemistry, 66, 3054-3059, **1994**.

NM Agyei, KH Gahm, and AM Stalcup, *Chiral separations using heparin and dextran sulphate in capillary zone electrophoresis*, Analytica Chimica Acta, 307, 185-191, **1995**.

NM Agyei, *Capillary zone electrophoretic enantioseparation of racemic antihistamines by dextran sulphates*, Analytica, 5(3), 14-20, **1997**.

NM Agyei, *Estimation of chloroquine-heparin binding constants by capillary zone electrophoresis*, South African Journal of Chemistry, 51(1), 60-62, **1998**.

REFERENCES

Adams, L.D., *Problems involving the analysis and use of fly ash in the cement industry*, Paper 9-T-80P, presented at the American Ceramic Society Pacific Coast regional meeting, 1980.

Adamson, A.W., *Physical Chemistry of Surfaces*, Wiley, New York, 1990.

Aggarwal, D., Goyal, M., and Bansal, R.C., *Adsorption of chromium by activated carbon from aqueous solution*, Carbon, 37, 1989-1997, 1999.

Ajmal, M., Khan, A.H., Ahmad, S., and Ahmad, A., *Role of sawdust in the removal of copper (II) from industrial wastes*, Water Research, 32, 3085-3091, 1998.

Akgerman, A., and Zardkoohi, M., *Adsorption of phenolic compounds on fly ash*, Journal of Chemical Engineering Data, 41, 185-187, 1996.

Aldrich, *A handbook of fine chemicals and laboratory equipment*, Sigma-Aldrich Corporation, 2003/2004.

Allen, T., *Particle size measurement*, Chapman and Hall, New York, 1974.

American Association of State Highway and Transportation Officials, *Standard specification for materials, Ground iron blast furnace slag for use in concrete and mortars*, AASHTO Designation: M302-86, 14th ed., 1986.

American Coal Ash Association (ACAA), *2000 Coal Combustion Product (CCP) Production and Use*, http://www.ACAA-USA.org/

American Concrete Institute, *Ground granulated blast-furnace slag as a cementitious constituent in concrete*, ACI Manual of Concrete Practice, ACI 226.1R, 1990.

Annachhatre, A.P., Win, N.N., Chadrkrachang, In: Stevens, W.J., Rao, M.S., and Chandrkrachang (Eds.), Proceedings of the Second Asia-Pacific Symposium, Asian Institute of Technology, Bangkok, Thailand, 169-173, 1996.

Annapragada, A., and Adjei, A., *An analysis of the Fraunhofer diffraction method for particle size distribution analysis and its application to aerosolized sprays*, International Journal of Pharmaceutics, 127, 219-227, 1996.

Apaka, R., Tutema, E., Hugula, M., and Hizala, J., *Heavy metal cation retention by unconventional sorbents (red muds and fly ashes)*, Water Research, 32(2), 430-440, 1998.

Aptak, R., Atun, G., Guclu, K., Tutem, R., *Sorptive removal of caesium-137 and strontium-90 from water by unconventional sorbents II*, Journal of the Atomic Energy Association of Japan, 33, 396-402, 1996.

Arnold, E., *Phosphorous*, In: Standard Methods For The Examination of Water and Wastewater, American Public Health Association, 1985.

Babcock and Wilcox Company, *Steam: its generation and use*, New York, NY, 1978.

Babi, B.M., Milonji, S.K., Plovina, M.J., Upi, S., and Kaludjerovi, B.V., *Adsorption of zinc, cadmium and mercury ions from aqueous solutions on activated carbon cloth*, Carbon, 40, 1109-1115, 2002.

Bailey, R.P., Bennet, T., and Benjamin, M.M., *Sorption onto and recovery of Cr(VI) using iron oxide-coated sand*, Water Science and Technology, 26, 1239-1244, 1992.

Bark, K., Sponner, A., Kampfer, P., Grund, S., and Dott, W., *Differences in polyphosphate adsorption by Acinetobacter isolates from wastewater producing phosphate: AMP phosphotransferase*, Water Research, Vol. 26(10), 1379-1388, 1992.

Bauer, H.H., Christian, G.D., and O'Reilly, J.E., Eds., *Instrumental analysis*, Allyn and Bacon, Inc., Massachusetts, 1978.

Bayvel, L.P., and Jones, A.R., *Electromagnetic scattering and its applications*, Applied Science, London, 1981.

Berry, E.E., and Malhorta, V.M., *Fly ash for use in concrete, Part II- A critical review of the effects of fly on the properties of concrete*, CANMET Report 78-16, Ottawa, Canada Centre for Mineral and Energy Technology, 1978.

Bhattacharya, A.K., and Venkobachar, C., *Removal of cadmium (III) by low cost adsorbents*, Journal of Environmental Engineering, ASCE, 110(1), 110-122,1984.

Black, L.B., McQuay, M.Q., and Bonin, M.P., *Laser-based techniques for particle size measurement: a review of sizing methods and their industrial applications*, Progress in Energy and Combustion Science, 22, 267-306, 1996.

Bockris, J.O'M., and Khan, S.U.M., *Surface Electrochemistry: A Molecular Level Approach*, Plenum Press, New York, 1993.

Bogue, R.H., *The chemistry of Portland cement*, 2nd ed., Reinhold, New York, 1955.

Borhen, C.F., and Huffman, D.R., *Adsorption and scattering of light by small particles*, Wiley, New York, 1983.

Bouck, D.W., *Nutrient removal in three-stage processing, In: Advances in water and wastewater treatment: Biological nutrient removal*, Wanielista, W.W., and Eckenfelder (Eds.), Ann Arbor Science, Michigan, pg. 65, 1978.

Bragg, W.L., Proceedings of the Cambridge Philosophical Society, v. 17, 43, 1913.

Braun, R.D., *Introduction to instrumental analysis*, McGraw-Hill, New York, 1987.

Brina, R., and de Battisti, A., *Determination of the specific surface area of solids by means of adsorption data*, Journal of Chemical Education, Vol. 64(2), 175-176, 1987.

Britannica, *Eutrophication*, 15th Edition, Encyclopaedia Britannica Inc., London, 1989.

Cabrera, J.G., and Gray, M.N., Specific surface, pozzolanic activity and composition of pulverized fuel ash, Fuel, Vol. 52, 213-219, 1973.

146

Campbell, W.J., *X-ray spectroscopy*, In: Instrumental Analysis, Bauer, H.H., Christian, G.D., and O'Reilly, J.E., Eds., Allyn and bacon, Inc., Boston, 1978.

Chakaravarty S., Dureja, V., Bhattacharyya G., Maity, S., and Bhattacharjee, S., *Removal of arsenic from groundwater using low cost ferruginous manganese ore*, Water Research, 36, 625-632, 2002.

Chantawong, V., Harvey, N.W., and Bashkin, V.N., Asian Journal of Energy and the Environment, 1, 33-48, 2001.

Chern, J-M., and Chien, Y-W., *Adsorption of nitrophenol onto carbon: isotherms and breakthrough curves*, Water Research, Vol. 36(3), 647-655, 2002.

Curkovic, L., Stefanovic, S.C., and Filipan, T., *Metal ion exchange by natural and modified zeolites*, Water Research, 31, 1379-1382.

Dasmahapatra, G.P., Pal, T.K., Bhadra, A.K., and Bhattacharya, B., *Studies on separation characteristics of hexavalent chromium from aqueous solution by fly ash*, Separation Science Technology, 31(14), 2001-2009, 1996.

Diamond, S., *The characterisation of fly ashes, In: Effects of fly ash incorporation in cement and concrete*, Proceedings Materials Research Symposium Annual Meeting, Boston, 1981, s.12-23.

Droste, R.L., *Theory and Practice of Water and Wastewater Treatment*, John Wiley & Sons, Inc., New York, 1997.

Eckenfelder, W.W., *Principles of Water Quality Management*, CBI Publishing Company, Inc., Boston, Massachusetts, 1980.

Emery, J.J., *Pelletized lightweight slag aggregate*, Proceedings of Concrete International 1980, Concrete Society, 1980.

Erdogan, Y., and Demirbas, A., *Partly-refined chemical by-product gypsums as cement additives*, Cement and Concrete Research, 24(4), 601-604, 1994.

Freundlich, H., *Colloid and Capillary Chemistry*, Methuen, London, 1926.

Frumkin, A.N., *Z. Phys. Chem.* (Leipzig), 166, p. 466, 1925.

Garcez, I., and Tittlebaum, M.E., *Investigation of leachability of sub-bituminous fly ash enhanced road base materials, In: Fly ash and coal conversion by-*

products: characterization, utilization, and disposal, Materials Society Symposia Proceedings, Vol. 43, p. 237, Pennsylvannia, 1985.

Guibal, E., Saucedo, I., Jansson-Charrier, M., Delanghe, B., and Cloirec, P., *Uranium and vanadium sorption by chitosan and derivatives*, Water Science and Technology, 30, 183-190, 1994.

Gupta, G.S., Prasad, G, and Singh, V.N., *Removal of colour from wastewater by sorption for water reuse*, Journal of Environmental science and Health, A23(3), 205-217, 1988.

Goodwin, D.G., and Mitchner, M., *Fly ash radiative properties and effects on radiative heat transfer in coal-fired systems*, International Journal of Heat and Mass Transfer, 32, 627-638, 1989.

Gouesbet, G., Grehan, G., and Maheu, B., *Generalised Lorentz-Mie theory and applications to optical sizing*, Combustion Measurements, N. Chigier, (Ed.), 339-382, Hemisphere, Washington DC, 1991.

Groenewold, G.H., Hassett, D.J., Koor, R.D., and Manz, O.E., *Disposal of western fly ash in the northern great plains, In: Fly ash and coal conversion by-products:*

characterization, utilization, and disposal, Materials Society Symposia Proceedings, Vol. 43, p. 213, Pennsylvannia, 1985.

Guiner, A., *X-ray crystallographic technology*, Hilger and Watts, London, 1952.

Han, I., Schlautman, M.A., and Batchelor, B., *Removal of hexavalent chromium from groundwater by granular activated carbon*, Water Environment Research, 72, 29-39, 2000.

Hayward, D.O., and Trapnell, B.M.W., *Chemisorption*, 2nd ed., Butterworth & Co., London, 1964.

Helfferich, F., *Ion Exchange*, McGraw Hill Book Company Inc., New York, 1962.

Helmuth, R., *Fly ash in cement and concrete*, Portland Cement Association, Illinois, 1987.

Hirleman, E.D., Oechsie, V., and Chigier, N.A., *Response characteristics of laser diffraction particle size analyzers: optical sample volume extent and lens effects*, Optical Engineering, 23, 610-619, 1984.

Hooton, R.D., *Permeability and pore structure of cement pastes containing fly ash, slag, and silica fume*, Blended Cements, ASTM STP 897, Fronhnsdorff, G., ed., American Society for Testing and Materials, Philadelphia, 128-143, 1986.

Huang, C.-P., and Blankkenship, D.W., *The removal of mercury (II) from dilute aqueous solution by activated carbon*, Water Research, 18, 37-46, 1984.

Huang, C.-P., Chung, Y.-C., and Liou, M.-R., *Adsorption of Cu(II) and Ni(II) by pelletized biopolymer*, Journal of Hazardous Materials, 45, 265-277, 1996.

Huang, C.P., and Ostovic, F.B., *Removal of cadmium (II) by activated carbon adsorption*, Journal of the Environmental Engineering Division, EE5, 863-878, 1978.

van de Hultz, H.C., *Light scattering by small particles*, Wiley, New York, 1957.

Ibrahim, K.M., NasserEd-Deen, T., and Khoury, H., Use of natural chabazite-phillipsite tuff in wastewater treatment from electroplating factories in Jordan, Environmental Geology, 41, 547-551, 2002.

Jarrige, A., *Les cendres volantes*, Paris, Editions Eyrolles, 1971.

Johansson, L., and Gustafsson, J.P., *Phosphate removal using blast furnace slags and opaka: mechanisms*, Water Research, 34(1), 259-265, 2000.

Joshi, R.C., Natt, G.S., Day, R.L., and Tilleman, D.D., *Scanning electron microscopy and X-ray diffraction analysis of various size fractions of fly ash, In: Fly ash and coal conversion by-products: characterisation, utilization and disposal*, Materials Research Society, Symposium Proceedings, Vol. 43, p. 31, Pennsylvania, 1985.

Joshi, A., and Chaudhuri, M., *Removal of arsenic from ground water by iron oxide-coated sand*, Journal of Environmental Engineering, 122, 769-771, 1996.

Kao, P.C., Tzeng, J.H., and Huang, T.L., *Removal of chlorophenols from aqueous solution by fly ash*, Journal of Hazardous Materials, 76(2-3), 237-249, 2000.

Khan, S.A., Rehman, R., and Khan, M.A., *Adsorption of chromium (III), chromium (VI) and silver (I) on bentotite*, Waste Management, 15, 271-282, 1995.

Knight, J.C., Ball, D., and Robertson, G.N., *Analytical inversion for laser diffraction spectrometry giving improved resolution and accuracy in size distribution*, Applied Optics, 30, 4795-4799, 1991.

Ko, D.C.K., Porter, J.F., and McKay, S., *Optimised correlations for the fixed-bed adsorption of metal ions on bone char*, Chemical Engineering Science, Vol. 55(3), 5819-5829, 2000.

Kocirik, M., Jiri, S., and Smutek, A., *The role of inert material in an adsorption bed*, Collect. Czech. Chem. Commun. Vol. 47(12), 3221-3229, 1982.

Kouloumbi, N., and Batis, G., *The anticorrosive effect of fly ash, slag and a Greek pozzolan in reinforced concrete*, Cement and Concrete Composites, 16, 253-260, 1994.

Kruger, R., South African Coal Ash Association, Personal Communication, Johannesburg, 2002.

Langmuir, I., *The adsorption of gases on plane surfaces of glass, mica and platinum*, Journal of the American Chemical Society, 40, 1361-1402, 1918.

Lea, F.M., *The chemistry of cement and concrete*, 3rd Edition, Edward Arnold (Publishers) Ltd, London, UK, 1970.

Leyva-Ramos, R., Rangel-Mendez, J.R., Mendoza-Barron, J., Fuentes-Rubio, L., and Guerrero-Coronado, *Adsorption of cadmium (II) from aqueous solution onto activated carbon*, Water Science and Technology, 35, 205-211, 1997.

Luke, W.I., *Nature and distribution of particles of various sizes in fly ash*, U.S. Army Engineers, Waterways Experiment Station, Technical Report No. 6-583, 21 pp., 1961.

Mantel, D.G., *The manufacture, properties and applications of Portland cements, cement additives and blended cements*, Pretoria Portland Cement (PPC), The Penrose Press, Johannesburg, South Africa, 1991.

Malliou, E., Loizidou, M., and Spyrellis, N., *Uptake of lead and cadmium by clonoptilolite*, Science of the Total Environment, 149, 139-144. 1994.

Malliou, E., Malamis, M., and Sakellarides, P.O., *Lead and cadmium removal by ion exchange*, Water Science and Technology, 25, 133-138, 1992.

McKay, G., Blair, H.S., and Findon, A., *Equilibrium studies for the sorption of metal ions onto chitosan*, Indian Journal of Chemistry Section A, 28, 356-360, 1989.

Michaels, A.S., *Simplified methods of interpreting kinetic data in fixed-bed ion exchange,* Industrial Engineering and Chemistry, 44(8), 1922-1930, 1952.

Michelsen, D.L., Gideon, J.A., Griffith, G.P., Pace, J.E., and Kutat, H.L., *Removal of soluble mercury from wastewater by complexing techniques,* Govt. Rep. Announce. Index (U.S.A), 75(24), 102, 1975.

Miller, J.C., and Miller, J.N., *Statistics for Analytical Chemistry,* 3rd ed., Ellis Horwood Ltd., Chichester, 1993.

Montemor, M.F., Simoes, A.M.P., Salta M.M., and Ferreira, M.G.S., *Carbonation of fly ash-containing concrete. Electrochemical studies,* Material Science Forum, 192-194:867, 1995.

Montemor, M.F., Simoes, A.M.P., and Salta, M.M., *Effect of fly ash on concrete reinforcement corrosion studied by EIS,* Cement and Concrete Composites, 22, 175-185, 2000.

Murakami, K., *By-product gypsum from various chemical industries as a retarder for the setting of cement,* Proc. 5th International Conference on the chemistry of cement, Tokyo, 457-510, 1968.

Namasivayam, C., and Ranganathan, K., *Waste iron (III)/chromium (III) sludge as flocculant for the treatment of dairy wastewater*, Environmental Pollution, 82, 255-261, 1992.

Netzer, A., and Hughes, D.E., *Adsorption of copper, lead and cobalt by activated carbon*, Water Research, 18, 927-933, 1984.

Noureldin, A,S., and McDaniel, R.S., *Evaluation of steel slag asphalt surface mixtures*, Presented at the 69th Annual Meeting, Transportation Research Board, Washington, 1990.

Nowacki, P., *Lignite Technology*, Noyes Data Corp., New Jersey, USA, 1980.

Ouki, S.K., Cheeseman, C.R., and Perry, R., *Effects of conditioning and pre-treatment of chabazite and clinoptilolite prior to lead and cadmium removal*, Environmental Science and Technology, 27, 1108-1116, 1993.

Ouki, S.K., and Kavanagh, M., *Performance of natural zeolites for the treatment of mixed metal-contaminated* effluents, Waste Management & Research, 15, 383-394, 1997.

Panday, K.K., Prasad, G., and Singh, V.N., *Removal of Cr (VI) from aqueous solution by adsorption on fly ash-wollastonite*, Journal of Chemical Technology and Biotechnology, 34(A), 367-374, 1984.

Panday, K.K., Prasad, G., and Singh, V.N., *Mixed adsorbents for Cu(II) removal from aqueous solution*, Environmental Technology Letters, 7, 547-554, 1986.

Pansini, M., Colella, C., and De'Gennaro, M., *Chromium removal from water by ion exchange using* zeolite, Desalination, 83, 145-157, 1991.

Pettijohn, F.J., *Sedimentary rocks*, Harper and Bros., New York, 1957.

Piekos, R., and Paslawska, S., *Fluoride uptake characteristics of fly ash*, Fluoride, 32(1), 14-19, 1999.

Piekos, R. and Paslawska, S., *Fluoride uptake characteristics of fly ash*, Research Report, International Society for Fluoride Research, 32(1), 1-6, 1999.

Portland Cement Association, PCA: *Take a virtual plant tour*, http://www.portcement.org, 2002.

Pusch, R., *Use of bentonite for isolation of radioactive waste products*, Clay Minerals, 37, 353-361, 1992.

Rangel-Mendez, J.R., and Streat, M., *Adsorption of cadmium by activated carbon cloth: influence of surface oxidation and solution pH*, Water Research, 36, 1244-1252, 2002.

Rasmussen, H., Bruus, J.H., Keiding, K., Nielson, P.H., *Observations of dewaterability and physical, chemical and microbiological changes in anaerobically stored activated sludge from a nutrient removal plant*, Water Research, Vol. 28(2), 417-425, 1994.

Ray, S.S., and Parker, F.G., *Characterisation of ash from coal-fired power plants*, EPA 600/7-77-010, Chattanooga, Tennessee Valley Authority, 1977.

Recycled materials Resource Centre RMRC), University of New Hampshire, http://www.rmrc.unh.edu, 2002.

Reed, B.E., and Arunachalam, S., *Use of granular activated carbon columns for lead removal*, Journal of Environmental Engineering, 120, 416-436, 1994.

Sakadevan, K., and Bavor, H.J., *Phosphate adsorption characteristics of soils, slags and zeolite to be used as substrates in constructed wetlands systems*, Water Research, 32, 393-399, 1998.

Schmuhl, R., Krieg, H.M., and Keizer, K, *Adsorption of Cu(II) and Cr(VI) ions by chitosan: Kinetics and equilibrium studies*, Water S.A., 27, 1-7, 2001.

Semmens, M.J., and Martin, W.P., *The influence of pre-treatment on the capacity and selectivity of clinoptilolite for metal ions*, Water Research, 22, 537-542, 1988.

Sen, A.K., and Arnad, K.D., *Adsorption of mercury (II) by coal fly ash*, Water Research, 21, 885-888, 1987.

Sharma, D.C., and Forster, C.F., *Removal of hexavalent chromium from aqueous solutions by granular activated carbon*, Water SA, 22, 153-160, 1996.

Shimadzu Corporation, *Instruction manual: Shimadzu digital double-beam spectrophotometer UV-150*, Kyoto, 1994.

Skoog, D.A., and Leary, J.J., *Principles of instrumental analysis*, 4th ed., Saunders College Publishing, Orlando, 1992.

Smethurst, G., *Basic Water Treatment*, Thomas Telford Ltd., London, 1979.

South African Bureau of Standards, *Compressive strength for concrete masonry units*, Standard No. SABS 1215-1984.

Spackman, W., Davis, A., Walker, P.L., Lovell, H.L., Essenhigh, R.H.; Vastola, F.J.; and Given, P.H., *Characteristics of American coals in relation to their conversion into clean energy fuels*, Quarterly Progress Report Fe-2030-3, ERDA, Pennsylvania State University, 1976.

Srivastava, S.K., Bhattacharjee, G., Tyagi, R, Pant, N., and Pal, N., *Studies on the removal of some toxic metal ions from aqueous solutions and industrial waste Part I (Removal of lead and cadmium by hydrous iron and aluminium oxide)*, Environmental Technolology Lettters, 9, 1173-1185, 1988.

Srivastava, S.K., Tyagi, R., and Pal, N., *Studies on the removal of some toxic metal ions Part(II) (removal of lead and cadmium by montmorillonite and kaolinite*, Environmental Technology Letters, 10, 275-282, 1989.

Srivastava, S.K., Tyagi, R., and Pal, N., *Adsorption of heavy metal ions on carbonaceous material developed from the waste slurry generated in local fertilizer plants*, Water Research, 23, 1161-1165, 1989.

Srivastava, S.K., Singh, A.K., and Sharma, A., *Studies on the uptake of lead and zinc by lignin obtained from black liquor- a paper industry waste material*, Environmental Technology, 15, 353-361, 1994.

Srivastava, S.K., Gupta, V.K., and Mohan, D., *Removal of lead and chromium by activated slag- a blast furnace waste*, Journal of Environmental Engineering, 123, 461-468, 1997.

Strong, F.C., *Theoretical basis of the Bouger-Beer law of radiation absorption,* Analytical Chemistry, 24, 338-342, 1952.

Stout, F.C., and Jensen, L.H., *X-ray structure determination*, John Wiley & Sons, New York, 1989.

Sundstrom, D.W., and Klei, H.E., *Wastewater Treatment*, Prentice Hall Inc., London, 1979.

Swithenbank, J., Beer, J.M., Taylor, M., Abbot, D., and McCreath, G.C., *A laser diagnostic technique for the measurement of droplet and particle size distributions*, Progress in Astronautics and Aeronautics, 53, 421-447, 1977.

Tabikh, A.A., and Miller, F.M., *The nature of phosphogypsum impurities and their influence on cement hydration*, Cement and Concrete Research, 1(6), 663-678, 1971.

Torrey, S., *Coal ash utilization: fly ash, bottom ash and slag*, Noyes Data Corp., New Jersey, USA, 1978.

Turriziani, R., *Aspects of the chemistry of pozzolans, pp 69-86, In: The chemistry of cements*, Taylor, H.F.W., Ed., Academic Press, New York, 1964.

Ulrich, G.D., *Theory of particle formation and growth in oxide synthesis flames*, Combustion Science Technology, Vol. 4, 47-57, 1971.

Ulrich, G.D., Milnes, B.A., and Subramanian, N.S., *Particle growth in flames, II. Experimental results for silica particles*, Combustion Science Technology, Vol. 14, 243-249, 1976.

Undaybeytia, T., Morillo, E., and Maqueda, C., *Adsorption of Cd and Zn on montmorillonit in the presence of a cationic pesticide*, Clay Minerals, 31, 485-490, 1996.

U.S. Department of the Interior, Bureau of Mines, Mineral Commodity Summaries 1993, Washington, DC, 1993.

Vorres, K., *Coal*, Kirk-Othmer Encyclopedia of Chemical Technology, 3rd ed., Vol. 6, 224-282, John Wiley & Sons, New York, 1979.

Wan-Ngah, W.S., Endud, C.S., and Mayanar, R., *Removal of copper(II) ions from aqueous solution onto chitosan and cross-linked chitosan beads*, Reactive and Functional Polymers, 50, 181-190, 2002.

Wan-Ngah, W.S., and Isa. I.M., *Comparison study of copper ion adsorption on chitosan*, Journal of Applied Polymer Science, 67, 1067-1070, 1998.

Washington, C., *Particle size analysis in pharmaceutics and other industries: theory and practice*, Ellis Horwood, London, 1992.

Watt, J.D., and Thorne, D.J., *Composition and pozzolanic properties of pulverised fuel ashes*, Journal of Applied Chemistry, Vol. 15, 585-594, 1965.

Williams, K.L., *Introduction to X-ray spectrometry*, Allen & Unwin, Boston,1987.

Yadawa, K.P., Tyagi, B.S., and Singh, V.N., *Effect of temperature on the removal of lead(II) by adsorption on China clay and wollastonite*, Journal of Chemical Technology and Biotechnology, 51, 47-60, 1991.

Yamada, H., Kayama, M., Saito, K., and Hara, M., *A fundamental research on phosphate removal by slag*, Water Research, 20, 547-557, 1986.